ÇUKUROVA UNIVERSITY
INSTITUTE OF NATURAL AND APPLIED SCIENCES

PhD THESIS

Volkan KORKUT

INVESTIGATION OF PROCESS PARAMETERS IN DIRECT MATERIAL DEPOSITION BASED OPEN-SOURCE ADDITIVE MANUFACTURING SYSTEMS

DEPARTMENT OF MECHANICAL ENGINEERING

ADANA-2022

ABSTRACT

PhD THESIS

INVESTIGATION OF PROCESS PARAMETERS IN DIRECT MATERIAL DEPOSITION BASED OPEN-SOURCE ADDITIVE MANUFACTURING SYSTEMS

Volkan KORKUT

ÇUKUROVA UNIVERSITY
INSTITUTE OF NATURAL AND APPLIED SCIENCES
DEPARTMENT OF MECHANICAL ENGINEERING

Supervisor : Prof. Dr. Hakan YAVUZ
Year: 2022, Pages: 193
Juries : Prof. Dr. Hakan YAVUZ
: Prof. Dr. Mehmet BİLGİLİ
: Prof. Dr. Selçuk MISTIKOĞLU
: Assoc. Prof. Dr. Mustafa ORAL
: Asst. Prof. Dr. Hürrem AKBIYIK

In this study, the Additive Manufacturing methods are investigated. They are considered to be revolutionary for the manufacturing industry. In this context, amongst many other research topics, it is observed that Fused Filament Fabrication and Metal Droplet Jetting systems are considered to be popular ones. The common feature of these methods is that they are based on the direct material deposition technique, which provides significant advantages in terms of manufacturing parts with complex geometry. However, both of the methods are fairly new and there are still some technical issues that are currently a research topic. To achieve the objectives of the presented study, firstly, a Fused Filament Fabrication device based on open-source concept is developed. The process parameters that affects the part strength are determined and optimized using the open-source device. During the optimizations, along with others, the issue of material consumption is also considered. The objective of this study is to achive controlled process parameters and steps to increase the part strength using the same amount of material. In the second stage; Owing to the open-source concept system developed, the same device is extensively modified to make it suitable for the Metal Droplet Jetting system related research. The production process is performed by controlled deposition of metal droplets. In order to give droplet form to the molten metal, a unique Metal Droplet Jetting mechanism including a mechanical actuation system is designed and manufactured. To achieve a deposition model with the desired morphology, the droplet ejection and deposition stages are first subdivided into groups, then each is examined in details. In this way, the droplets are not only produced homogeneously, but the need for pneumatic gas support, which makes it difficult to control and increases the processing cost, is eliminated. As a result of experimental studies supported by theoretical calculations, a low-cost and practical metal material deposition method that can be used effectively, especially in the electronics industry, is presented.

Keywords: Direct Material Deposition, Fused Filament Fabrication, FDM, Material Jetting, Metal Droplet Generation, Deposition Morphology, Additive Manufacturing

ÖZ

DOKTORA TEZİ

DOĞRUDAN MALZEME BİRİKTİRME TABANLI AÇIK-KAYNAKLI EKLEMELİ İMALAT SİSTEMLERİNDE İŞLEM PARAMETRELERİNİN ARAŞTIRILMASI

Volkan KORKUT

ÇUKUROVA ÜNİVERSİTESİ
FEN BİLİMLERİ ENSTİTÜSÜ
MAKİNE MÜHENDİSLİĞİ ANABİLİM DALI

Danışman	: Prof. Dr. Hakan YAVUZ
	Year: 2022, Pages: 193
Juriler	: Prof. Dr. Hakan YAVUZ
	: Prof. Dr. Mehmet BİLGİLİ
	: Prof. Dr. Selçuk MISTIKOĞLU
	: Doç. Dr. Mustafa ORAL
	: Dr. Öğr. Üyesi Hürrem AKBIYIK

Bu çalışmada, imalat endüstrisi açısından bir devrim niteliği taşıyan Eklemeli İmalat yöntemlerine dair araştırmalar yapılmıştır. Bu kapsamda, direkt malzeme depolama tekniğine dayalı Fused Filament Fabrication ve Metal Droplet Jetting sistemlerinin, ürün üretimi açısından önemli avantajlar sağladığı gözlemlenmiştir. Bununla birlikte, üretim performanslarının arttırılmasına yönelik bir takım eksikliklerin giderilmesi de gerekmektedir. Bu amaçla, ilk etapta, Fused Filament Fabrication işlemlerinin gerçekleştirilebileceği, açık-kaynak konseptine dayalı bir cihaz kurulumu yapılmıştır. Bu cihaz aracılığıyla, parça dayanımına etki edecek işlem parametreleri belirlenmiş ve optimize edilmiştir. Dahası, optimizasyonlar yapılırken, malzeme tüketimi konusu da ön planda tutulmuştur. Bu sayede, malzeme israfına yol açmadan, parça dayanımının arttırılmasına yönelik umut verici, çevre dostu işlem adımları açığa çıkarılmıştır. İkinci etapta; Benimsenen açık-kaynak konsepti sayesinde aynı cihaz, kapsamlı bir şekilde modifiye edilerek, metal bazlı ürün üretimine elverişli hale getirilmiştir. Üretim işlemi, metal damlacıkların kontrollü bir şekilde depolanması ile gerçekleştirilmiştir. Ergiyik metale damlacık formu kazandırabilmek amacıyla, bir mekanik aktüasyon sistemi içeren özgün bir Metal Damlacık Jetleme mekanizması tasarlanıp, üretilmiştir. İstenen yapıda bir depolama modeli elde edebilmek için damlacık ejeksiyonu ve depolama aşamaları sınıflandırılmıştır. Bu sayede dropletler sadece homojen bir şekilde üretilmekle kalmayıp, kontrolü güçleştiren ve maliyeti önemli ölçüde arttıran pnömatik gaz desteği ihtiyacı elimine edilmiştir. Teorik hesaplamalar ile de desteklenen deneysel çalışmalar sonucu, özellikle elektronik endüstrisinde etkin bir şekilde kullanılabilecek, düşük maliyetli ve pratik bir metal malzeme depolama yöntemi sunulmuştur.

Anahtar kelimeler: Direkt Malzeme Depolama, Eriyik Filament Üretimi, FDM, Malzeme Jetleme, Metal Droplet Üretimi, Depolama Morfolojisi, Eklemeli İmalat

EXTENDED ABSTRACT

Within the scope of this study, methods based on Additive Manufacturing technology and their process performances are investigated in detail. Among these methods, the ones that are based on direct material deposition are observed to be future promising in terms of low cost production by eliminating many manufacturing process steps. However, it is noticed that there are some problems in increasing the performance of such processes. In addition, AM-based part production allows product production by consuming only the material needed for the part, hence reducing waste to minimum. In this context, these methods are accepted as a game-changing technologies for the manufacturing industry. However, when AM methods are classified within themselves, they contain a number of weak points, primarily in terms of difficulty in installation and usage stages. Considering that time and cost are the two most important factors from an engineering point of view, related research and development to solve problems is a necessity rather than a choice. In this thesis study, these issues are considered and a systematic study is carried out to solve the problems identified in relevant direct material deposition methods.

A part of the study is focuses on solving the problems faced in the Fused Filament Fabrication (FFF) method, which is one of the most widely used AM methods worldwide. In this context, previous studies reported in literature are examined in detail. In these studies, it is determined that the efforts were mainly focus on increasing the strength of the parts. It has been suggested that the first reason for this situation is that the dynamics of this relatively new production method have not yet been set to a certain standard and the process settings are not understood well enough. In this process, the products are basically formed by the permanent coalescence of layers that are deposited on top of each other. Material bonding conditions, both within and between layers directly affect all physical properties of the manufactured part, such as strength, surface quality, production

efficiency, and material consumption, etc. In addition, in the deposition processes, there is a need to determine tens of interacting process parameters for each part separately. Hence, this is the only way that FFF-based manufacturing processes become viable through a standard procedure. In order to make a contribution to the solution methods, the process parameters that have an effect on the part strength are examined in this study. While determining the effective parameters in terms of strength, material consumption amount is also kept fixed. Although the increase in strength and material consumption issues has been comprehensively presented in literature, the number of studies in which the two critical factors considered together is found to be limited. In order to be able to address the consideration of process parameters in a combinational manner, an open-source concept 3D printer system is developed.

The developed open-source systems provide users with an infrastructure that allows the flexibility of setting many process parameters freely. In this type of systems, the users can access the necessary process parameters and related information directly. Moreover, since the existing database is open to everyone, problems are solved very quickly and can be adapted to the application areas in a very short time. The same issue is valid for FFF systems, the use of which is increasing day by day. The open-source concept gains further importance when it is considered that even the smallest improvement to be made in FFF-based production processes, which are used extensively both on an individual scale and in high-budget business areas. At this point, it is also important to consider that there is a necessity to provide an environmentally friendly production process that is in line with the Green Deal objectives.

Considering all these factors, an open-source FFF device is installed and the part production performance is evaluated as the first stage of the study. During the preparation of the parts for production, important process parameters such as line width, number of lines for shell walls, infill orientation and infill overlap are concentrated on. In the experimental process, in the first place, the interactions of the polymer-based lines to be deposited with each other and the amount of coalescence are determined on the digital platform. By using the Taguchi-based experimental planning technique, a series of samples are produced by means of parameters determined with different combinations, in a minimum but sufficient number. The samples are then subjected to mechanical testing and the results are evaluated using statistical tools. With the help of the findings and results of the statistical evaluations, a new part with a parametric combination is produced. While a significant increase in strength is achieved in this part, it is also ensured that there is no significant increase in material consumption. Experimental studies are then made adaptable to different FFF processes, based on a series of mathematical calculations.

Later, the device is extensively modified and the study is carried one step further. Through these modifications, the device is made suitable for metal deposition processes. This conversion is accomplished by replacing the region where the polymer material is extruded by a metal ejection system. The system is modified not only in hardware but also in software. The metal deposition process is provided by melting the metal in the form of droplets and storing it on a suitable surface. All these processes are carried out by means of a droplet generator with a unique design. The droplet generator is structurally composed of a solenoid actuator, a vibration transmitting, rod connected to the actuator, and an orifice. In addition, there is an induction heater surrounding the body and a material inlet where the material can be fed to the heated area. As a working principle, the metalic material in the form of wire is driven into the melting zone (reservoir) and then melted by using an induction heater. Then, the vibrations generated by the actuator operated with suitable electrical inputs are transmitted to the molten pool via a piston-like rod. The liquid is then forced to flow out through the mechanical impacts of the piston tip. Due to intermittent movements, it is observed that the liquid takes the form of a droplet as soon as it is thrown out of the orifice.

There are two main points that ensure the originality of the developed droplet generator. Firstly, the amount of pressure required to form the droplet is provided only by mechanical impacts. At this point, the theorems containing a series of dimensionless numbers are used to ensure that each successive droplet has the similar characteristic. It should be stated that it is necessary to apply a certain amount of thrust pressure in order to form the droplets with the desired properties. In the mechanical-impact based droplet generators that have been developed so far, this pressure range is provided by an auxiliary gas support. This additional system significantly increases the installation cost and complicates the overall control problem. In this thesis, this pressure balance is achieved not only by mechanical impacts, but also by characterizing the amount of material fed into the interior. In other words, the material to be fed into the melting zone directly determines the liquid height in the reservoir. In the experimental study, the need for pneumatic pressure supporting the mechanical pressure is provided by the hydrostatic pressure obtained with this fluid height. In order to keep the liquid height at the desired level, a controlled material is fed into the interior. For this process, a material feeding system is developed both in software and hardware terms and the amount of feeding is kept under control. This constitutes the second originality of the study. It is also important that the deficiencies detected in direct material deposition-based AM processes can be resolved through open-source-based systems. This thesis study is important in terms of reducing investment costs while improving the manufacturing performance, which play a critical role for the production industry.

GENİŞLETİLMİŞ ÖZET

Çalışma kapsamında, resmi olarak Eklemeli İmalat (Eİ) ailesine hem üye olmuş hem üye olmaya aday yöntemler kapsamlı olarak araştırılmıştır. Yöntemler arasında, direkt malzeme depolama tabanlı olanların, bir çok işlem adımını elimine ederek, düşük maliyetli üretim açısından umut verici olduğu gözlemlenmiştir. Bununla birlikte, bu tür işlemlerin performansının arttırılması hususunda bir takım problemlerin de mevcut olduğu fark edilmiştir. Ayrıca, Eİ tabanlı parça üretimi, sadece ihtiyaç kadar malzeme tüketerek ürün üretimine olanak sağlamaktadır. Bu durum, hem zaman hem de malzeme ihtiyacını belirgin bir şekilde azaltmaktadır. Bu bağlamda bu yöntemler, üretim endüstrisi açısından oyun değiştirici bir niteliğe sahip bir teknoloji olarak kabul görmüştür. Bununla birlikte, Eİ yöntemleri kendi içinde sınıflandırıldığında, başta kurulum ve kullanım zorluğu bakımından, bir takım zayıf nokta ihtiva etmektedir. Mühendislik bakış açısından, zaman ve maliyet konularının en önemli iki faktör olduğu göz önünde bulundurulduğunda, sorunların çözümüne yönelik araştırma ve geliştirme işlemlerinin yapılması bir tercihten çok zorunluluktur. Bu tez çalışmasında da bu hususlar ön planda tutulmuş olup, direkt malzeme depolama yöntemlerinde tespit edilen sorunların çözümüne yönelik sistematik bir çalışma yapılmıştır.

Çalışmanın çıkış noktası olarak, dünya çapında en yaygın kullanılan Eİ metolarından biri olan Fused Filament Fabrication (FFF) yöntemindeki sorunların çözümüne yönelik araştırmalar yapılmıştır. Bu kapsamda daha önce yapılan kalifiye çalışmalar detaylıca incelenmiştir. Bu çalışmalarda daha çok parça dayanımının arttırılması konusuna yoğunlaşıldığı tespit edilmiştir. Bu durumun ilk sebebinin, görece yeni sayılabilecek bu üretim yönteminin dinamiklerinin henüz belirli bir standarta oturtulamamış olduğu öne sürülmüştür. Çünkü ürünler temelde, üst üste biriktirilmiş katmanların birbiriyle kalıcı olarak birleştirilmesiyle oluşur. Hem katman içinde, hem de katmanlar arası malzeme birleşme koşulları, parçanın dayanımı, yüzey kalitesi, üretim verimliliği, malzeme tüketimi gibi istisnasız tüm

özellikleri̇ni doğrudan etkilemektedir. Ek olarak depolama işlemlerinde, birbirleriyle etkileşim halinde olan onlarca işlem parametresinin her parça için ayrı ayrı belirlenmesi ihtiyacı bulunmaktadır. Ancak bu şekilde FFF tabanlı üretim işlemleri, standart bir prosedür aracılığıyla uygulanabilir hale gelebilecektir. Çözüm yöntemlerine bir katkıda bulunabilmek amacıyla, bu çalışmada da parça dayanımına etkisi olan işlem parametreleri incelenmiştir. Dayanım konusunda etkili parametreler belirlenirken malzeme tüketim miktarları da ön planda tutulmuştur. Çünkü, geçmiş çalışmalarda dayanımın artışı ve malzeme tüketim konuları her ne kadar kapsamlı bir şekilde sunulmuş olsa da, iki faktörün birlikte işlendiği çalışma sayısının kısıtlı olduğu görülmüştür. Çözüme yönelik çalışmalarda, açık-kaynak konseptinden faydalanılmıştır.

Açık-kaynaklı sistemler, kullanıcılara oldukça verimli üretim işlemleri gerçekleştirilebilecek bir altyapı sağlamaktadır. Çünkü bu konsept sayesinde kullanıcılar; maddi anlamda herhangi bir telif hakkı ödemeden, gerekli bilgilere direkt olarak ulaşabilmektedir. Dahası, mevcut veritabanı herkese açık olduğundan dolayı, problemlerin çözümü çok hızlı gerçekleşmekte ve uygulama alanlarına çok kısa bir sürede uyarlanabilmektedir. Kullanımı her geçen gün artan FFF sistemleri için de aynı durum geçerlidir. Hem bireysel ölçekte hem de yüksek bütçeli iş alanlarında oldukça yoğun kullanılan FFF tabanlı üretim işlemlerinde sağlanacak en küçük bir iyileştirmenin bile global bir etki yaratacağı düşünüldüğünde, açık-kaynak konsepti ayrıca bir önem kazanmaktadır. Bu noktada, çevre dostu bir üretim işlemi sağlayabilmek de bir zorunluluk haline gelmektedir.

Tüm sayılan faktörler göz önünde bulundurularak açık-kaynaklı bir FFF cihazı kurulmuş ve parça üretim performansı değerlendirilmiştir. Parçaların üretime hazırlanma aşamasında, çizgi genişliği, duvar sayısı, dolgu oryantasyonu ve dolgu binme miktarı gibi önemli işlem parametrelerine yoğunlaşılmıştır. Deneysel süreçte, ilk etapta, depolanacak polimer bazlı hatların birbirileriyle olan etkileşimleri ve birleşme miktarları, dijital platformda belirlenmiştir. Taguchi tabanlı deneysel planlama tekniği kullanılarak, minimum ama yeterli sayıda, farklı kombinasyonlarda belirlenen parametreler aracılığıyla bir seri numune üretimi gerçekleştirilmiştir. Numuneler daha sonra mekanik testlere tabi tutulmuş olup sonuçlar, güçlü istatistiksel araçlar aracılığıyla değerlendirilmiştir. Elde edilen bulgular ve istatistiksel değerlendirmelerin de yardımıyla, yeni bir parametrik kombinasyona sahip parça üretimi gerçekleştirilmiştir. Bu parçada belirgin oranda bir dayanım artışı elde edilirken, malzeme tüketiminde kayda değer bir artış olmaması da sağlanabilmiştir. Deneysel çalışmalar, bir dizi matematiksel hesaba dayandırılarak, farklı FFF proseslerine de uyarlanabilir hale getirilmiştir.

Daha sonra cihaz kapsamlı bir şekilde modifiye edilerek çalışma bir adım öteye taşınmıştır. Bu modifikasyonlar aracılığıyla cihazın metal depolama işlemlerine elverişli hale getirilmesi sağlanmıştır. Bu dönüşüm, polimer malzemenin dışarı atıldığı bölgenin, bir metal ejeksiyon sistemi ile değiştirilmesi araclığı ile gerçekleştirilmiştir. Sistem, sadece donanımsal olarak değil, yazılımsal olarak da modifiye edilmiştir. Metal depolama işlemini metalin ergitilip, damlacıklar formunda dışarı atılması ve uygun bir yüzeyde depolanması aracılığıyla sağlanmıştır. Tüm bu işlemler, özgün bir tasarıma sahip bir damlacık üreteci aracılığıyla gerçekleştirilmiştir. Damlacık üreteci yapısal anlamda; bir solenoid aktüatör, aktüatöre bağlı bir titreşim iletici çubuk ve bir orifisten oluşmaktadır. Ayrıca üreteçte, gövdeyi çevreleyen bir indüksiyon ısıtıcı ve ısıtılan bölgeye malzemenin sürülebileceği bir malzeme girişi de bulunmaktadır. Çalışma prensibi olarak, tel formundaki metal malzeme ergitme bölgesine (rezervuara) sürülerek ergitilmesi sağlanır. Daha sonra, uygun elektriksel girdiler ile çalıştırılan aktüatör aracılığıyla oluşturulan titreşimler ergiyik havuza, piston benzeri çubuk aracılığıyla iletilir. Piston ucunun oluşturduğu mekanik darbeler aracalığıyla da sıvı dışarıya akmaya zorlanır. Akıtılan sıvı kesintili darbeler sayesinde, orifis çıkışında damlacık formu kazanır.

Geliştirilen damlacık üretecinin özgünlüğünü sağlayan iki temel nokta bulunmaktadır. Birincisi, damlacık oluşturabilmek için gerekli basınç miktarı, sadece mekanik darbeler aracılığıyla sağlanmıştır. Bu noktada, ardışık bir şekilde oluşturulacak damlacıkların her birinin aynı karakterde olmasını sağlamak amacıyla, bir dizi boyutsuz sayı içeren eşitlikten yararlanılmıştır. Çünkü, damlacıkları istenen özelliklerde oluşturabilmek için belirli bir miktar aralığında itiş basıncı uygulamanın zorunlu olduğu belirtilmelidir. Şu ana kadar geliştirilmiş olan, mekanik darbeye dayalı damlacık üreteçlerinde bu basınç aralığı, kurulum maliyetini önemli miktarda arttıran ve kontrolü zorlaştıran yardımcı bir gaz desteği aracılığıyla sağlanmıştır. Bu tez çalışmasında ise bu basınç dengesi, sadece mekanik darbeler ile, ama içeriye beslenen malzeme miktarı da kontrol edilerek sağlanmıştır. Başka bir anlatımla, ergitme bölgesine beslenecek malzeme, rezervuar içindeki sıvı yüksekliğini direkt olarak belirlemektedir. Bu deneysel çalışmada, mekanik basıncı destekleyici pnömatik basınç ihtiyacı ise, bu sıvı yüksekliğine bağlı hidrostatik basınç aracılığıyla sağlanmıştır. Sıvı yüksekliğini istenen seviyede tutabilmek için ise içeriye kontrollü bir malzeme beslemesi yapılmıştır. Bu işlem için hem yazılımsal hem donanımsal anlamda bir malzeme besleme sistemi geliştirilmiş ve besleme miktarı kontrol altında tutulmuştur. Bu da çalışmanın ikinci özgün noktasını oluşturmaktadır. Direkt malzeme depolama tabanlı Eİ işlemlerinde tespit edilen açıkların, açık-kaynak tabanlı sistemler aracılığıyla çözümlenebiliyor olması önemli bir husustur. Aynı anda hem yatırım maliyetlerini düşürmenin hem de üretim verimliliğinin arttırılmasının, üretim endüstrisi için kritik birer faktör olduğu göz önünde bulundurulduğunda bu tez çalışması önem arz etmektedir.

ACKNOWLEDGEMENT

This thesis work is the final step towards the completion of my PhD education. But I know that this is surely not the end on behalf of the lifelong learning process. When I look back on the efforts I have made over the years on the path of mechanical engineering, I see that I have perhaps passed the best years of my life.

In the last years of my education, I had the privilege of studying on advanced production techniques, additive manufacturing and control systems, which I worship to work on. I therefore would like to express my gratitude to those who helped me to reach the fulfilment of my thesis.

I would like to thank my thesis advisor, Prof. Dr. Hakan Yavuz for giving me the opportunity to perform the research on this interesting topic and for his insightful ideas regarding the problem encountered during the whole period. Also, I would like to thank Prof. Dr. Hasan Kurtaran and Prof. Dr. Hüseyin Akıllı for their contribution and reassuring support in every stage of this thesis study.

Furthermore, I am indebted to Asst. Prof. Dr. Aysun Baltacı, Asst. Prof. Dr. Barış Oğuz Gürses, Asst. Prof. Dr. Hürrem Akbıyık and Dr. Res. Asst. Alper Burgaç for their valuable supports during my thesis work. Besides, I also thank to Muhammet Yıldırımcan and Murat Yılmaz for their helps in setting my experimental setup.

Finally, I would like to thank my wife Didem Güneş Korkut, my mother Rahime Korkut, my father Feyzullah Korkut, my brother Mustafa Korkut and his dear wife Müge Çakır Korkut for their limitless supports and patience in all circumstances. I would not be able to handle my PhD period without them.

CONTENTS **PAGES**

LIST OF TABLES **PAGE**

LIST OF FIGURES **PAGE**

LIST OF ABBREVIATIONS

LW	:*Line width*
ST	:*Shell thickness*
OL	:*Overlap length*
We	:*Weber number*
ρ_g	:*Droplet density*
U	:*Droplet velocity*
D	:*Droplet diameter*
σ_d	:*Surface tension of liquid*
V	:*Voltage applied*
P_{atm}	:*Atmospheric pressure*
P_{hs}	:*Hydrostatic pressure*
P_p	:*Mechanical pressure*
P_{rf}	:*Reflow pressure*
P_c	:*Constant pressures of* (P_p, P_{st}, and P_{rf})
V_{molten}	:*Volume of molten liquid*
h_f	:*Liquid height*
d_s	:*Solder alloy density*
g	:*Gravitational acceleration*
m_u	:*Mass of single droplet*
f	:*Ejection frequency*
V_{out}	:*Ejected liquid volume*
V_{wire}	:*Volume of wire*

r_{wire}	*:Radius of wire*
U_{wire}	*:Wire feed velocity*
ω	*:Gear angular velocity*
r_g	*:Gear radius*
t_{feed}	*:Necessary feeding time*

1. INTRODUCTION

The Additive Manufacturing (AM) technology has growing popularity due to the capability of manufacturing a part using digital model directly. This feature allows manufacturing complex shapes that are difficult or almost impossible to achieved using conventional techniques such as material removing, cutting or bonding processes. The AM process involves several steps to convert virtual model into a physical object. Fundamentally, it begins with modeling desired geometry using any professional 3D modeling software. Afterwards, the completed model file is converted to the Stereolithography (.stl) file format to be able to configure the model in the slicer software. In the slicer software, found in both commercial and open-source form, the digital model is sliced into horizontal layers. This procedure is also called as "slicing step". Besides the slicing, various parameters those determine the final part quality are also configured. During this process, the software also simulates material adding action depending on the time and location. The data of sliced model including the time and the location is then recorded in form of G-Code (".gcode") file. The G-Code file is a universal code that maintains connection between digital processing and actual manufacturing processing. Although there are many different devices, materials and mechanisms available, the principle of AM operation relies on the g-code as a key feature of the AM industry. Technically, the base material is deposited on a suitable deposition platform (substrate) continuously layer by layer according the data received from the G-Code. This process continues until the last layer is completed and the physical object is obtained as shown in Figure 1.1, (Gibson et al., 2010). The definition of the AM process is also standardized by American Society for Testing and Materials (ASTM) as "*a process of joining materials to make objects from 3D model data, usually layer upon layer, as opposed to subtractive manufacturing methodologies. Synonyms: additive fabrication, additive processes, additive* *techniques, additive layer manufacturing, layer manufacturing, and freeform fabrication*" (ASTM International, 2012).

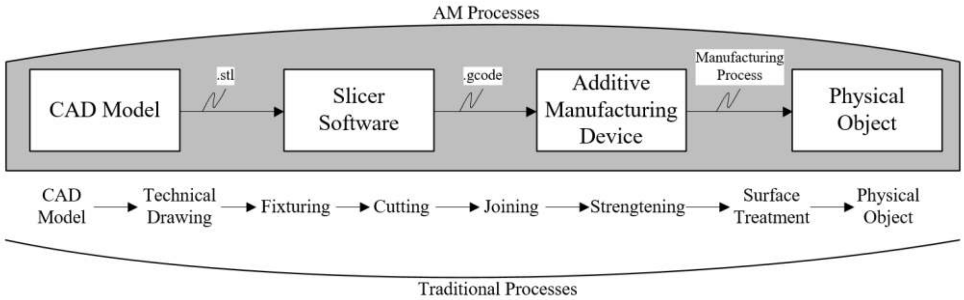

Figure 1.1. Main steps of Additive Manufacturing process (top) and conventional manufacturing steps (bottom).

The main advantage of the AM technology is that the part manufacturing can be achieved regardless of its geometric complexity. For further, the AM production offers manufacturers an exact time estimation of the processing period. This is because, the model preparations are made in digital environments and the actual manufacturing process occurs generally in a single step. This factor also benefits the elimination of many time-taking steps involved in the conventional techniques such as turning, milling or drilling. Moreover, when a small modification is required in a part desing, the time and the labour required for the process dramatically increases in the subtractive methods. In contrast, the AM provides flexibility in the production period due to the digital based process control. At the same time, manual dexterity is usually not required during the production period. To sum up, the AM is a game changer operation that enables faster, precise and energy-time-cost efficient part creation processes (Gibson et al., 2014).

The main types of AM processes were standardized under the "*ISO/ASTM standard 52900*" under seven main titles as VAT Polymerization, Material Extrusion, Powder Bed Fusiton (PBF), Material Jetting (MJ), Binder Jetting, Direct Energy Deposition (DED) and Sheet Lamination (ISO-ASTM-52900, 2015). The need to classify these technologies has arisen from the fact that the technologies used in the layering process are different in general.

In the VAT Photopolymerization, the photosensitive, thermoset resins are cured by focusing a laser beam or a cetain type of a projector light layer by layer. In Material Extrusion process, a certain type of material is extruded by a specific drive mechanism and the deposited on a deposition platform. Generally the heating operation is required in the extrusion region in order for the material to be heated, extruded and deposited respectively. However, some of viscous materials are also available for the extrusion process such as concrete, clay, biomaterials, metals and even the foods. The layering process in the PBF operation is done via a laser head directed on a container full of powder. The heat accumulation where the beam is pointed melts the powder particles. In this way, the particles are held together when the cooling finishes. This method is mostly used for producing the metals parts by the helpings of a polymeric binder agent. As a definition of the MJ process, the droplets are first generated using a specific ejection mechanism, then deposited on a platform. The conventional 2D inkjet printers those have a similar operating principle, can be said as the ancestors of the MJ method. The polymer based liquid or liquefied materials are generally adopted for this type of layering processes. However, there are lots of studies on metal droplet generation-deposition technqiues which makes the MJ method as a candidate to be an official member of AM family. Having the similar principle to the MJ, the bonding agent made of polymers is deposited on a powder bed in the Binder Jetting process. This method can be basically assumed as a combination of MJ and PBF. The desired parts made of materials such as sand, glass, metals etc. can be manufactured additively via binder jetting. In DED processes, the high powered energy source is directed on a continuously fed metal material. The form of the material can be either powder or a wire. The material fed is simultaneously melted on the deposition point. The layering process occurs in this way. Lastly, the materials in form of sheet are cut by a specifically followed path. When the tracing of a desired contour is finished, the next sheet is fed into the same area. The layers are then fused and etched together and the layering process is finalized. Many types of materials can be employed in this methods such as, paper, metals and various plastics (ISO-ASTM-52900, 2015; Molitch, 2018)

Not limited to the given AM methods, there are several additional techniques made of a combination or a derivation on these methods. However, in order to produce parts with AM, the process parameters must be configured correctly, as a common point of all methods. The expectations from the parts' property are directly related to the operational parameters which are focused in numerous research and investigation activities so far.

Although the devices used in AM operations differ in terms of the adopted layering technology, there are some common processing steps and considerations for all related operations. In the first place, a suitable Design for Additive Manufacturing (DfAM) process is required (Gausemeier, 2011). Only in this way, the production process can be carried out in accordance with the model design to be produced. Afterwards, the CAD model must be sliced using a special slicer software and made ready for production step. This stage is the most important stage in AM processes. Because the most critical process outputs such as the strength of the part, surface quality, production time and material consumption are determined at this stage. That is, the layer thickness of the part, its placement on the deposition platform, its orientation, how much material will be consumed per unit time, the deposition morphology, the density, the processing temperature, atmospheric conditioning if necessary, and many more parameters are determined in this step. Another important factor is that a device and component setup capable of meeting the parameters is required. The selection of the device specific to the expectation from the product is of critical importance as it is responsible for a large amount of the initial cost.

In this thesis, detailed research and experimental studies on AM methods, process parameters and the devices to implement them are presented. In the first place, the FFF method, which is the most widely used technique worldwide, is investigated in detail. In addition, the effect of the determined process parameters on the strength of the printed product is examined. During the printing processes performed, observations and examinations are made on the deposition and the layering morphologies. Afterwards, the produced samples are subjected to a series of mechanical tests. As a result, it has been observed that the strength of the parts can be increased by configuring the process parameters appropriately. The most important point is that while increasing the strength, the issue of material consumption is also kept same. In this way, an environmentally friendly production process is realized by keeping material consumption under control, and at the same time, physical properties of the produced parts are improved. Production processes are carried out through a custom-made device based on open-source logic. In this way, software/hardware improvements and modifications needed in the experimental process are achieved easily.

In the second stage, the focus is directed on metal droplet generation and deposition techniques, on which considerable amout of research has been done in in literature. Because the part production via metal droplets is a candidate technique to become an official AM method due to its future promising potential. The devices developed so far based on this method have a structure consisting of inflexible and expensive components produced for a specific operation. Moreover, obtaining smooth metallic droplets can be accomplished by grueling control processes, often requiring multiple sub-applications (supportive thrust mechanisms, atmospheric control, and more). This situation is the motivation of this study; in this context, the device built for the FFF process was subjected to various modifications and evolved into a metal droplet generator. Through the developed open-source droplet generator, metal-based droplets can be created without the need for cost-increasing and difficult-to-control processes such as atmospheric control and pneumatic gas support. The thrust pressure required for the droplet ejection was provided by mechanical impacts, and the sustainability of the storage process is ensured by optimizing the hydrostatic pressure. Thanks to the droplet production and characterization, the deposition operations in the desired morphologies are able to be realized. A flexible metal droplet generator, offering the advantage of low cost operation, custom metallic material deposition, unlike existing systems is obtained.

1.1. Contribution of the Thesis

In this study, the critical process parameters examined are of those used in the FFF method and the MDJ method. The contributions of the thesis are as follows;

- A low cost and flexible 3D printer frame is modified both for its software and hardware. With this device, FFF processes are succesfully performed using polymer-based filament and the process parameters are examined in detail.

- Using results of the parameters examined in study, it is seen that "infill overlap" and some other certain parameters affecting this parameter; has observed to have vital impact. It affects the product mass at a negligible level, but has a significant effect on the part's physical strength. The examinations are performed using microscopic observations and tensile tests.

- While making the experimental planning, Taguchi-based experimental design technique is used, and the mechanical test results are evaluated with the help of statistical tools such as ANOVA. In this way, a minimum but significant combination of tests and parameters is established. As a result, it is determined that the infill overlap parameter is a critical process parameter that increases the strength without increasing the material consumption in FFF type printing processes. In this context, critical information related to this parameter, which has not been adequately researched before, is contributed to the relevant literature.

- The device used in the FFF process is later modified to form a droplet generator capable of producing metallic droplets. With the developed droplet generator, metallic droplets are obtained by using only vibrational mechanical impacts without pneumatic pressure support. It is found that the material feed rate plays a critical role when it comes to the continuity of droplet production without auxiliary gas support.

- The work is taken a step further and a unique wire feeding system has been developed and controlled. It is observed that with a suitable wire feed rate and mechanical impact input, stable and continuous metal droplets can be formed. The relationship between thrust pressure and droplet formation is related to the hydrostatic pressure created by the amount of material in the molten reservoir.

- The droplet deposition operations are carried out with different process parameters in order to obtain metallic patterns suitable for use in different areas. Based on the amount of merging or non-merging of the deposited droplets, the types of deposition morphologies were examined under different categories. As a contribution to the literature; It is experimentally proven that useful metallic patterns can be created by means of amplitude-variable mechanical vibrations, provided an appropriate material feed rate, pulse frequency, voltage, and axial travel speeds are determined. In terms of performing all these operations with a modifiable, low-cost and sustainable device infrastructure, it is promised that users will be able to create droplets with desired properties and deposite in desired morphologies in the future.

1.2. Organisation of the Thesis

The rest of this thesis is organized as follows. In the Section 2, the previous studies conducted on the process parameters adopted in the FFF and MDJ technologies are presented. In these sections, firstly the classification of all techniques, including their description, advantages and disadvantages are presented. For further, the general overview to the classified methods with their features as well as the issues related to the technical problems requiring further investigations are discussed. In addition, the available materials, manufacturing abilities and the main drawbacks for each method are compared.

In the Section 3, the material and methods and related issues are discussed. The details about the deposition methods of the devices, actual layering proceses and the parameter optimisations adopted are described. The relationship between the used methodologies in the past and the methods applied in this study is presented. The further information about the developed devices is referred by highlighting the important findings from the related studies.

In the Section 4, the details about the developed device for the experimental procedure are provided in a proper timeline. The methods used in the experimental runs, the hardware, the software and the inspection are also explained step by step. The modifications in the device during the transformations between the two AM methods due to the demands and requirements are presented.

In the Section 5, the results obtained from the experiments are evaluated using the theoretical assumptions as well as the statistical approaches. The reasons of the resultant deposition processes are then discussed.

2. PREVIOUS STUDIES

In this section, the classification of AM technologies is presented. Afterwards, the presented methods are defined separately while providing details that include comparison of these techniques. These comparisons are achieved by considering the materials, the prominent features and drawbacks in the production processes. The research directions for these methods are determined based on this approach. Subsequently, the reviews of reported studies from literature to fill these deficiencies are presented in detail.

2.1. The Types of AM Technologies

***VAT Photopolymerization*:** In this process, photosensitive resins are solidified by curing by means of UV light directed at certain coordinates. The resins are stored in a chamber that can move up or down with a certain precision for the layering process. The time-dependent location information of the points to be cured on digital platforms is transferred to the device. The UV source is directed to the desired point according to the position information and the curing process is performed. Layering is continued until the physical model is complete. The VAT photopolymerization process can be examined under several different categories that are similar in principle. The most widely used among these methods is the Stereolithography (SLA) technique. In SLA technique, the UV source, in the form of a single beam, is directed on the resin to follow the desired contour. In this way, the area where the beam focused is cured and the layer is completed (Figure 2.1).

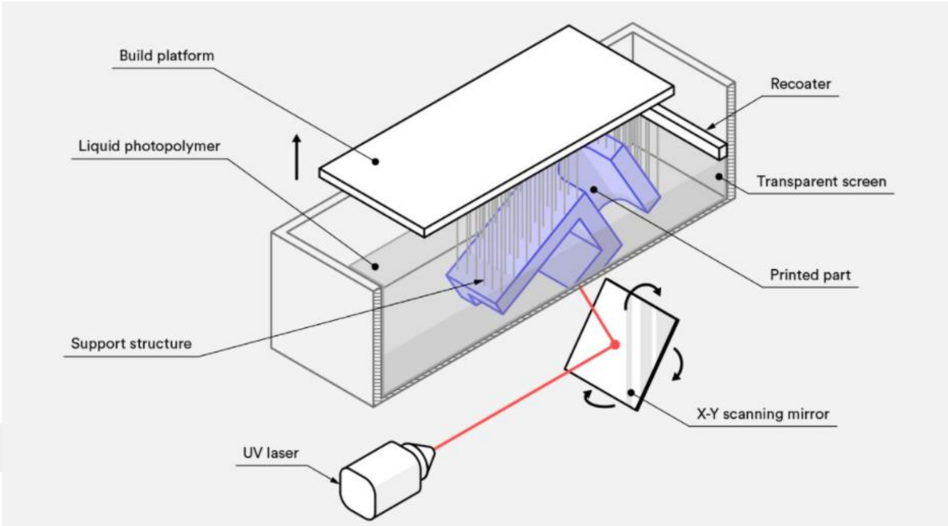

Figure 2.1. A representative view of SLA methodology (Website, 2021a)

The Direct Light Processing (DLP) method, is similar in principle to SLA in terms of the process of curing the resin. But this time, instead of a movable light source, the UV source is provided via a projector screen consisting of digital pixels or LEDs that can cure the entire layer at once. However, in this curing process it takes place the form of square pixels. This results in the final resolution being lower than the SLA. This method is considered to be the ancestor of the AM technology, as it is the first example of the layered manufacturing technique (Molitch, 2018).

The VAT photopolymerization process provides high part accuracy and better surface finish compared to the other AM techniques. These systems are advantageous in that they can be used with a variety of light sources and can be modified relatively easily. However, it requires photosensitive materials with complex chemical structures such as acrylates are required to be used leading to high processing costs. It has been also reported that the strength of parts produced with these materials is lower than that of the other AM methods. For these reasons, the use of this method amongst others is relatively limited (Gibson et al., 2010a).

***Material Extrusion*:** This method is based on the logic of layering the material along the appropriate pathways, with a certain extrusion mechanism. This technology is commonly called Fused Filament Fabrication (FFF). As a working principle, a filament made of thermoplastic material is driven into the heated zone with by means of a geared mechanism. Then, the heated filament softens and it is forced to flow towards a deposition surface through an orifice (nozzle). This way, the material is deposited by tracing a certain pathway, in form of lines on the surface. The deposition operation contiues line by line, then layer upon layer, until the part geometry is completed (Figure 2.2). This method can also be found in the literature under the name of Fused Deposition Modeling (FDM), patented by Stratasys Corporation (Vyavahare et al., 2020).

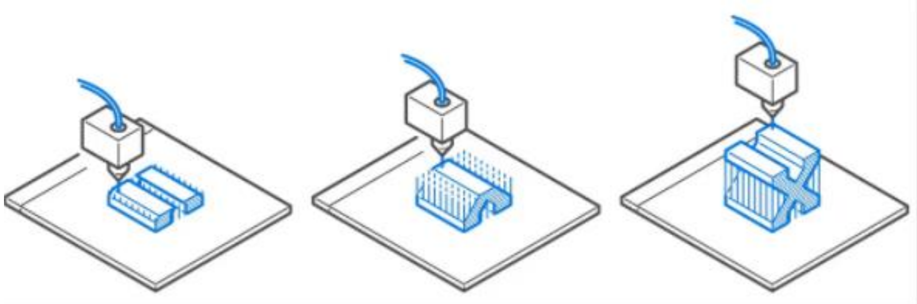

Figure 2.2. The representative image of Fused Filament Fabrication (FFF) operation (Website, 2021b).

The choice of materials that can be used in this method is quite wide. Examples of these are Polylactic Acid (PLA), Acrylonitrile Butadiene Styrene (ABS), Polycarbonates (PCs), Polyether Ether Ketone (PEEK), Nylon, High-impact Polystyrene (HIPS), Polyetherimide (PEI), Thermoplastic Polyurethane (TPU), Bio-composite filaments and other composite material filaments (Website, 2021c,d,e). However, it is reported that the PLA is the most preferred material due to the fact that it is biodegradable and more cost-competitive compared to others (Sin et al., 2012).

The FFF technique does not require hard-to-control equipments such as high-power laser heads for heating/curing purposes. In addition, since the initial costs of FFF-based systems are relatively affordable, their annual sales continue to increase exponentially (Huang et al., 2013, Rayna et al., 2016). Currently, wide ranges of applications are available for both the professional and the individual use; such as rapid tooling, functional part manufacturing, architectural modelling and household items production (Short et al., 2015; Gibson et al., 2010b).

On the other hand, in order to produce qualified parts with this method, many process parameters must be configured in a harmony. In addition, part production with FFF is relatively slower than other method and laborious post-processing efforts are often required due to the rough surface finish of the manufactured part. Moreover, the issue of increasing the strength of manufactured parts through parameter optimizations is still up to date (Molitch, 2018a).

Powder Bed Fusion**:** The Powder Bed Fusion (PBF) technology is one of the firstly commercialized AM operations. Although this method was primarily emerged for the purpose of processing polymer materials, the material options are expanded today. That is, the ceramics, composites and metal alloys become possible to be processed in PBF operations. The operational principle relies on melting a powdered material by focusing a high-power laser beam along the desired pathways (Figure 2.3). The focus route as well as the layering data is received from the G-Codes generated by slicer software that of a common AM processes. Differently, the powdered material is readily being placed in a suitable powder container before the melting process in contrast to the material extrusion based AM operations (Gibson et al., 2010c).

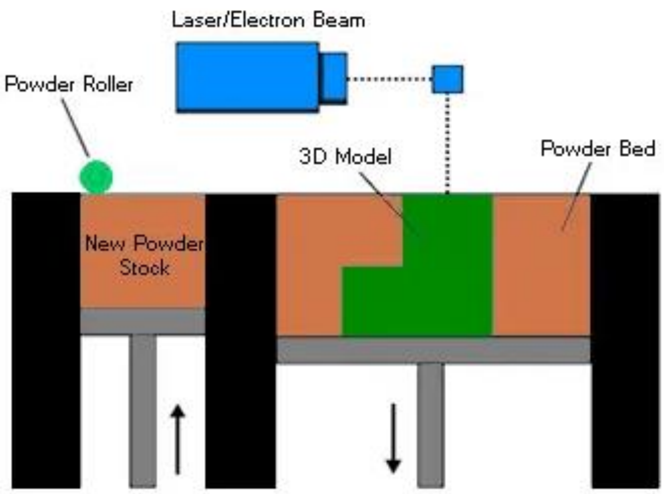

Figure 2.3. A schematical shown of PBF technique (Website, 2021f).

In the PBF process, the laser beam is directed on to the powder which may consist of multiple material types. Today, mainly metal-based powder materials are started to be used effectively in this method. In metal processing based PBF operations, the powder contains nearly %60 percent of metallic particles while the polymeric grains occupy the rest. The PBF process involving both polymer and metal powder at the same time is called as Selective Laser Sintering (SLS) (Badrinarayan and Barlow, 1992). In SLS, in the focus point of the laser beam, the heat accumulation is generated and the polymer portion of the powder is melted. By doing this, the metallic grains are binded by polymeric melt then are held together. After one layer is completed, a new powder layer is spread by a special-made cylindric bar, commonly called as “sweeper”. Owing to the high-quality surface finish of the bar, the powders are distributed homogeneously. This way, the layering process is achieved. On the other hand, the requirement of the specific components such as sweeper, laser head, powder container and the axial motion system cause the investment costs to increase. Besides, the final part manufactured by SLS requires post-processing to make the part functional. This is because, the product do not present a metallic part properties unless the metallic coalescence is provided via an additional process such as sintering. Even after the sintering process, the part density becomes low (around 60% depending to the base powder content) due to the porous structure. Here, the porosity causes inevitable strength reduction as well as the poor surface finish in the end-product (Murr and Johnson, 2017; Yamaguchi et al., 2000).

There is another PBF method that allows producing metallic parts with a high density, called as “Selective Laser Melting (SLM)” or “Direct Metal Laser Sintering (DMLS)”. The operation basics rely on the similar concept with SLS. However the pure metals or alloys are directly melted trought the laser beam instead of binding them with a polimeric material. As the process requires higher heat input to melt the metal, the power of laser beam should be higher than on SLS. The surrounding ambient also needs to be controlled strictly on behalf of both the work safety and preventing the chemical interactions on the base metal. With the SLM method, the parts having higher strenght can be manufactured with wider material options due to the higher melting capacity (Yadroidsev et al., 2009). On the other hand, the need of the high setup investment and the experienced operator requirement for a safe and consistent production operation is the main drawbacks of the SLM method (Yamaguchi et al., 2000). These factors limit this methodology to be used in routine engineering applications such as prototyping, rapid-tooling or in-place repairments.

Using the powder bed technology, the parts having a higher accuracy level and higher complexity in shape can be produced using an Electron Beam Melting (EBM) approach. It was first commercialized by *Arcam AB*, Sweden, in 2001 (Website, 2021g). In the EBM process, the high-power electron beam is employed to initiate the fusion between the metallic particles. This nanoscale fusion process allows scanning a very thin layer of metal powders result in high resolution in the end-product. Similar to the SLM, the EBM operation requires advanced control engineering applications as well as the extreme physical conditions of the manufacturing areas.

***Material Jetting*:** Being a part of an AM technology, the Material Jetting (MJ) is an emerging technique that allows a wide range of manufacturing options. The MJ may influence the future of manufacturing industry with its promising features such as high density, high strength, reduced costs, shorter leading times and eco-friend production (Campbell and Weiss, 2007). In this method, the deposition process is achieved by ejecting the consecutive droplets in a controlled manner. That is, the liquid (or liquefied) base material is first collected in a suitable reservoir (container) then forced towards the orifice region using a specific mechanism generating a thrust pressure. By applying the intermittent impacts repeatedly, the liquid material is transformed into the droplet form and evacuated towards the deposition substrate. The droplets are then collected at the certain coordinates predefined by slicer software (Jiao et al., 2018). Depending on the demand, the droplets can be deposited as both single horizontal layer and multiple layers vertically. In horizontal deposition, a layer is created by discrete or combined droplet arrays. When the deposition occurs layer upon layer the 3-dimensional (3D) objects are manufactured (Figure 2.4).

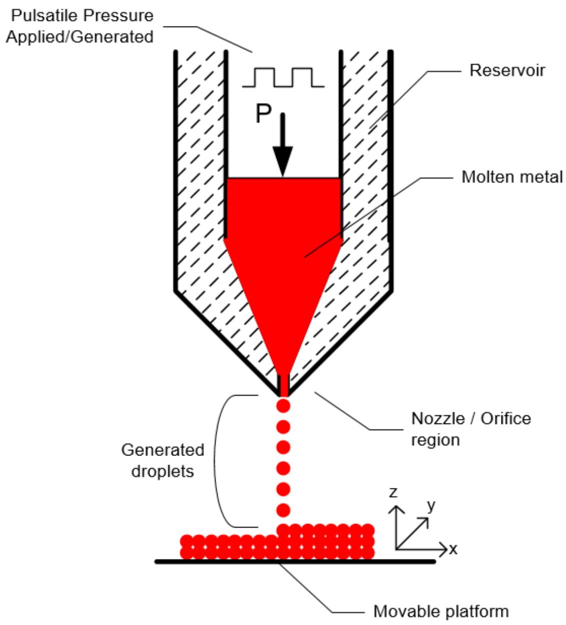

Figure 2.4. The conceptual image of a material jetting operation

The principle of droplet generation is derived from conventional 2D ink-jet printers used for printing the ink on a paper. Parallel to the developments in the manufacturing industry, inkjet printers have begun to be modified to eject various materials such as photopolymers, biological compounds, ceramics, composites even metals. Due to its wide choice of materials and ease of use, the MJ process is named as one of the promising methodologies for AM techniques (Wijhoff, 2010). The commercial version of a droplet generator is first developed by IBM Corporation using the term *Jetting* in 1972 (Northrup, 1972) and continued with the researches on the process stabilisation by Bogy and Talke, (1984), then the patented device proposed by Hewlett-Packard company using the term *Inkjet Printing* (Vaught et al., 1984) and followed by MicroFab company under the name of “Microdispensing Technology” (Hayes et al., 1999).

Meanwhile, with the developments in control techniques, it is also become possible to jet the metal materials (Wang et al., 2014). Since the materials can be deposited directly with this method, the number of studies and the popularity of the subject are increasing. Although the method of direct metal jetting has not been officially included in the AM classification yet, the usable objects have begun to be produced with this method. Some examples of the products obtained by the metal droplet deposition method are as follows (Figure 2.5);

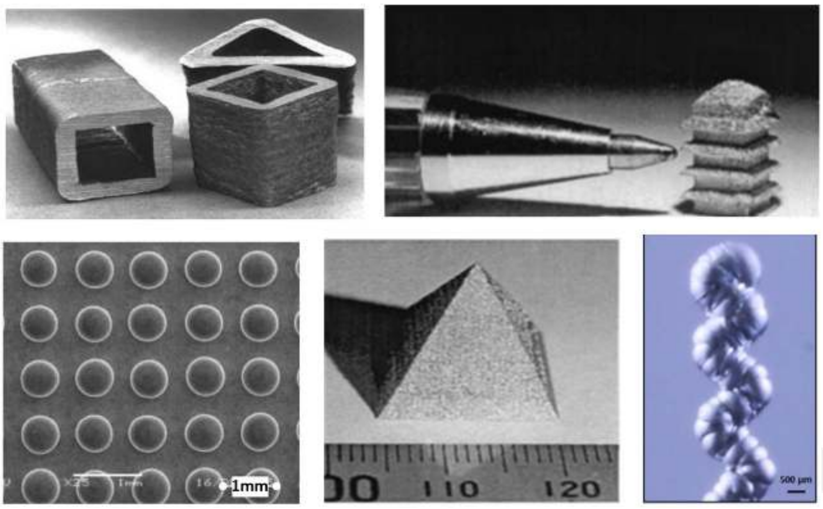

Figure 2.5. The various examples of the droplet based products (Yamaguchi et al., 2000; Zhang et al., 2017; Yokoyama et al., 2009)

The use of Metal Droplet Jetting (MDJ) operation serves many critical areas. With this method, very small metallic parts can be obtained by depositing them directly on the surface at a high resolution. The possibility of producing complex and conductive metallic parts are used or candidates for use in many important fields such as aviation and aerospace (Wohlers, 2013). Especially, for the fields of Micro-Electro-Mechanical-Systems (MEMs) and the electronics industry (Wang et al., 2014; Luo et al., 2012), MDJ is a promising method in metal-based part manufacturing. The Metal droplet generation and deposition processes offers many advantages in production flexibility. Therefore, this method is investigated with more details regarding its techniques and the application areas in the next sections of the thesis.

Binder Jetting**:** In the Binder Jetting (BJ) method, the polymer based droplets are generally used as binder agents. This is to say, the polymer based resins those are photosensitive or thermally curable are jetted onto the container filled with metallic powder. In these processes, the binder agents are used to hold base material particles (metal, ceramic etc.) together in a specific geometry. While the layer pattern is being scanned by the binder droplets, curing or heating is performed simultaneously. After the all layers completed, the solid part is removed from the powder container in order to be sintered (Meteyer et al., 2014). As shown in the Figure 2.6, the stucture of the BJ system can be related to the PBF system basics. However, in contrast to PBF, the agent droplets are ejected on the powdered base material container rather that directing a light source.

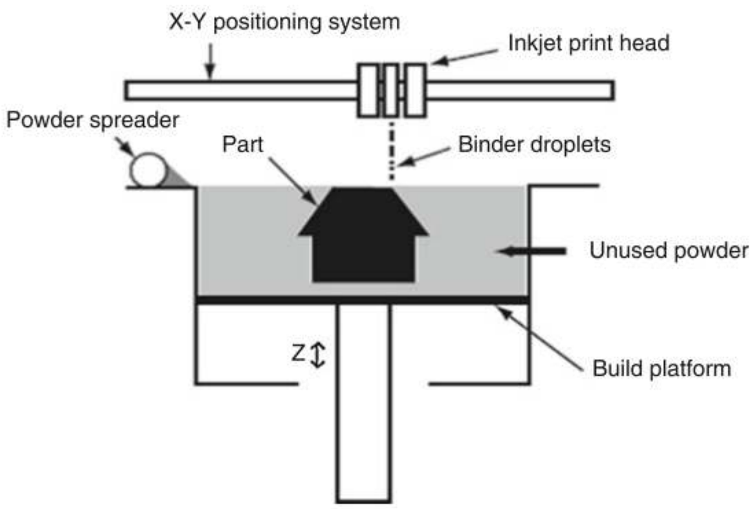

Figure 2.6. Schematical view of BJ process (Gibson et al., 2010c).

In fact the BJ process has a similar advantage to the PBF process. However in BJ, the material used can be adjusted to the exact amount that is needed. Furthermore, the number of nozzles can be increased that operates at the same conditions with the original one. The use of Multiple nozzles increase the deposition rate and thus the layering speed, resulting in shorter processing times. From the perspective of energy consumption, the BJ can be advantageous by eliminating the need of high-power laser source which is required in PBF during the whole process (Sachs et al., 1992).

Direct Energy Deposition**:** The parts can be manufactured with the Direct Energy Deposition (DED) method with a high precision additively. Althought the method can be applied to process polymers, ceramics or composites; it is mostly adopted for metal processing due to the working ability with high melting point metals such as Titanium, Aluminum and Chromium (Liu and Dupont, 2003). The one of the first commercialization of the DED device has been presented under the name of Laser Engineered Net Shaping (LENS) by "*Optomec*" (Molitch, 2016). The way DED machines work involves the continuous feeding of material onto a given substrate instead of a ready-made powder bed. However, the form of the fed material can be powder or wire as illustrated in Figure 2.7.

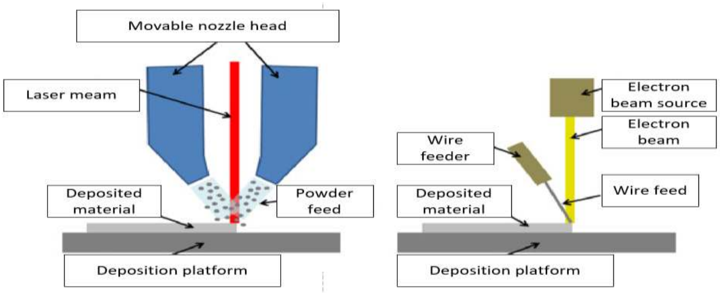

Figure 2.7. The schematical view of the Powder-based DED operation (left), wire-based DED operation (right) (Stress et al., 2021).

The continuous feeding of the material provides high deposition rates as in DED operations. Furthermore, the amount of feed can be configured precisely according to need of material amount. This factor prevents wasting material and the energy in the production. The DED processes can be done in various working areas which result in high mobility in a device (Beuth and Klingbeil, 2001).

Nowadays, such that even the conventional arc-welding machines have started to be utilized as a DED operation effectively (Astarita et al., 2021; Koli et al., 2021). In the DED method, high-power laser source can be focused to fuse a feedstock powder material. When using an electron beam source as the laser source, the focal point can be significantly reduced. In this way, high resolution layers can be obtained. This methodology is named as Electron Beam Additive Manufacturing (EBAM).

In DED processes, high-budget components such as high-power laser systems are required for part manufacturing. Also, the production processes that can take days have to be carried out in strictly conditioned environments. Moreover, all operations must be conducted under the supervision of experienced operators. Due to all these situations, DED procedures both require high costs and are far from being practical (Yamaguchi et al., 2000; Lu et al., 2009; Stress et al., 2021; Bourell et al., 2009).

***Sheet Lamination*:** This AM technique is the most primitive layered manufacturing techique. Principally, a roll of a sheet is fed towards a building platform, the feed is cut and then the laser cutting operation is done in contours with appropriate coordinates. The cut part is collected on a vertically moving platform. The process continues until all layers are completed. Besides the laser source, CNC milling, water-jet cutting can be preferred to cut the sheet to form layers instead. This low cost technology allows very large format parts while sacrificing from the complexity of the geometry (Website, 2021h). The representation image is given in the Figure 2.8.

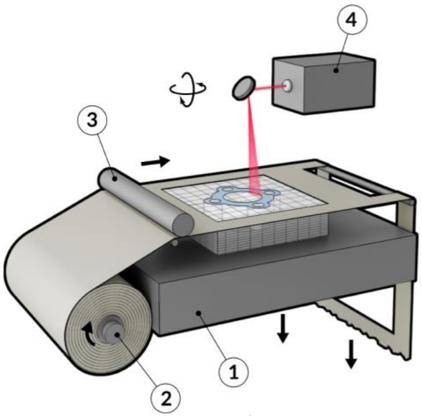

Figure 2.8. The representative image of Sheet Lamination technique. 1-Built platform 2-Feeder roller 3-Lamination roller 4-Laser cutter (Website, 2021i)

In the following section, the all AM techniques with their advantages, disadvantages and the gaps belonging to relevant method are discussed.

2.2. An Overview to the AM Processes

In this section, a comparison between these methods are made and details such as the types of materials, the application areas, the properties of the products, production costs, times and process parameters are presented. First of all, the materials types that can be used in the relevant AM method are compiled in the Table 2.1 as follows;

Table 2.1. Types of AM according to the materials used (MIT, 2021; ISO-17292; 2015).

AM Types	Sub-categories	Material form	Thermoplastics	Photopolymers	Metals	Ceramics	Composites	Bio-materials	Multimaterial
VP	SLA, DLP	*Liquid*		●	○	○	●	●	
ME	FFF	*Filament*	●	●	●	○	●	●	○
PBF	SLS, SLM	*Powder*	●	●○	●○	●	●		
MJ	MDJ, BJ, PolyJet	*Liquid Powder Wire*	●	●	●○	○	○	●	●
DED	LENS, EBAM, UAM	*Powder Wire*			●		○		●
SL	LOM UAM	*Sheet*	●		●		●		○

● : Direct process, ○ : Indirect process

According to the table, the range of materials that can be used in AM is quite wide. Moreover, it can be observed that the most diverse material processing capacity is in the FFF and MJ processes. In addition to the material option, direct material deposition feature is also available in both methods. With this feature, the part manufacturing operations can be carried out efficiently as mentioned in the previous sections. It is also the additional processing steps and high-budget component requirement which are involved in PBF and DED are eliminated.

Therefore, it becomes the subject of many research and development efforts according to the literature. In the next sections, the issues of configurating the process parameters, deposition conditions and production efficiency are examined from many different perspectives. In the Table 2.2, the outputs obtained during and after the production process are summarized. While tabulating, the classifications made by ASTM are taken as basis and The MDJ method is added into the MJ group as a subcategory. It should be noted here that the MDJ method has not yet been defined as an officia AM operation according to ASTM. However, due to its production potential, it has recently been referred to as an AM method and it is a strong candidate to become an official member in the near future as reported by Murr et al., (2017). In addition, some methods such as SLS and SLM belonging to the same family are added to the table under separate headings since they are used frequently in production.

Table 2.2. The general comparison of AM operations with their general features and drawbacks (Abdulhameed et al., 2019; ASTM, 2013; Gao et al., 2015)

	LOM	***DED***	***LENS***	***EBM***	***(DMLS)***	***SLS***	***(DLP)***	***(MJ)***	***FFF***
Surface Finish	Low	High	Very high	Very high	Medium	Low	High	Low	Medium
Support Requirement	No-req	Rare Often	No-needed Rare	No-needed Rare	No needed	No needed	Rare	Often	Often
Operating Temperature	Low-High	High	Very high	Very high	High	Low-Medium	Low	Low-High	Low
Energy Needed	Low-High	High	Very high	High	High	Medium-High	Low	Low	Low
Production Feature	Big scale Strength	Tooling, Prototyp. Nanoscale	Nano-scale High complex. High Strength	Nano-scale lay. High complex. High Strength	Tooling, Prototyping Nano-scale	Prototyping Microscale layering	High complex. Microscale	Conductivity Microscale deposition	Strength Prototyp
Multiple Material.	Good	Fair	Bad	Bad	Bad	Good	Bad	Good	Fair
Final Resolution	Low	High	Very high	Very high	High	High	High	Low	Medium
Prod. Rate	Low	Low	Low	Low	Low	Low	Low	Fair	Low
Production Drawbacks	Low resolution	Post-process Labour Low t. Res	Mass. prod. Post-process Labour	Cost prod. Post-process Labour	Post-process Labour High warpage	Porous Low Strength	Low Str. UV sens. Low ther.	Porous Low Strength	Brittle Low t.res
Invest. Cost	Low	High	Very high	Very high	Very high	High	Medium	Medium	Low
Maintenance and repair	Medium	High	High	High	High	High	Medium	Often	Often
Effort	Low	High	Very High	Very High	High	High	Low	High	Medium

Up to this point, standard definitions of AM processes, what materials they can be applied to, and what characteristics product outputs usually exhibit, are explored. When the engineering concerns shown in the table (energy consumption, product durability, operation cost, fields of activity, operational difficulties, etc.) are evaluated as a whole, it appears that more in-depth investigations should be conducted in FFF and MDJ processes. Specifically, FFF operations are recognized as the most frequently used AM technique worldwide compared to all other methods in terms of ease-of-use, cost and product facilities. For this reason, it is considered that even the smallest improvement in this process will have a global impact. In this context, minimizing the waste of material and increasing the strength of the produced parts also become a necessity.

According to the table, it is also observed that some remarkable features are available in the MDJ method. That is, the metallic structures can be produced with a direct material deposition technique in more practical way in the MDJ systems compared to other methods. So far, the droplet-based production techniques have been developed up to a certain point under the MJ category. However, there are still some problems to be solved in *metal-based* droplet deposition processes. The process dynamics must be well understood in order to first generate droplets properly and then deposite them suitably. Because there are many process parameters involved that need to be controlled at the same time. In order to achieve successful operation, detailed investigations should be carried out both on the structure of the device itself and on the process parameters. When the current studies performed in the literature and the devices used are examined, it is also observed that the device structures are still not flexible enough. Moreover, the need for more detailed configuration of the process parameters arises so that metal materials can be properly processed. These issues limit the production of metal parts with MDJ. By solving these problems, the accessibility of this method can be increased and its use can be facilitated. If these devices can be developed in the mentioned direction, they will be a solid candidate to be used as a practical AM processes.

Therefore, both the methods of FFF and MDJ are investigated in detail within the scope of this study. The systematic procedure is adopted for the solution of the above-mentioned problems. As a starting point, the process parameters for both methods are examined and it is aimed to eliminate the deficiencies in these operations. In the following sections, the gaps in these methods and the performed studies to eliminate them are discussed in more detail.

2.3. The Current Situation, Feature and Gaps of FFF Processes

When the studies done so far are examined, it is noticed that the AM method, which has the highest number of users and has the highest accessibility in terms of cost and installation, is the FFF method. That is, the annual sales of these devices are increasing and it is predicted that the amount of increase will also increase in the coming years (Huang et al., 2013; Rayna and Striukova, 2016). The main reason for the increase is that FFF-type processes also appeal to individual users besides the industrial use. In this context, rapid tooling, functional part manufacturing, architectural modeling, and even the production of household items can be given as examples of individual uses (Gibson et al., 2010; Short and Daniel, 2015). Another reason for the frequent use of FFF processes is that such devices are easier to operate than powder and resin-based AM processes. This is because there is no need for processes such as curing with laser heads that consume excessive power (Wendel et al., 2008). Another important research topic is to increase the strength of the materials produced by this method. Because the strength of the parts produced with FFF is generally medium-low. An example of this is the case where the strength of the parts produced by injection molding using the same material is higher than the parts produced with FFF (Ahn et al., 2009; D'Amico et al., 2017; Kim et al., 2016; Vyahare et al., 2019). The main reason for obtaining low strength parts in FFF is that there are dozens of important parameters that need to be configured in a harmony. There are researches on the production of parts with this method, to increase the strength by configuring the process parameters suitably. However, there is no standard configuration methodology that can be applied to all parts. In other words, in FFF, an appropriate parametric combination should be determined according to the expectations (strength, surface roughness, printing time, energy saving, functionality) from the part to be produced, which is often not possible to meet all expectations with the same process. For this reason, only one or few product features are generally taken into account during the parameter definition. As a result, concessions have to be made on other product/production options other than the desired features. Commonly compromised features include high material consumption, prolonged printing time, high surface roughness, or lack of functionality. In particular, the issue of material consumption has become a prominent issue in new generation production processes. That is, the issue of using only the necessary amount of material for the part production was also discussed in the annual report, published by Wohler Associates (2018). In this report, besides the energy consumption, the importance of the studies carried out for AM operations to gain an eco-friend quality has been emphasized. Both the issues of controlling the material usage and increasing the part strength in the FFF process needs to be further investigated together. This is because; the studies available in the literature are mainly focused either only on increasing material strength or only on material consumption. In addition, the number of studies examining both issues together is also limited. In order to fill the mentioned gap found in the literature there is a need for systematic optimization of the process parameters (Ivanova et al., 2013).

2.4. Process Parameters for FFF Operations

There are many parameters affecting the final condition of the part manufactured with the FFF devices. The parameter determination is done in the slicing step using Slicer software. Althought there are both open-source (Cura, Slic3r, Repetier etc,) and commercial (Simplify3D, Autodesk Fusion 360, NetFabb) software available, the working principles are mostly similar with a slight differences. The most important parameters which are generally adjusted in the slicing step are layer thickness, build orientation, extrusion temperature, built plate temperature, infill density, infill pattern, infill orientation, line width, print speed and flow rate (Dey and Yodo, 2019).

- *Layer height*: The thickness of each layer deposited horizontally on the built plate. It is generally responsible from the final resolution, print time and the surface finish in a part. When the layer height increases; the print time reduces while the resolution decreases (Figure 2.9.a to b.)
- *Build orientation*: The angular position of the part along the axes of X, Y and Z in the build chamber.
- *Extrusion temperature*: The temperature where the heating process occurs. In this region, the filament is fused and squeezed out of the nozzle to the deposition platform. The level of temperature is determined according to the filament material (e.g. 200-230 ^{o}C for PLA, 240-250 ^{o}C for ABS).
- *Built plate temperature*: The temperature on where the extruded material is deposited. Although the most of FFF device have this feature, this is not a must for all types of materials. However this feature is generally required in order not to cause the deformation in the deposited part due to the sharp temperature transition. This parameter can be found in the literature under the names of hot bet, heated bed, built platform, deposition plate or heated platform.
- *Infill pattern*: It is the geometric model of the infill structure. It can be in many various forms such as grid, cubic, octet, concentric etc. The shape of pattern is generally takes its importance when a specific feature from the part is desired such as lightness, high-speed production, compressing or tensile strength etc. (Figure 2.9.c)

- *Infill density*: The density of the inner structure of the part. In FFF processes, the outer wall (shell) of the part is generated in full density. However the most of job do not require the 100% density in the inner region where the high strength in part is not critical. This parameter is mainly responsible from the material consumption, part's mass, the printing duration as well as the strength. The term "infill" can be called as a "raster" in some of sources and software (Figure 2.9.d).
- *Infill orientation*: The angular direction of the deposited infill lines along the horizontal axes (X or Y)
- *Line width*: The width of the deposited bead on the platform. The nozzle diameter is mainly responsible from the width of line extruded.
- *Print speed*: The speed of the translational movements of the extruder head along the axis. Although this parameter is related to the layering speed in the Z axis, it is generally referred as the horizontal speed of the along X and Y axes.
- *Air gap*: It is determined by the distance between the infill lines. It can be determined by both the percentage of infill density and entering a specific value manually for the gap distance.
- *Flow rate*: The amount of material extruded in a unit time. In most of FFF device, this value is set to be 100% as default. However in some devices, the deposited line width may not match to the value defined in the slicer software due to the faulty calibration of the extruder gears or the excessive friction in a certain points along the feed route. In this case, this parameter is changed until the deposited line width exactly matches to the digital value. It is can be found under the name of Extrusion Multiplier in some Slicer software. The 100% percentage in Flow Rate is equal to 1.0x of the Extrusion Multiplier parameter.

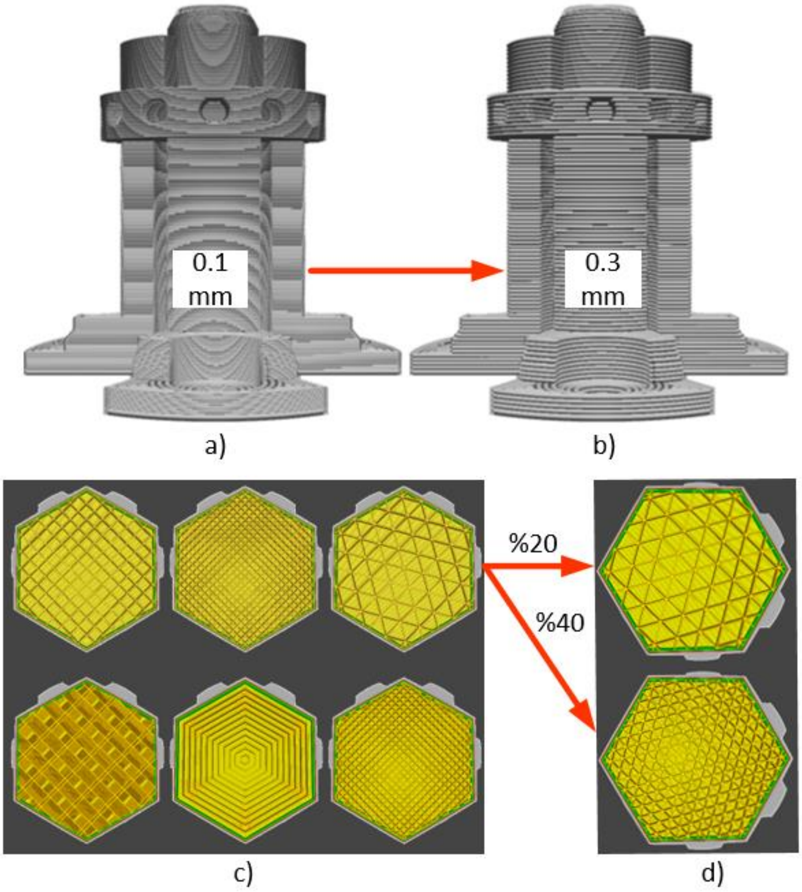

Figure 2.9. a. 0.1 mm layer height, b. 0.3 mm layer height, c. Various infill models, d. Various infill densities (Website, 2022a).

However, the print settings are not limited to the given ones. In the next sections, other print parameters are also introduced when needed. In the comprehensive study of Sood et al. (2010), the mechanical properties of the produced parts via FFF were investigated by focusing the parameters of layer thickness, orientation, raster angle, raster width and air gap. The effects of these parameters were configured in different combinations to see their effects over the tensile, flexural and impact strength of the printed samples. The findings indicated that when the number of layers increases, the strength of the part also increases.

However, the heat accumulation also increases with the increase in the amount of the coalescence between the layers, which result in an increment in a layering profile, as reported. The similar results were found for the specimens to be valid those have a high density of infills and sharp turns in the route. The findings showed that the amount of bonding in the deposited lines both horizontally and vertically determine the final strength of the part. That is, the heat dissipation must be maintained in a harmony with the amount of coalescence between the lines. Furthermore, the selected parameters play an important role in both thermal interaction and bonding characteristic those determine the mechanical property of a part. The study evaluating the similar parameters was conducted by Liu et al., (2016) over the mechanical properties of the fabricated parts. This time the different statistical approach was adopted during the evaluation of the mechanical test results. Although the similar findings were obtained, the optimum parameter combination for the acceptable level of strength in the printed samples was also revealed.

In a study, the tensile strength, rupture profile and the impact resistance of the parts produced with FFF method were investigated taken into account the five different layer orientation (Es-Said et al., 2000). As shown in the Figure 2.10, the lines were deposited with different angles along the horizontal plane. In the left microscopic image, the lines were deposited in -45^{o} and +45^{o} degrees in turn, until the last layer, while only the -45 ^{o} degree was adopted in the whole process in the right image.

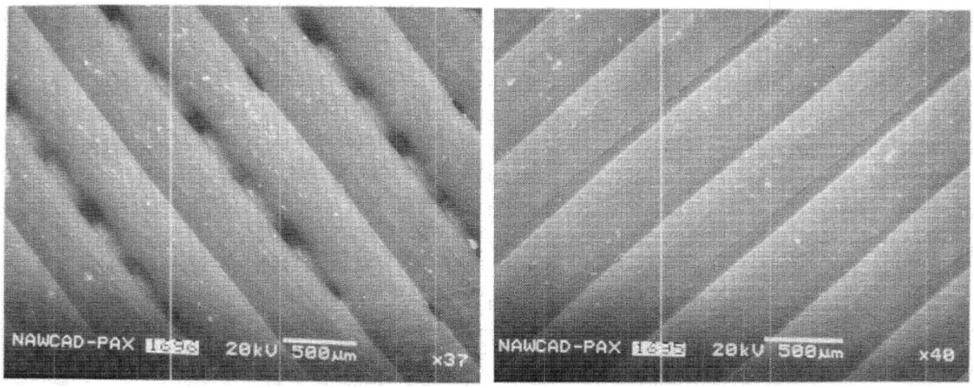

Figure 2.10. The layer orientation having the angles of ±45° (left) and 45° (Es-Said et al., 2000).

In the crosswise deposition (±45°), the air gap formations were observed. The reason for the gap formation is that when the lines are deposited crosswise; the amount of contact with the lower layer tends to decrease gradually. It was also added that anisotropy increases as the contact cross-sectional area decreases, so sufficient and permanent bonding does not occur. It was noted that these porosities have a negative effect on the above-mentioned strength properties of the material.

The ultimate tensile strength of FFF-printed parts were examined by adjusting the parameters of layer thickness, infill orientation and the number of shell walls in the study of Lanzotti et al., (2015). According to the tensile tests and microscopic observations, it is reported that when the number of surrounding contour (shell) increases, the tensile strenght is parallelly increases. The shell and the infill structure can be clearly seen from the images in Figure 2.11.

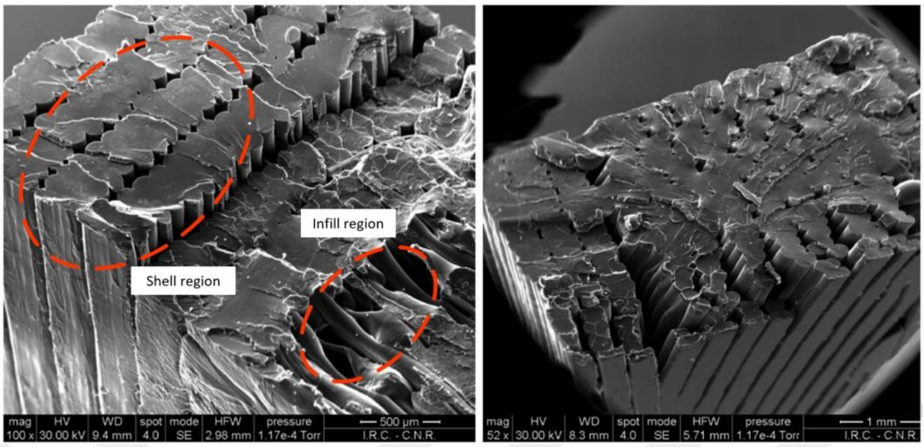

Figure 2.11. The SEM image of the rupture area in the tensile specimen (Left: ductile specimen, Right; brittle specimen). Adopted from (Lanzotti et al., 2015).

In this study, the relationship between the shell width and the part strength was attributed to the fact that the lines in the shell region are significantly more intense compared to the infill region. In other words, as the amount of bonding between the lines increased, the strength of the part increased, as stated. This phenomenon can be seen from the SEM images.

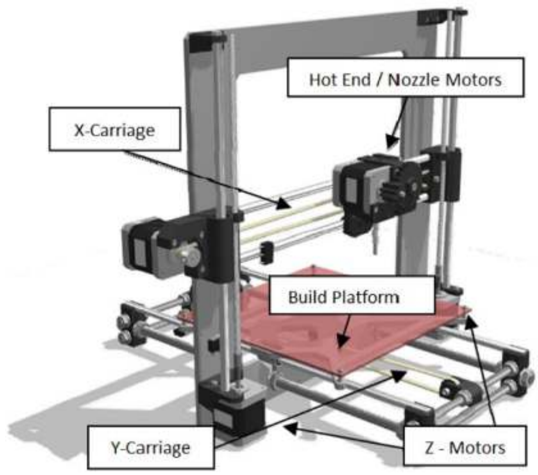

Figure 2.12. Open-source based Prusa i3, FFF-type printer (Lanzotti et al., 2015).

Another important point in this study is that all samples were produced with an open-source, Prusa i3 printer with a high quality (Figure 2.12). The fact that both academic and industrial activities can be carried out successfully through these printers once again pointed the importance of the open-source concept. Owing to the open-source concept, the use of FFF devices has become very practical. Apart from reducing device costs, open-source based devices have become self-manufacturing almost 60% of their parts. In this regard, these devices are also referred to as self-replicating rapid prototyping devices (Anzalone et al., 2013). These devices, which are generally operated with open-source microprocessors such as Arduino, have reached the capacity to produce scientific instruments with very low costs, especially in the prototyping processes (Pearce, 2012; Pearce, 2014). In this thesis study, this concept is mainly adopted in the period of establishing the device.

The flexural strength is investigated on printed parts via open-source FFF device in another study of Rajpuhorit and Dave (2018). The change in the strength due to the different combinations of the layer height, infill orientatin and the line width in part configuration is the main focus. It is observed that the layer height has the biggest effect on the flexural properties. This issue is related to the amount of bonding between the layers. That is, the smaller layer thickness results in more number of layers to accomplish the part printing. Therefore the improved bonding tends to increase the overall strength of the part. In addition, at the average line width values, it is stated that the thermal load accumulated on the deposited lines causes the part to cool more slowly. This study is important since it is emphasized that the bond strength between the lines increases due to the delay in cooling, and the increase in the strength of the part in parallel with this. It was also suggested to examine the strength characteristic by varying the shell thickness in addition to the focus parameters as a future study.

It is common practice for parts printed with FFF to use a certain number of drawn lines surrounding the outer profile of the model (Figure 2.13). This is done because the outer texture of the part can be salvaged from the messy appearance of the infill line ends. It is worth noting that the amount of physical bonding increases with increasing infill and contour lines. This also determines the shell thickness.

Figure 2.13. The different shell thickness in the same model geometry (Website, 2022b).

In this context, also by considering the recommendation in the given study, the shell thickness is included into the parameter examinations in this thesis study.

2.4.1. Bonding Chacateristic between Deposited Lines and Layers

The coalescence between the deposited lines determines the grade of the parts' functionality. This is to say, the printed part should have a sufficient strength in order to satisfy the purpose of the manufacturing processes. Therefore, the bonding conditions of the extruded lines needs to be understood well. For this purpose, Tymrak et al., (2014) were conducted an experimental study on characterizing the tensile property of the parts. The infill density of the specimens are determined as 100%. It is observed that deposited lines form a structure which more close to a solid part than a part consist of single lines. This formation is relied on the excessive heat accumulation which yields to a superior fusion between the lines and then the layers. In fact, the experiments are planned based on comparing the print quality of different FFF-type 3D printer brands, adopting the open-source concept. Overall, the results shows that fully dense parts could be functional enough to be used where tensile strength is required. Particularly, parts with infill direction parallel to the tensile load direction is reported to exhibit high strength. It was stated that the basis of this situation is related to the very strong coalescence of the lines. This issue was experimentally proven also in the studies of Rodriguez et al., (2003), and Li et al., (2002), that the spacing between the lines, and therefore the amount of bonding, has a significant effect on the tensile strength.

The issue of bond strength was evaluated from a different perspective in the study of Pierson and Chivukula (2018). In the study, instead of the bonding situation in the internal structure of a single piece that is routinely printed; the bonding phenomenon that occurs when another piece is printed on a previously printed and cooled piece was investigated (Figure 2.14). It has been experimentally demonstrated that the bonding dynamics obtained in these two different scenarios are different.

Figure 2.14. White piece: Primarily printed and cooled specimen, Red piece: Secondary specimen (Pierson and Chivukula, 2018)

At this point, in almost all the studies described so far, statements were made that as the line width grows, the bonding strength also increases. However, an opposite argument is presented in the mentioned study. In other words, the polymeric bonding phenomenon can have both positive and negative effects on the tensile strength of the part, depending on the situation. Therefore, it appears that this parameter needs to be examined in more detail. Only in this way, the effects of this parameter on the bonding characteristic and the consequent part strength can be better understood. For this reason, in this thesis study, the line width parameter is considered as one of the parameters that have an effect on the strength and is included among the parameters to be focused on.

The Ultimate Tensile Strength (UTS) of the printed specimens are increased by configuring the raster angle, contour width, raster width and raster-to-raster air gap suitably in the study of Hossain et al., (2014). Although the authors named the parameters differently, the definitions of these parameters are exactly the same with the terms mentioned earlier. The visual explanations of the mentioned parameters are as follows (Figure 2.15);

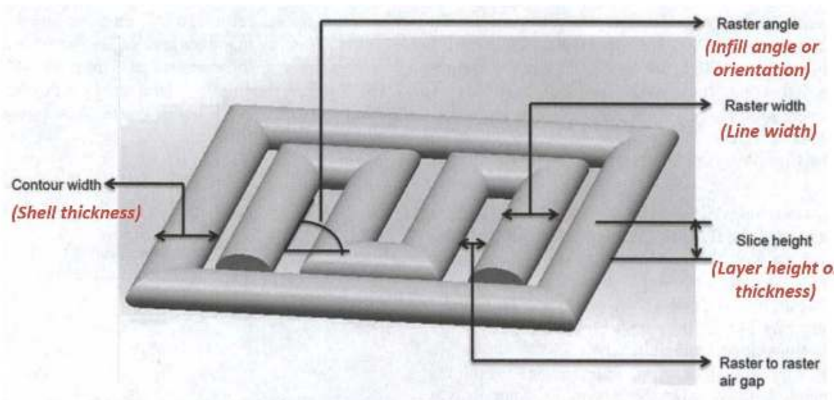

Figure 2.15. The visual definitions of oftenly used process parameters (Hossain et al., 2014)).

In the study, the smaller the raster (line) width parameter, the less air gap formation was observed on the outer surface. Accordingly, it was proposed that a higher quality finish can be obtained. Moreover, the reduction of air voids also resulted in increased UTS. Based on the results; It was commented that the less air gaps between the lines, or if possible, they are completely eliminated, the higher UTS increase can be achieved. Another conclusion that can be drawn from this study is that the regions where air gaps occur also cause different effects in terms of strength. In other words, as shown in Figure 2.16, air gaps can occur in the inner regions of the part (a, b) and near the edges.

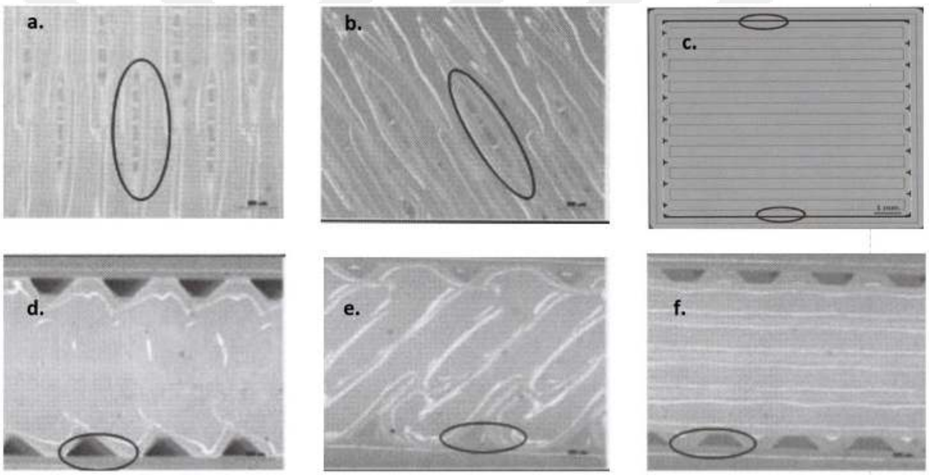

Figure 2.16. The air gaps in different location in deposited part (Hossain et al., 2014)

In fact, this is a general opinion in many studies that voids have a negative effect on strength. However, it was also stated in most of them that the case of the gaps in the inner regions or close to the edges affects the UTS and tensile strain of the material in different amounts. This study was important in that the effects of cavities formed in the part's inner and outer regions on the strength were focused in detail. On the other hand, the issue of what changes in strength will occur when the void amount is reduced to zero or even adjusted to be negative was not addressed.

In other words; the parts are obtained in the FFF process as a result of depositing two main structures on the platform. These are infill and shell structures. The areas of focus in this study are limited to the infill area and the gaps that occur inside the interior shell wall. Therefore, there is a need to examine the infill lines overlapping the shell wall (negative air gap). The definitions of the infill overlap parameter determined during the slicing phase are visually summarized in Figure 2.17.

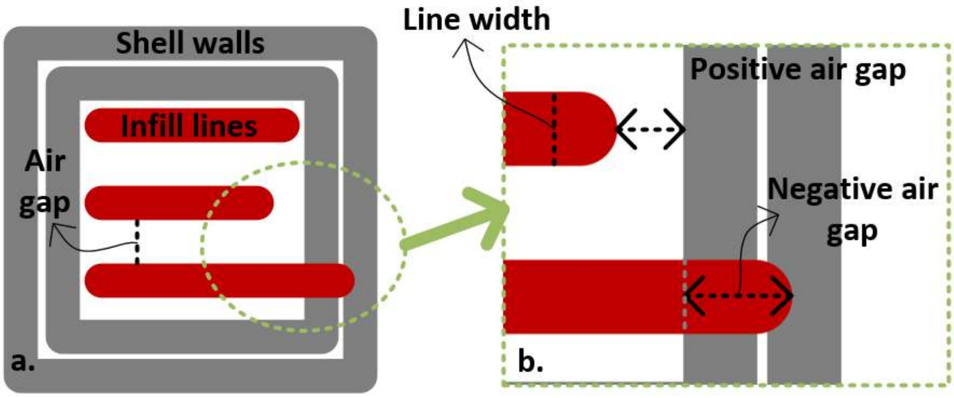

Figure 2.17. a. Shell structure and infill lines, b. Infill overlap parameter (Positive and negative air gap)

In the light of the mentioned studies, it can be interpreted that; since the infill overlap parameter determines the amount of bonding between the lines, it has a direct effect on the strength and bonding strength. In addition, this parameter is in direct interaction with the dominant parameters such as line width, shell thickness and infill density. However, there is a lack of research on this parameter in the literature. Therefore, this parameter is included in this thesis study as one of the main parameters to be examined. In the studies examined up to this point, the effects of process parameters on strength are researched and it is concluded that; the strength varies considerably as a result of different configurations of the parameters. Moreover, the relationship between parameters and strength is investigated through deposition and bonding morphologies. As observed, there is a common opinion that the amount of bonding of lines and layers with each other has a critical importance in terms of strength. From the different point of view, it is also seen that the printing devices are either open-source or adaptable to open-source. This factor indicates that the open-source concept is capable of and allows the part manufacturing for scientific purposes.

2.5. The Analogy of the Operational Factors in FFF and MJ Processes

The parameters examined in FFF processes and the developments in modifiable devices have also shed light on the solution of the problems in Material Jetting (MJ) systems using metal materials. Because, the subjects listed below are common issues in principle in both of them;

- Expulsion of a material through an orifice via certain parameter configurations,
- The fact that the extruded materials are deposited directly on the surface (digital based direct deposition),
- The direct effect of micro-level bonding (coalescence) conditions of the deposited materials and the resulting macro-deposition morphologies on the final product,

However, when the material to be processed in the MJ method is chosen as metal, deposition operations become more complicated compared to FFF. This is because, in order for metals to be deposited on a surface, they must first be collected in a suitable reservoir and then melted. Afterwards, the molten liquid must be ejected out in the form of a droplet with a suitable thrust mechanism. The devices capable of performing these operations are already available in use according to the literature. On the other hand, the costs of these devices seemed to be high. The operating and controlling such activities are also very complex engineering problems as observed. Moreover, available devices are far from flexible in their production processes. This is because, they are mainly meant to be established in order to perform only one dedicated operation. At this point, open-source systems with a modifiable structure, which are also used for FFF processes, promise a solution to the mentioned problems in MJ operations.

2.6. The Developments in the Metal Droplet Jetting Processes

The Metal Droplet Jetting (MDJ) is promising methodology in terms of direct material deposition. In the MDJ processes, metallic droplets are generated and the deposited in a certain substrate. The way of deposition is similar to the other AM methods that rely on a digital-based direct deposition steps. However, the material deposition is done via generated droplets one by one, rather than continuous lines extruded as in FFF. The droplets are first ejected from a nozzle towards a deposition area in sequential order. Then the droplets are deposited with a desired gap (positive and negative) to form a 3D object. Metallic droplet generation process enables many various applications areas such as:

- Soldering applications (Tomaszewski, 2017; Lin et al., 2006, Schuhmacher e al., 2007),
- Electronic Packaging (Gallagher, 2005; Park et al., 2006),
- Ball Grid Array (BGA) production (Chun and Hsiao, 2003; Luo and Lui, 2009; (Zhong, 2014),
- MEMs field (Wallace 1989; Luo et al., 2012),
- Aircraft industry and the aerospace engineering (Wohlers, 2013; Cooper et al., 2004; Muntz and Dixon, 1986).

Although different methods are available to create metal droplets, they have common points in their working principle. A concept design for metallic droplet production is shown in Figure 2.18 below in general terms. (Johnson et al., 2016);

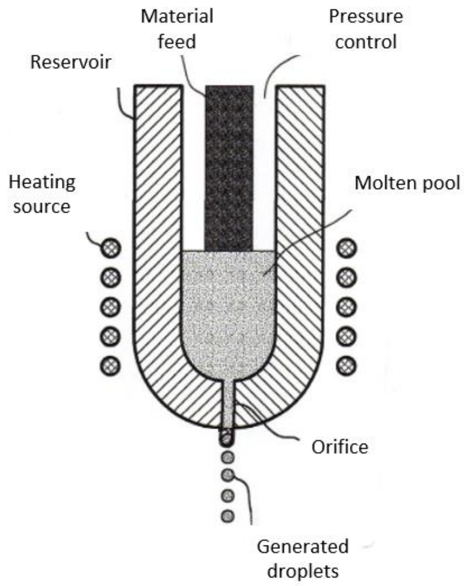

Figure 2.18. The representation of a fundamental metal droplet generator (The image is adapted from drawn patented by Johnson et al., (2016))

In the study of Priest et al., (1997), the subject of direct metal deposition based on droplet generation was investigated under the term of Solid Freeform Fabrication (SFF) process. It is stated that there are three main parameters to be able to achieve good quality metal parts. First, the sustainability of the metal jetting process depends on the purity of the molten liquid. In other words, impurities and oxidation formation in the metal that may cause nozzle clogging should be eliminated. Secondly, droplet jetting processes need to be classified as ejection process, flight period of droplet and the cooling period of landed droplet, respectively. It was also stated that each of these steps individually is critical on the deposited parts' quality. In other words, the detailed analysis of the velocity, viscosity, surface tension, density and temperature of a single drop is essential for successful printing. Additionally, the ejection properties such as voltage, frequency, the orifice diameter and the wetting characteristic of the liquid material are determinant on the deposition morphology as reported by Priest et al., (1997); Orme and Huang, (1997), Chun et al., (1997).

The jetting operation was categorized according to the ejection frequency in the given study into two groups as; Drop-on-Demand (DOD) and Continuous Jetting. The properties of the two methods are tabulated as follows in Table 2.3;

Table 2.3. The main differences of the Drop-on-Demand and Continuous Jetting Priest et al., (1997)

Parameters	**Drop on Demand Jetting**	**Continuous Jetting**
Deposition Rates	< 10 kHz	up to 100 kHz
Droplet size (in diameter)	Better for small droplets	Generally larger droplets
Material consumption	Low, generally no waste	High, requires droplet elimination
Control process	Highly controllable individual droplets	Only the droplet stream can be controlled

Mainly, the difference between two is the droplet deposition rates. In the continuous jetting, the frequency of droplets ejected can reach up to the 100 kHz if the generator mechanism is equipped with suitable ejection mechanism. However, droplet generation at these high frequencies requires costly and relatively complex systems to use. The examinations over the continuous method were first initiated by Savart, (1833), and were first defined mathematically by Rayleigh, (1879). That is, the studies on the phenomenon of droplet formation are a comprehensive research topic starting from the 19^{th} century and extending to the present day. As a result of these studies, it is observed that the operation of continuous systems has both a complex structure and a low controllability. As an example, in continuous jetting, it is very difficult to stop and start droplet formation in a controlled manner while ejection is in progress. This issue precludes the droplet deposition on a surface to be in a selective manner. For this reason, its usage areas are limited (Liu and Orme, 2001). In the DOD method, the droplet generation frequency is usually in Hz scale, but in some of applications, it is observed that it can be reach up to a several kHz. Although the low deposition rates cause the production process to be prolonged, much higher quality part production is promised. This is because, the droplets are ejected so that they do not touch each other during the flight period, and it is allowed the droplets to be individually controlled much more effectively. The schematical shown of the two methods are presented in Figure 2.19.

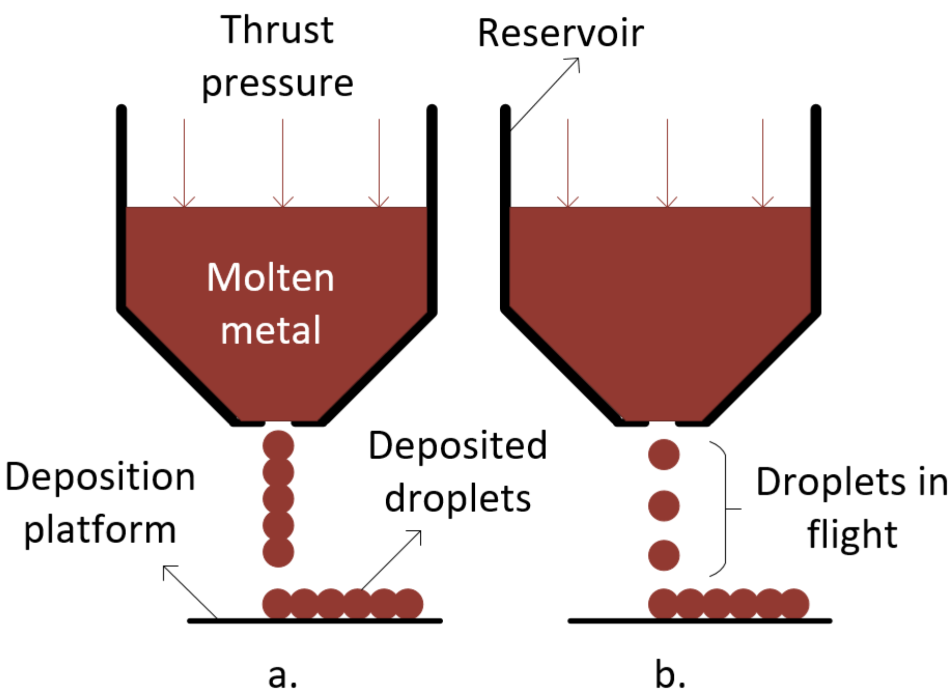

Figure 2.19.a. The continuous jetting b. the Drop-on-Demand (DOD) jetting

From an environmental point of view, only as much material is used as is required in the DOD method, thus avoiding material wastage. In contrast, the uncertain amount of droplets must be eliminated from the stream those are deviated from the streamline using special equipment in continuous jetting. The elimination operation is generally done by charging the droplets electrostatically during the flight and deflecting them by using the charged electrodes, as first demonstrated by the Stanford Research Institute in 1965 (Sweet, 1965). All processes related to the droplet elimination increase the cost of equipment and labor considerably which limits the application area of continuous jetting. On the other hand, if droplets are generated one by one then every single droplet can be controlled in size, velocity and other critical droplet properties. This phenomena enables the uniformity in all of the droplets generated. Thereby, more consistent deposition characteristics, more controllable, low cost and eco-friend operations especially for the electronic applications can be achieved in the DOD systems (Fischer et al., 2020).

2.6.1. The Elements of Metal Droplet Generation Processes

The droplet generation processes have been studied in many ways as observed in the studies done so far. These can be roughly classified under the mechanical and electrical inputs of the ejection mechanism, the properties of the droplets and the analysis, observation and inspection methods employed in the processes. As mentioned earlier, the control and characterization of individual droplets can be done much easier compared to the continuous method. In this way, the quality of the deposition process is also positively affected by their proper configuration. As a result of the analysis made on the studies investigated, the main elements to be considered in the droplet generation process are presented in Table 2.4 below.

Table 2.4. The main aspects and the elements of the metal droplet generation operations

Fundamental Properties	Base Material • High melting point • Low melting point • Raw material type -Powder -Wire -Liquid	Ejection Type • Pneumatical eject. -Direct inert gas supply • Mechanical eject. -Vibration Transfer • Combined (Hybrid) -Inert gas assisted mechanical impact • Other (Thermal, Acoustic, MHD)	Nozzle & Reservoir • Components -Orifice, reservoir, nozzle, sensors insulators, fixtures • Geometry -Inlets, outlets, slots dimensional design • Material selection	Material Feed • Manual Feed -Powder, liquid • Dynamic Feed -External container -Liquid -Wire
Control Applications	Temperature • Heating Method -Resistive heating (Cartridge, coil, jacket) -Inductive heating • Heated components -Reservoir, deposition platform, external storage, atmosphere	Pressure • Direct ejection pressure • Assistive supplement • Atmosphere content -Vacuum, -Oxygen, -Inert	Motion • Actuation • Axial motion setup -X,Y,Z • Feeder Mechanism -E	Software • Slicer software -Open-source -Commercial • Numerical Analyses -Simulations • Image Processing
Post ejection period	Droplet Properties • Diameter • Sphericity • Flight velocity • Flight distance • Wetting characteristic • Coalescence • Splat, satellite form.	Inspection Methods • Destructive testing -Tensile, flexural, compression • Non-destructive testing -Ultrasonic, SEM, XRD, • Image processing	Final Product • Horizontal Lines -printed circuits, conductive lines • Horizontal Array -Solder bump array • Inclined deposition • 3D (layered) parts -Miniaturization	

The first factor to be considered in the droplet generation systems is the melting point of the metal material to be melted. This factor, which is a starting point, is decisive for all remaining device and droplet features. This is because, the equipment used must not lose its function and must handle the whole operation at the required temperature levels. The second critical factor is the type of ejection in which the droplets are transformed into a droplet form, by providing the necessary pressure for the droplet ejection. In metal droplet generators, the hybrid systems involving both the pneumatic and the mechanical thrusts pressure are generally preferred ones as observed in the literature. Although there are mechanisms that operate on different principles, the mentioned mechanisms have some advantages in their own right. The comprehensive studies on droplet generators that allow metal droplet generation were primarily conducted by Orme and Muntz, (1987). In their pioneering study, the breaking and bonding conditions of droplets on-flight, and the droplet size modulation related to these issues were examined. These examinations are masterpieces in terms of achieving highly stable droplet formation, detailed method introduction and detailed analysis of droplets in terms of fluid mechanics. This work was further developed by the same group (Orme and Muntz, 1990; 1992; 1998) and patented in 1990. In the following years, patent studies continued based on similar droplet generator systems (Chandra and Jivraj, 2002). However, the first droplet generator developed for the production of relatively high melting point metals was presented by Orme and Smith in 2000 (Orme and Smith, 2000). The study presented a very impressive device, and the production of 24.000 Aluminum droplets per second was achieved. The image of the device is shown as in Figure 2.20.a.

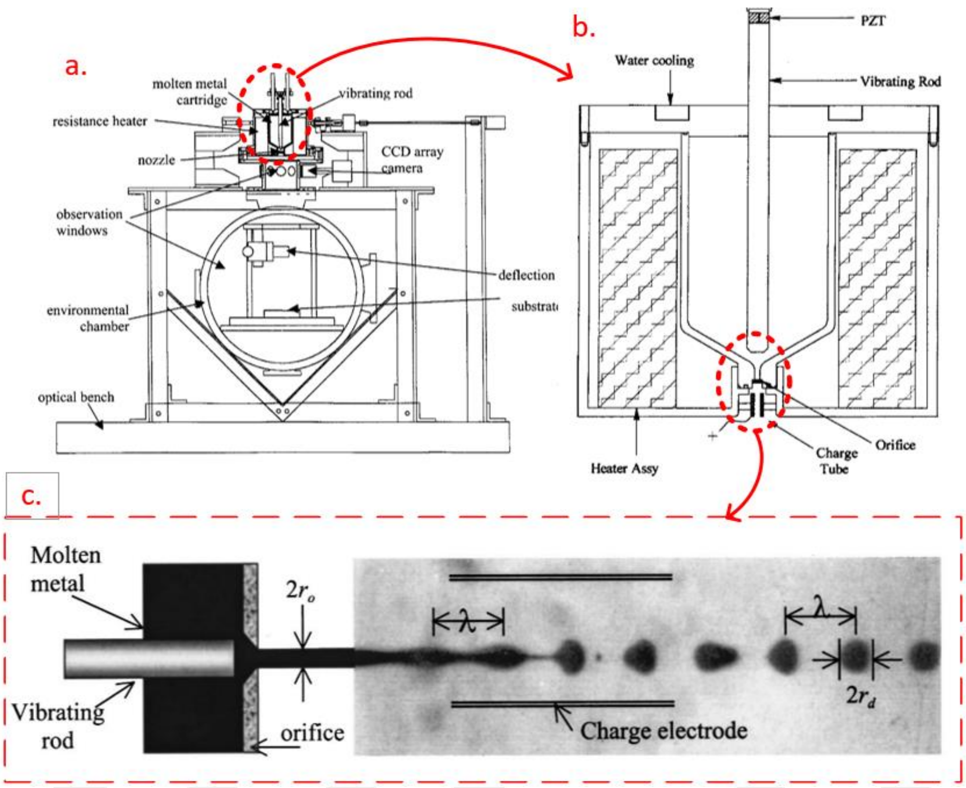

Figure 2.20. a. The general view of Aluminum based droplet generator. b. The detailed view of the ejection area. c. The schematic view of the ejection and generation process (Orme and Smith, 2000).

The sensitivity of the device was quite high and the droplet placement with a precision of 12.5 micrometers was able to be made by deflecting (eliminating) unwanted droplets. For droplet ejection, mechanical impulses, assisted by inert gas were used. The piezoelectric ceramic type actuator (PZT) was used as the impulse generator (Figure 2.20.b). Although the continuous jetting method in the device, they are important for being the first of their kinds. It should be noted that the droplets were formed in a similar way to the DOD method and their flight forms were able to be analyzed individually during the flow (Figure 2.20.c). All this operation has been brought to the literature with the definition of Precision Droplet-based Net-form Manufacturing. The subject of droplet jetting application areas employing solder materials is detailed in the study of Liu and Orme (2001). The practical application examples mostly in the field of electronics are presented in Figure 2.21 below;

Solder droplet printing capability	Applicable for
Bumps on chips, tape, board	Flip–chip, TAB, MCM, SMT, COB and BGA
Varying thickness, composition	Mixed packages or chip types
Rework, application of replacement solder	Flip–chip, TAB, MCM and SMT
Connection of redundant circuitry	MCM, multi-wire boards
Top layer personalization	Prototype boards, MCM, COB
Via filling	MCM
Non-contact 3D lines/dots	Lid attach, 3D packaging
Produce uniform microspheres	Flip–chip, via filling, anisotropic adhesives, solder paste
High precision deposition	Product labeling

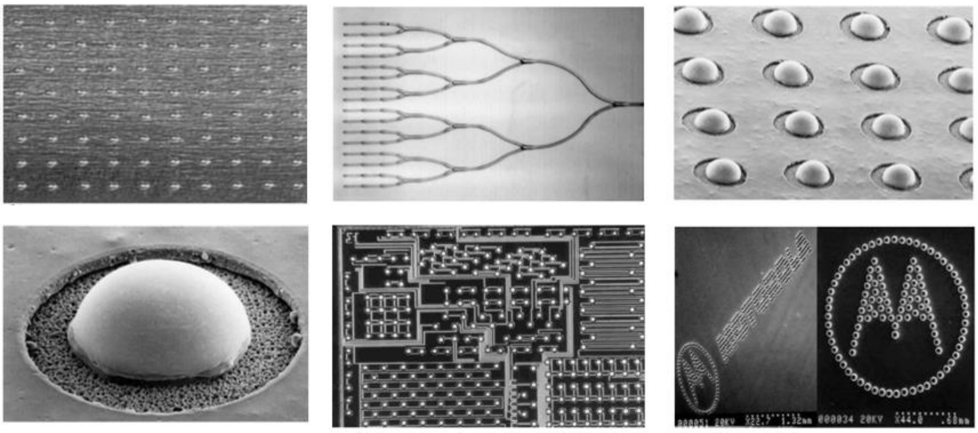

Figure 2.21. The detailed application areas and the implementations of solder-based droplet jetting operations (The images are compiled from (Liu ve Orme, (2001))).

It can be interpreted from the examples that how critical the application areas of metal droplet jetting processes are. This has brought with it the necessity of examining every aspect of this method in a much more detailed way. Due to the production potential it promises, especially for the electronics industry, the MDJ method needs to be further investigated.

In another comprehensive study, the production of metal parts through droplets was discussed under the name of Free Form Fabrication (Tseng et al., 2001). In this study of, the droplet characterization was carried out on the nozzle diameter, jetting velocity and frequency. Through the configuration of these parameters, it was reported that the droplet size can be effectively controlled. The experiments were constructed on a set of analytical formulations based on Weber's theory, and a great deal of theoretical-practical compatibility was observed. The experimental setup and images of the applications are as in Figure 2.22 below.

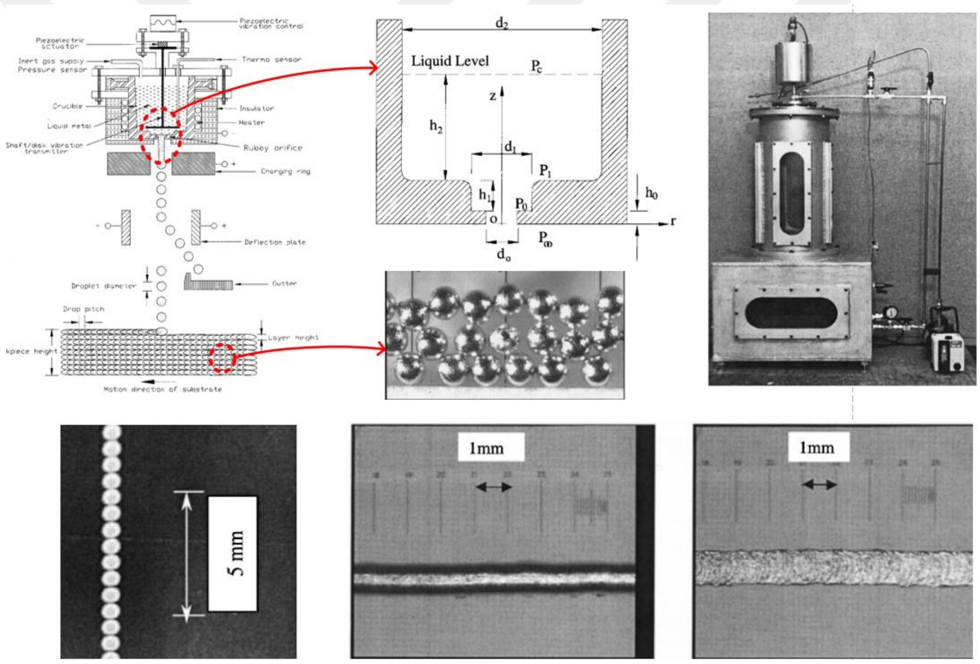

Figure 2.22. The novel metal droplet generator and its applications (Tseng et al., 2001)

The system shown in this figure uses almost all the hardware that can be found in a droplet generator. In detail, vibratory actuator, inert gas supply, controlled environment and temperature, sensors, crucible, heater, piston-type shaft, charging, deflecting components and many more operations were involved.

With the setup installed, a droplet flow with a very high homogeneity was obtained. With the deposition of solder-based fine lines, the production of products that can be used in many electronic applications such as circuit printing processes has been promised. There are two more important points of the study. First of all, the geometric design in the region where the ejection process takes place was investigated in detail. Almost every point was handled separately and the points to be considered in the design were introduced. The second important point is that the droplet size and deposition control was done with the help of dimensionless numbers such as Reynolds, Weber, and Ohnesorge. These numbers allow to greatly predicting flow formation and associated droplet formation criteria. This way, owing to these numbers, controlled and sustainable droplet formation can be achieved to a large extent. Technically, these numbers can be determined through a number of operating conditions related to the fluid's viscosity, flow velocity, gravitational acceleration, surface tension, droplet diameter, and in some cases their ratio to each other (Tseng et al., 2001; Weber and Passow, 1993). The products obtained by utilizing these numbers have been developed to serve many fields, especially the production of electronic parts. It should be noted that these dimensionless equations are also adopted in this thesis study.

In this context, in the study of Murr et al., (2017), droplet jetting operations were classified and droplet operations based on droplet formation and post-jetting operations were presented (Murr and Johnson, 2017). The main focus was on;

- The ejection conditions
- The flight distance of the droplets
- Density, surface tension, viscosity and the size of droplets and,
- Orifice (nozzle) diameter.

In addition to the parameters listed, the formation of the droplets at the time they hit the surface was also included in the examinations. The representative image of the study, which also examines the "wetting characteristic" topic, related to the dimensional condition of the landed droplet, is presented in Figure 2.23.

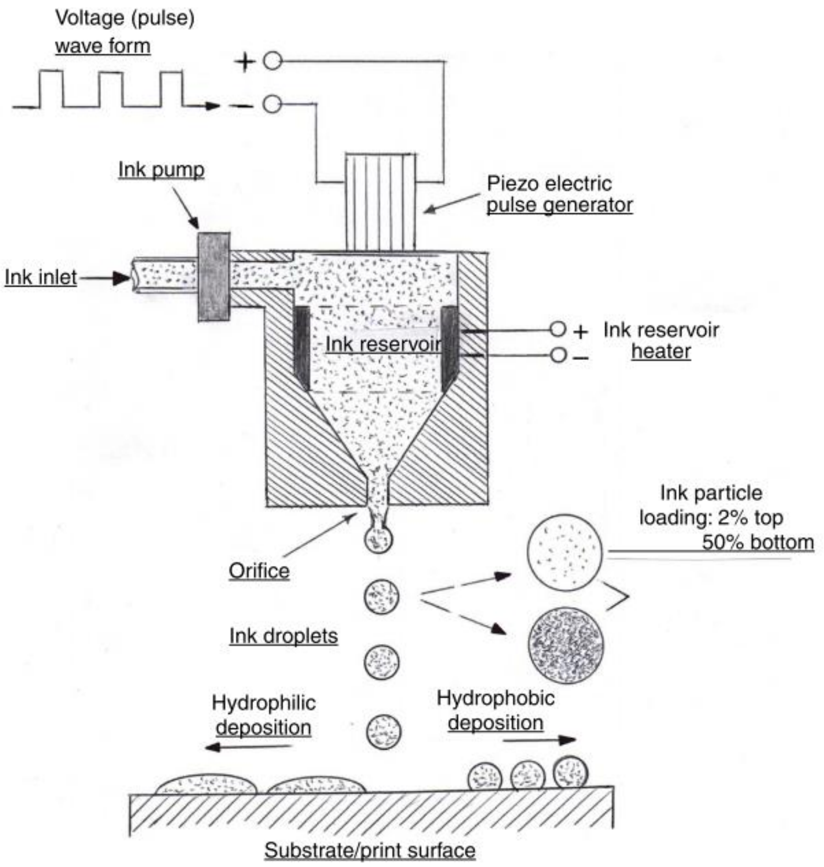

Figure 2.23. A conceptual image of the drop-on-demand method (Murr and Johnson, 2017)

It was concluded in the study that homogeneous parts in terms of strength and surface quality are in a sharp relationship with a single droplet quality.

2.6.2. The Process Parameters of the Droplet Generation Operations

Up to this point, the studies that enable these activities to gain an AM qualification are reviewed. These studies generally were focused on the continuous jetting method. However, in the same stuies, it is also mentioned the advantages to be gained when such systems are evolved to the DOD method. For this reason, especially in recent years, DOD-type metal droplet deposition processes have been the main subject of many researches. The studies conducted for this purpose are presented in Table 2.5, including the operational elements adopted in the relevant study. Moreover, it is also indicated the focal points of the study (marked with an x) and in which subjects it has not examined but may be studied in the future (hollow gray box). Most importantly, studies that presented critical findings that focused on and/or should focus on in the future were also shown (grey boxes with "x" filled in). While tabulating;

- ✓ The studies are given in chronological order,
- ✓ The studies that made a serious impact, and which constitute the motivation of this study, are shown in bold,
- ✓ The droplet generation and deposition stages are divided into main classes as ejection input parameters, inspection and evaluation and outputs, respectively.
- ✓ All the issues discussed and focused in the relevant study are included,
- ✓ The parameters marked in red indicate the ones also included in this thesis study.

Table 2.5. The review of the investigated droplet jetting operations

				Bogy and Talke, 1984	Yang et al., 1997	Orme and Smith, 2000	Tseng et al., 2001	Sohn and Yang, 2005	Cheng et al., 2005	Lee et al., 2005	Lin et al., 2006	Lee et al., 2008	C.Pita et al., 2008	Kim and Cherng, 2008	Fang et al., 2008	Ham et al., 2010	Wu and Lin, 2010	Jiang and Qi, 2010	Qi and Chao, 2012	Liu, 2014	Zhong et al, 2014	Vega et al., 2014	He et al., 2014	Harris et al., 2015	Li et al., 2015	Liao et al., 2016	Luo et al., 2016	Wang et l., 2017	Murr and Johnson, 2017	Zhang et al., 2017	Himmel et al., 2018	Zhang et al., 2019	Ma et al.,2019
				40	41	42	43	44	45	46	47	48	49	50	51	52	53	54	55	56	57	58	59	60	61	62	63	64	65	66	67	68	69
	Jetting Type		DOD	x	x	x	x	x	x	x	x	x	x	x	x	x	x	x	x	x	x		x	x	x	x	x	x	x	x	x	x	
	Jetting Type		Continuous			x							x	x				x		x		x							x				x
Input	Base Material		Pure Metal			x		x	x	x		x		x	x			x	x		x	x	x			x	x	x	x	x	x	x	x
Input	Base Material		Alloy				x		x	x					x				x			x	x			x	x		x			x	x
Input	Base Material		Polymer				x										x																
Input	Base Material		Composite & Other	x	x						x		x			x	x	x		x				x	x			x					
Input	Actuation	Thrust	Piezoelectric	x	x	x	x			x	x	x	x	x		x	x	x		x			x	x	x			x	x	x		x	x
Input	Actuation	Thrust	Solenoid Coil					x													x						x						
Input	Actuation	Thrust	Pneumatic			x		x	x			x			x				x		x	x				x				x	x	x	x
Input	Actuation	Nozzle & Reservoir	Geometry	x	x	x	x	x	x	x	x	x	x	x		x	x			x	x		x	x			x		x				x
Input	Actuation	Nozzle & Reservoir	Diameter		x			x	x			x			x		x		x		x	x	x		x			x		x		x	x
Input	Motional Structure	Axial	X, Y, Z, E Setup			x		x	x	x					x	x						x	x		x	x			x	x	x	x	x
Input	Motional Structure	Material feed	(Passive) liquid	x		x	x	x	x		x		x	x	x	x	x	x	x				x		x	x	x	x	x	x	x	x	x
Input	Motional Structure	Material feed	(Dynamic) wire																			x							x				
Input	Ambient		Room temp.		x			x			x		x			x				x			x	x	x			x				x	
Input	Ambient		Inert Gas			x	x		x	x		x		x	x	x		x	x		x	x	x			x	x			x	x	x	x
Input	Electrical		Voltage	x					x		x	x	x	x	x	x	x						x	x	x		x	x		x		x	x
Input	Electrical		Frequency			x	x	x	x		x	x	x	x	x	x	x	x	x	x	x			x	x	x	x		x	x	x	x	x
Input	Temperature		High Temp			x	x		x	x		x									x								x	x	x	x	
Input	Temperature		Low Temp	x	x			x	x		x	x		x	x	x	x	x	x	x		x	x	x		x	x	x				x	x
Input	Temperature		Platform Heating					x						x	x				x											x	x	x	x
Inspection & Evaluation	Type of Investigation		Theoretical	x		x	x		x	x	x	x			x		x	x	x			x			x		x			x		x	x
Inspection & Evaluation	Type of Investigation		Numeric & Opt.			x				x				x			x					x					x	x	x			x	
Inspection & Evaluation	Type of Investigation		Experimental	x	x	x	x	x	x	x	x	x	x	x	x	x		x	x	x	x	x	x	x	x	x	x	x		x	x	x	x
Inspection & Evaluation	Type of Investigation		Metallurgical			x			x			x		x	x				x							x			x	x	x		x
Inspection & Evaluation	Type of Investigation		Image Processing		x			x	x		x	x	x	x	x	x		x		x		x	x	x			x			x	x	x	x
Output	Droplet	Generation	Satellite & Ligament	x	x	x	x	x	x	x			x			x	x	x		x	x		x	x	x		x	x					x
Output	Droplet	Generation	Volume & Formation	x	x		x	x	x		x	x	x	x		x	x		x	x	x	x	x	x	x	x			x	x	x	x	x
Output	Droplet	Generation	Velocity & Distance	x		x	x	x		x	x	x	x	x	x		x	x	x			x				x	x	x	x	x	x	x	x
Output	Droplet	Generation	Deflection			x	x							x															x				
Output	Droplet	Generation	Surface tension		x	x	x	x	x	x	x	x	x	x	x		x	x	x	x		x	x		x		x			x		x	x
Output	Droplet	Generation	Viscosity	x	x		x	x	x	x	x	x	x	x	x		x		x	x		x					x			x		x	x
Output	Droplet	Deposition	Cooling rate			x								x	x												x		x	x	x	x	
Output	Droplet	Deposition	Wetting Charac.				x		x					x	x				x					x			x		x	x		x	x
Output	Droplet	Deposition	Splat form			x		x						x	x				x							x			x	x		x	
Output	Droplet	Deposition	Oxidation			x			x	x		x			x			x	x			x				x	x		x			x	x
Output	End-product	Engineering Concern	Resolution				x		x		x	x			x		x	x				x	x		x		x			x	x	x	x
Output	End-product	Engineering Concern	Strength			x	x		x									x	x		x								x	x	x		
Output	End-product	Engineering Concern	Density			x									x			x	x								x			x	x	x	
Output	End-product	Engineering Concern	Surface Quality				x								x			x	x							x	x		x	x	x		
Output	End-product	Engineering Concern	Post-Process Req.					x	x																					x	x		
Output	End-product	Industrial Concern	Leading Time			x				x								x					x	x	x			x	x				x
Output	End-product	Industrial Concern	Investment		x				x	x		x						x		x	x	x	x	x		x	x		x		x	x	x

x: Focused | :Not focused, Open to developments | x : Focused, Qualified, Open to developments

The studies presented in the table are discussed in terms of the factors that should be determined in the droplet creation process. According to the table, it can be seen that the focus is generally on the studies conducted with the DOD method. In terms of actuation source, it is seen that mostly mechanical and pneumatic ejection systems are preferred. In addition to these, it should be noted that droplet creation using different methods is also included in the review. The reason for this is that although different methods are applied, it has common features in terms of examinations made on the generated droplets. The main purpose of the table is to reveal which properties of the generated droplets should be examined. Technical details such as the mechanisms adopted in these studies, the equipment used, the materials and methodologies used, the observation and inspection methods are given in more detail in the material and methods section. But it is important to present an overview on studies including their entire subject of focuses. In the table, it can be deduced that as the years progressed, the number of subjects covered in the studies increased owing to the observation and examination methods proposed in parallel with the developing technology. The topics related to droplet formation are detailed through qualified studies. In this way, the difficulties, obstacles and gaps encountered in the developed systems and droplet production periods can be revealed in more detail.

Rumschoettel et al., (2016) developed a droplet generator on behalf of depositing of soldering droplets on built platform directly. In this way, it was reported that the processes of producing products that are much more feasible and at lower cost than metal production methods such as EBAM and SLM is possible. Piezoelectric materials were used as the actuation source in the generator, and solder alloy was preferred as the base material. The image of the generated droplets via this system is as follows (Figure 2.24);

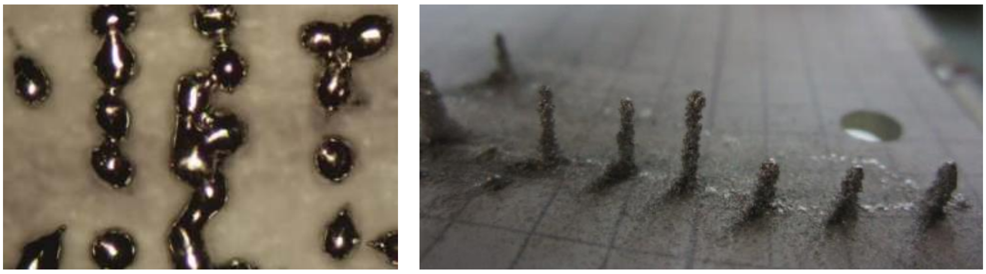

Figure 2.24 a. The microscopic image of solder droplets. b. Deposited droplets (Rumschoettel et al, 2016).

It was emphasized that droplets produced by DOD method can easily handle electronic part production processes. In the study, there are 3 main problems were observed in the ejection and deposition processes. First, a piezoelectric sourced actuator, which is not suitable for operation above the Curie Temperature, was used as the actuation source. Although it was reported that the operating temperature can be increased up to 1200 ^{o}C degrees with various insulation applications (Zhong et al., 2014), it was seen that the maximum operating temperature at which the presented device can only be increased slightly above the Curie temperature. Second, the issues of the bonding and the coalescence in the resulting droplets are not addressed in any ways. The third weak point is considered as the most critical factor for this thesis study. That is, it was stated that the liquid height in the container where the melt was hold decreases very rapidly due to the high-speed liquid discharge. After a short time the container becomes completely empty. In order to eliminate this problem, the emptied reservoir was filled manually each time. In this context, the necessity of automatic filling of the melt reservoir for a continuous droplet formation process was highlighted. This study is important because its importance the automatization of material feeding was emphasized although it was not provided detailed information. In this and subsequent studies, the subject of material feeding was either not focused at all or defined in a limited way. Moreover, the importance of the material feed rate is not grounded theoretically at no point. For this reason, in this thesis study, the subject of material feeding operation is taken as one of the focus for the uninterrupted metal droplet deposition processes.

In the study of Fan et al., (2008), a mechanism by which the droplet can be ejected by mechanical impacts was described. The ejection system based on mechanical impact, was defined under the name of Push-mode Driven droplet generator. After then, push-mode driven methods were compared with squeeze-mode (Takahashi et al., 2002; Wu et al., 2005), shear-type mode (Brunahl and Grishin, 2002) and bend-mode (Laurell et al., 1999) propulsion methods. As a result of the comparison, it was emphasized that the impact-based (push-mode) droplet ejection method is the most controllable and the least costly method. The actuation source in push-mode was provided by means of piezoelectric transducers which are very easily available in the market. The mechanical impulses were generated by a solenoid actuator instead of a piezoelectric material in the study of Sohn and Yang, (2014). In the jetting process, the solder alloy was melted and the liquid was pushed out of the nozzle by a rod connected to the actuator, and droplets were obtained in this way. In this study, it was stated that the jetting quality is directly related to the melting temperature, the ejection frequency, and the internal geometry of the ejection zone in the reservoir. In other words, as the melting temperature increases, the droplet surface tension and viscosity decrease, and the necessity of adjusting the mechanical impact parameters accordingly with the increasing temperature was presented through tests. Mechanical parameters were defined as the actuator pulse amplitude, frequency, the tip geometry of the rod transmitting the vibration to the orifice region and the internal reservoir geometry in the same region. The mentioned regions are presented in Figure 2.25.

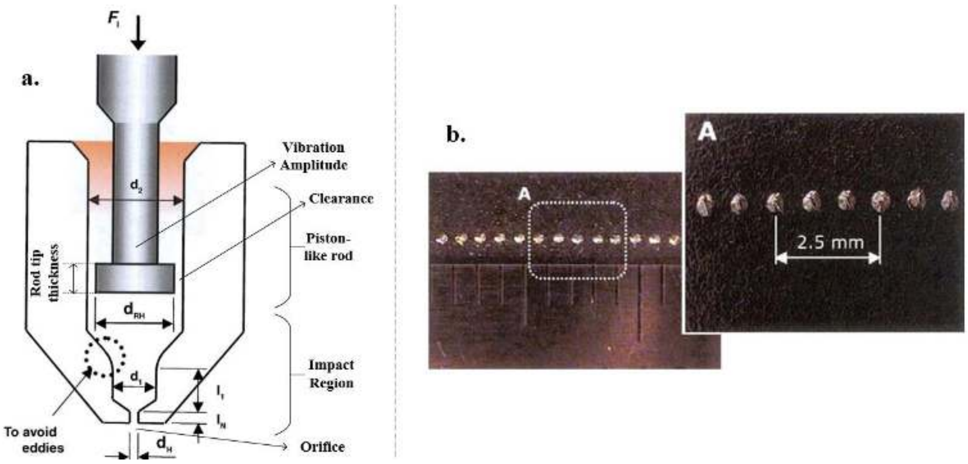

Figure 2.25. a. The cross-section of the reservoir including the important dimensions, b. The deposited solder droplets (Sohn and Yang, (2014))

As a result of droplet production experiments, it was observed that the diameter of the droplet is significantly affected by the reservoir geometry and vibration amplitude. It was also stated that the rod end thickness and clearance distance are also critical parameters. The term clearance here was defined as the gap distance between the lateral surface of the piston tip and the inner wall of the reservoir. In addition, the solder material used in the experiments was melted at temperatures well above its melting point. It was also stated that at elevated temperature, the surface tension and viscosity of the material decreased significantly, and accordingly, the tendancy of the flow into the reservoir increased by re-flowing through clearance into the reservoir instead of being thrown out by the impact (Beer, 1972). According to the results obtained in the study; If the clearance distance is too much, the material to be ejected cannot be transferred to the orifice area sufficiently, if it is too little, the backflow occurs. As another finding, it was stated that if the distance between the orifice-piston tip is too small, satellite occurs, and if it is too much, a blob (big drop) appears. Although the specified operating parameters are unique to the presented device, it is understood that it is critical to adjust these parameters to be able to deposite the droplets stably. This study showed that the quality and the homogeneity of the deposited droplets (Figure 2.25.b) are strictly depended on the geometrical design of the ejector and reservoir. For this reason, in this thesis study, the geometric structure of the droplet generator is focused, and all important dimensions are analyzed.

2.6.3. The Determination of Suitable Droplet Deposition Conditions

The DOD method allows the deposition process to be controlled effectively. It is possible to modulate a single droplet in its properties such as diameter, velocity and the deposition form. Due to the fact that the final object is made of combined droplets, each droplet appears to have a critical importance. That is, the quality of the deposition operations is directly related to the properties of a single droplet. To be able to achieve the desired the geometry of the deposition, it is first necessary to classify the deposition models according to the droplet's arrangements. That is, the droplets can be both deposited horizontally (2D deposition) and/or vertically (3D deposition). The droplet deposition models along the three axes are given in the Figure 2.26.

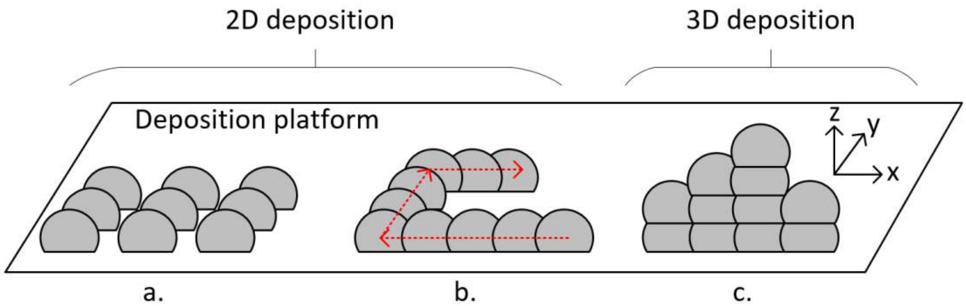

Figure 2.26. The droplet deposition models, a. Controlled discrete array, b. Continuous line c. 3D (layered) deposition

In the horizontal deposition, the droplets may be placed in an array form having a certain distance between them. In this way, a specific geometric patterns made of droplets can be produced in order to be used in many applications, especially in electronics. The Ball Grid Array (BGA) production is one of the application area of the droplet deposition technique. The examples of the BGA type droplet depositions are provided in the Figure 2.27.

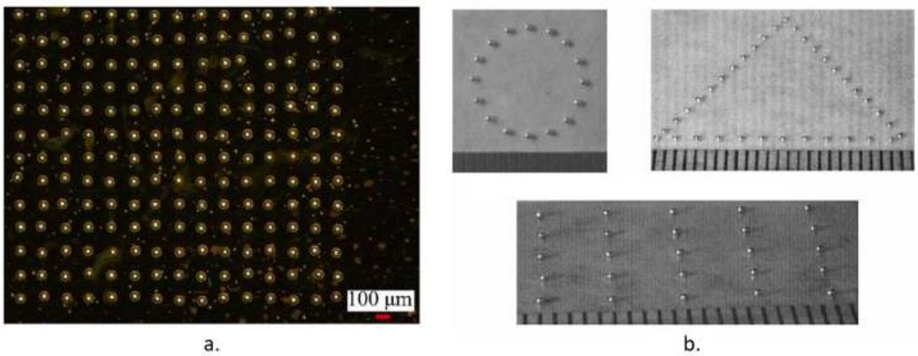

Figure 2.27. The various examples of metal droplet arrays made of solder alloys ejected a. Mechanical impacts (Ma et al., (2019)) b. Pneumatic impacts (Cheng and Chandra, (2005))

The BGA technology is one of an electronic packaging technique used in electronic component manufacturing. The electronic packaging technologies enable smaller, lighter and compact components production. The size of a product is reduced with this technique while improving its operational performance. Thereby, it is already adapted for the the integrated circuit production such as the chips, boards, printed circuits and so on. Specifically, BGA is a kind of a carrier for the surface mount devices. It is necessary to provide conductive pins in order for the electronic parts to be attact on. The tiny droplets are placed appropriately at the connection point between the electronic element and the relevant module (Rocha, 1997). The quaility of BGA package depends on many factors such as ball diameter, sphericity, cleanliness, planarity, uniformity and radial/placement errors (Ries et al., (1993)). Since all of these parameters are depended on the droplets generation conditions, it is a must to determine suitable ejection parameters as a first step. It is then become possible to deposite usable droplets for such applications as BGA or Flip-chip packaging. So far, the modern soldering techniques such as reflow soldering and wave solder were in use to deal with the electronic packaging operations. Although these methods provide mass-manufacturing advantage, the devices are difficult to use, require multi-step process for a single operation, occupy large area in the production zone. In addition, these devices are not flexible enough for the varying processes and they are quite high in cost (Abtewa et al., (2000); Kumar and Ting, (2006)). Similar to electronic packaging, the metallic droplets –especially the solder alloys- can be deposited for use in MEMs manufacturing processes. The conductive connectors, pinpoint slots and carrier joints can be created for the MEMs device in terms of both new-product and repair operations. As mentioned, metal droplets have wide range of usage area that of given examples, but not limited to. The applicability of the metal jetting techniques into the mentioned operations is one of the reasons for focusing the proper droplet generation via such technique.

When the droplets are deposited in a sequence, having a contact to each other, the conductive lines as well as 3D structures can be achieved (Figure 2.24.b, c.). Here, the amount of coalescences between the droplets determines the final shape. In the given for both 2D and 3D droplet deposition, there are critical parameters need to be further investigated and understood. To classify, the ejection parameters, the droplet condition during flight and the deposited droplet properties are the fundamental periods of a droplet based manufacturing operation. There are also many subcategories within the periods those can be found in the Figure 2.28.

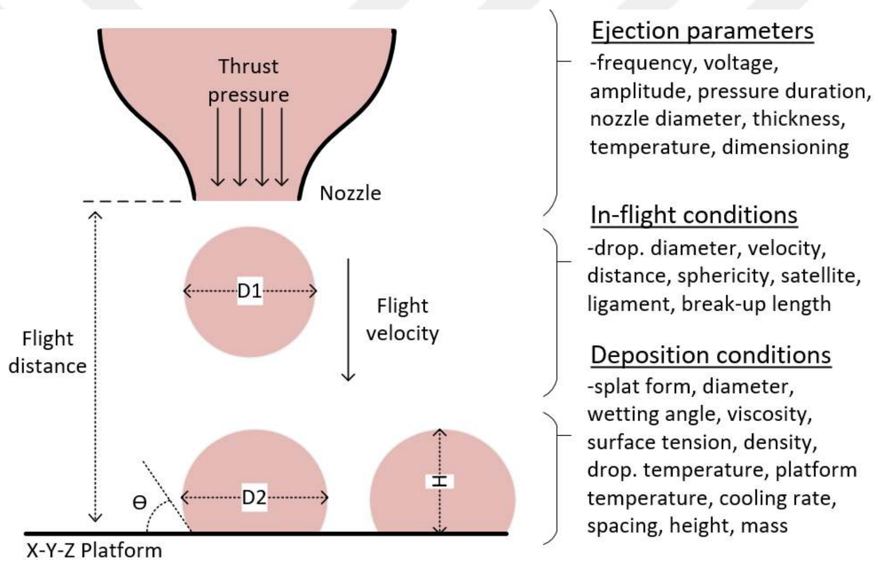

Figure 2.28. The main operational parameters and conditions of a droplet generation and deposition

In order to cope with all the dynamics of the droplet production operations, the extensive investigations and observations are required at every point possible. In the study of Bhola and Chandra, (1999), the droplet impact dynamics were examined to be able to predict the shape of the droplet hit the surface. In the experiments impact velocities and the deposition platform temperatures were varied controlledly. It was observed that the diameter of solidified droplet is proportial to the platform temperature and the impact velocity.

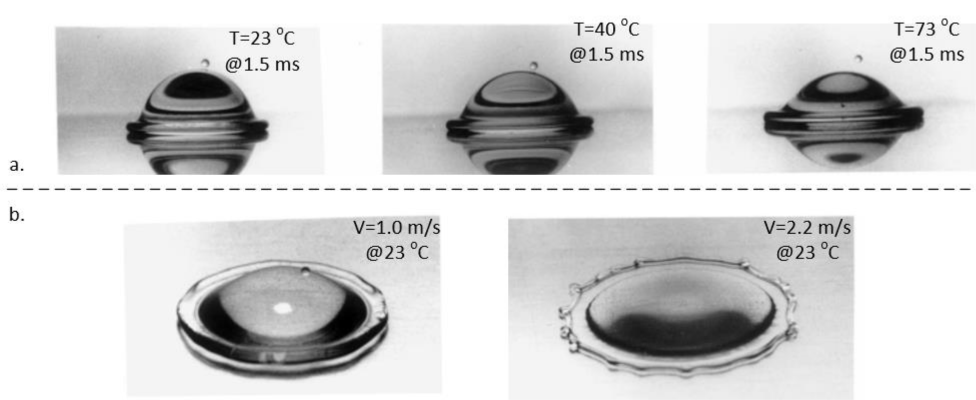

Figure 2.29. a. Impact of a droplet at various platform temperatures, b. With various impact velocities (Bhola and Chandra, (1999))

The reasons of these droplet formations attributed to the change in surface tension and the viscosity. That is, when the platform temperature decreases, the surface tension increases and tends to hold droplet in a more spherical shape. In addition, the solidification time prolongs at the elevated platform temperatures. During this time, the droplet keeps oscillating until it totally solidifies. It spreads and recoils repetitively. In the meantime, the surface tension cannot pull back the droplet from its perimeters towards its centre. Thus, the shape of solidified droplet tends to be in more eliptical form with wider droplet width and lower height (Figure 2.29.a). As the impact velocity increase (at equal platform temperatures), the same situation occurs for the shape of solidified droplet. The variation in the shape depending on both the viscous forces and the impact velocities are correlated to the energy transformations within the droplet. That is, in order to predict the spreaded diameter of a solidifed droplet, it is necessary to calculate the droplet's energy before and after impact. More specifically, the energy balance of the droplets conditions can be expressed with the Equation 2.1 as;

$$K_1 + S_1 = S_2 + W \tag{2.1}$$

the K_1 is the initial kinetic energy, S_1 and S_2 are surface energies before and after after the impact in turn, and the W is the work done against the viscosity of the liquid (Pasandideh-Fard et al., 1996). At the time the droplet hits the surface and gains its maximum diameter value, the value of velocity, thus the kinetic energy becomes zero. Then the remaining energy is spent on deforming the droplet shape against the viscous forces. At this point, the maximum spread diameter can be calculated using the dimensionless equations as below ((Pasandideh-Fard et al., 1996; Bhola and Chandra, 1999));

$$\xi_{\max} = \frac{D_{\max}}{D} = \sqrt{\frac{We + 12}{3(1 - \cos\theta) + 4(We / \sqrt{\mathrm{Re}}}} \tag{2.2}$$

$$We = \frac{\rho_g U^2 D}{\sigma} \tag{2.3}$$

$$\mathrm{Re} = \frac{\rho_g U D}{\mu_g} \tag{2.4}$$

Using the Equation 2.2, called as maximum spread factor, (by first calculating the values in Equations 2.3 and 2.4), the final shape of the droplet can be predicted taken into account its velocity, temperature, density, viscosity and the surface tension of the droplet. In the presented study, the experiments in order to conrol the physics behind the droplet conditioning are conducted. The impact, spread and the solidification periods are examined. It is stated that the applicability of the dimensionless equations to the real-time droplet modulation and control, as the theoretical calculations are well-agreed to the experimental results.

With the method of metal droplet deposition, miniaturized, thin-walled 3D metallic parts were succesfully manufactured by Chao et al., (2012) (Figure 2.30.f).

It was stated for the proper droplet deposition that the deposition accuracy depends on both the flight distance and the properties of the landed droplet that of contact angle and spread diameter. In the first step, the minimum distance necessary for the droplet to be able to break-up from the nozzle is measured by image processing. According to the measurements, the break-up length (Figure 2.30.a) is in direct proportion to the jetting velocity.

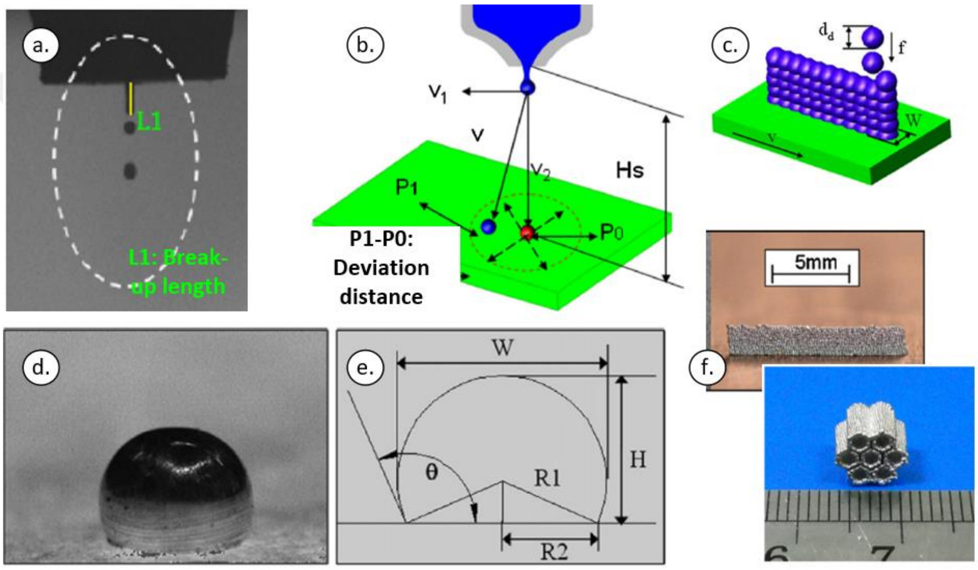

Figure 2.30. a Break-up length, b. Landing deviation, c. Representative thin wall d. Microscobic droplet image, e. Shape parameters of droplet, f. Manufactured thin-walled parts (Chao et al., (2012))

For the maximum distance, the incremental flight distances are set and droplets generated. They measured the distance of the deviated droplets from the target point. Until a certain flight distance, the droplets are deposited with a distance deviation smaller than their diameters which are referred as an acceptable level of a landing error (Figure 2.30.b). The optimal flight distance in final is found in between 1-20 mm. Secondly, it is reported that the uniformity of a wall thickness is directly related to the individual droplet's width since the wall is made of single droplets (Figure 2.30.c, .d and .e). To be able to predict the wall thickness, it is adopted a serie of dimensionless equtions based on conservation of the mass. The parameters necessary for predicting the droplet spread diameter are the shape properties as; wetting (contact) angle of droplet and ideal diameter of droplet during flight. The Equation 2.5, developed by Fang and Chandra, (2008), is given below;

$$W \approx 2R_1 = d_d \left(\frac{4}{\left(1-\cos\theta\right)^2 \left(2+\cos\theta\right)} \right)^{1/3} \quad (2.5)$$

It is firstly performed a serie of experiments with four different nozzle diameters, and measured the droplet's diameters and the contact angles. Then the deposition experiments are initiated. Owing to the great agreement between the theoretical equations and the actual wall thickness, the system is proven to be feasible. It is an important finding that the shape parameters of a droplet significantly determine the accuracy of the part's shape. Moreover, theoretical calculations can be used as an effective predictor, as also demonstrated in the study.

The deposition morphology of the droplets are investigated by implementing the similar theoretical equations but this time, taking into account the axial motion of the deposition platform along X and Y axis in the study of Qi et al., (2012). The main focus is on revealing the effects of the axial velocity of the platform, droplet ejection frequency and the gap distance between the deposited droplets and the bonding amount over the deposition morphology (Figure 2.31).

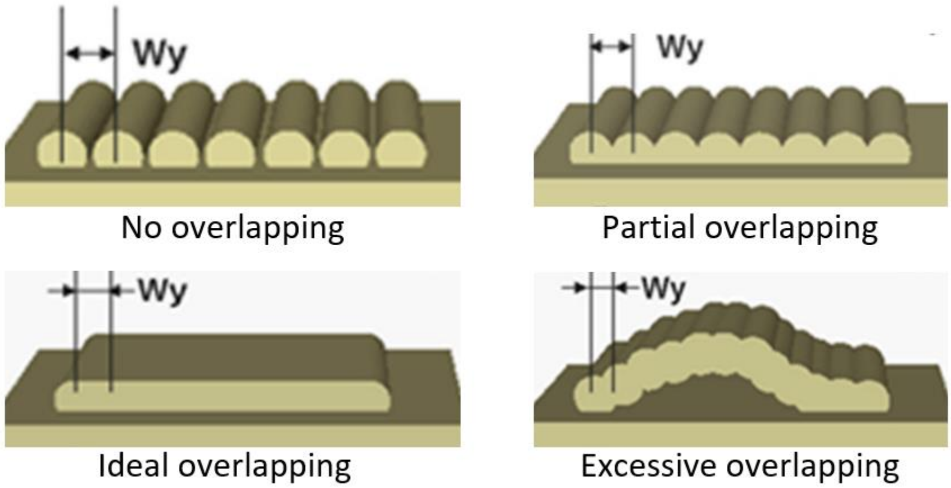

Figure 2.31. The classification of the overlapping due to its amounts.

It is characterized the amount of overlapping between the droplets, the lines and the layers by configuring the frequency, platform velocity and the spacing between the single droplets. The experiments are done by characterising the droplets wetting properties as shown in Figure 2.30.e. It is intended to control the porosity and the accuracy of the final shape. According to the experimental results obtained, good metallurgical bonding by eliminating the porosity can be achieved. It is suggested it can be done by implementing a theoretical assumptions (Equation 2.5) in order to obtain the necessary amount of maximum droplet width. The study also indicates that the coalescence between the droplets not only depends on the solidifed droplet's size, but also the velocity of the moving platform and the ejection frequency.

As a complementary study made by Zhang et al., the metallic structures were formed by droplets made of both solder and Aluminum alloys (Zhang et al., (2017); (2019)). The droplet deposition process under the term of parametric mapping is studied by classifying the droplet sequences according to the spacing between them which are; inclined, wave-shaped and horizontal placement. The horizontal placement is also sub-categorized as overlapped, clustered and discrete morphologies. The images belonging to the original deposition operations, showing the categories are given in the Figure 2.32.

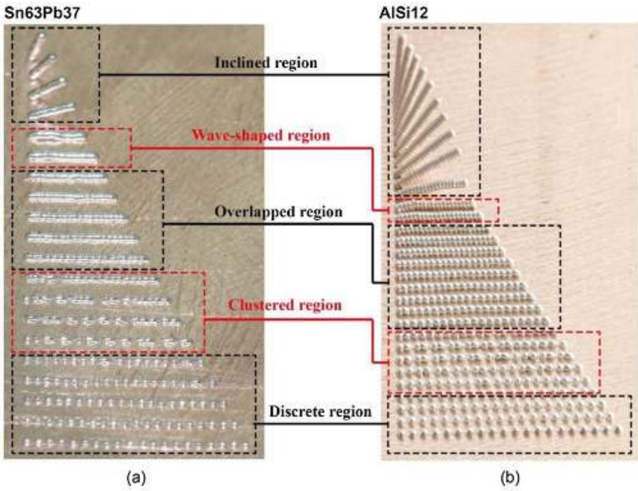

Figure 2.32. The droplet deposition morphologies made of a. Solder alloy, b. Aluminum alloy

Before the experimental stage, the mathematical definitions were developed by taking into account the velocity, contact angle, spread diameter and Offset ratio and the Merge ratio in the first place. The main target was determined as controllling the spacing and the bonding characteristics of the droplet arrays. The parameters of landing error, the frequency and the axial translation velocity were also included in the calculations. Here, the distance between the droplets is stated as a dominant factor in morphology designs. This expression is explained by the correlation between the offset and the Spreading ratio. The Offset ratio is defined as the ratio of the spacing between the two centers of the droplets to the diameter of single droplet (Equation 2.6). The spreading ratio indicates the ratio of the spread diameter of the solidified droplets to its ideal (fully spherical) diameter (Equation 2.7). The mathematical expressions of these equations are as follows;

$$\xi = \frac{w}{2r} \tag{2.6}$$

$$\lambda = \frac{W_s}{D} \tag{2.7}$$

$$\theta = \arccos\frac{\xi}{\delta} \tag{2.8}$$

Fundamentally, the correlations are based on three different scenarios. If the Spreading ratio is much bigger that the Offset ratio, the pillar-type (inclined) formation is obtained (Equation 2.8). If the difference between the two ratios are set to be a fair enough, the overlapped form of droplets are deposited. In the third case that where the offset ratio begins to pass the spreading ratio, the discrete morphology is achieved. However, it is required to determine the interval values of three scenarios in order to avoid the transitional formations such as wave-shaped and clustered regions. It is necessary due to the fact that only the three cases can be useful to the application areas such as printed circuit production (with the overlapped form), BGA production (with the discrete deposition) and the miniaturized, 3d metal objects (with the inclined region) as stated. These two studies provide some critical information to the literature because almost all of the crucial parameters for the desired droplet deposition operations were focused, evaluated and configured through the experiments. The more important is that the good agreement between the predictions based on mathematical calculations and the real-time observations was achieved. These studies has a great influence on the droplet-based manufacturing processes, because of presenting the ability of predicting and characterizing droplet deposition morphologies with a number of mathematical calculations.

So far, the investigations mostly focused on the process parameters affecting both the individial droplet condition and the final deposition morphologies are subjected. The glittering achievements in the relevant studies about the process characterisation are also provided. However, the information related to both hardware and software used is observed to be limited. The biggest reason behind this issue can be related to the several reasons. The one, the devices used in relevant studies were individually patented which precludes the possible improvements on device where the further examinations are required. Althought for the ones that provided detailed information about the operations performed, the cost of devices are very high. Besides the cost, the structures of the generators were far from modifiability due to the fact they were designed for specific droplet generation purposes. Similary, the software or the code in order to operate the whole system are not provided sufficiently. Fortunatelly, there are increasing number of studies based on open-source concept which may eliminate the mentioned drawbacks. Owing to the open-source based systems, the droplet generation operations are promised to be carried out at a lower cost. Furthermore, the structure of the system can be made modifiable in contrast to the commercial ones. Due to this and similar advantages, more research is needed on the open-source concept. For the same reason, it is considered as one of the focal points in this thesis, and more detailed information is provided.

2.7. The Implementation of Open-source Concept into the AM Processes

The scientific instrumentation, the devices and tooling required for manufacturing processes are being improved day to day. However, the majority of these devices consists of high-budget components and can only be operated through licensed software. This also limits the ability of the devices to be modified on demand. Fortunately, owing to the open-source concept, manufacturers, researchers, and even the individual users have started to produce their own devices, significantly reducing the operating costs. The term open-source basically describes generally free resources that allow users to access, modify, and develop a project with its all aspects which can be found in both hardware and software forms (Pearce, 2013). In other words, users can easily access all necessary resources, such as parts list, installation guide, and digital source codes to obtain a desired device and have the opportunity to realize the results obtained with commercial systems with much more affordable costs (Kentzer et al., 2011). There are many associations, communities and research groups available those support this concept to spread all around to the world. The Open Source Hardware Association (OSHWA) is one example of these organisations made a definiton of the open-source hardware. The definition provides a comprehensive methodology for open source-based processes to encourage researchers and manufacturers to adopt it. The main target of the OSHWA movement is to provide the hardware information that anyone can study, modify, distribute and even sell the original project under some open-licencing conditions. For further, the way to spread this features is standardised under some sort of checklist ensuring the scientific infrastructure of the job (Website, 2022c). It should be noted here that the widespread use of the open source concept does not mean that it does not require or cannot be licensed. Licensing in this context, unlike commercial licenses, is made to ensure that fully functional information can be disseminated in a more standardized way in the open source ecosystem, free of charge. In this manner, there are some criterias declared by the Open Source Initiative community conforming the open-source definition (Website, 2022d).

Today, open-source based 3D printers; especially the FFF-types can be established with very low costs. Moreover, the reduced cost leads the researchers to demonstrate more intensive investigations related to the physics behind the AM principles. This is because, the work with open-source compatible equipment have allowed a flexible interference in both the software and the hardware modifications. To be more specific, the movable structure of a device -as the chassis of the entire system- heaters, extruders, nozzles and their side parts are already available on the commercial market at an affordable cost as ready-to-use. Moreover, by the widespread inplementation of the open-source concepts, their control issues are also facilitated, owing to the availability of the source codes for free of charge. This issue enabled for researchers to concentrate more effectively on process parameters, eliminating the need of spending time for solving the investment and budget problems. In the study of Tymrak et al., (2014), the mechanical properties of test specimens printed via commercial FFF printers and the open-source based ones were compared. For the experiments, four different types of open-source, desktop device and two types of polymer material (PLA and ABS) were selected. As process parameters, three parameters of part orientation, layer thickness and infill density are chosen which can be said as the most effective parameters on part's strenght as mentioned in the previous sections. According to the experimental results, the tensile strength of specimens is not much differs from the printed ones via commercial devices since the components used are similar derivations of each other.

Besides the FFF operations, the AM devices become capable of processing metal materials with flexible devices at much lower costs due to the integration of the open source concept. It was first announced in the study of Anzalone et al., (2013) that the ability to manufacture the parts additively using the open-source structure is possible. The motivation of the study was the lack of affordable metal printers that could be used in the standart laboratories under routine circumstances. In the mentioned study, the device which works with the FFF principle is modified into a metal printer by some sort of utilizations benefiting from the open-source concept. It is included in the device description the list of materials, their prices, schematical flow diagram of process as a proof of concept. The device used and the product manufactured are shown in the Figure 2.33.

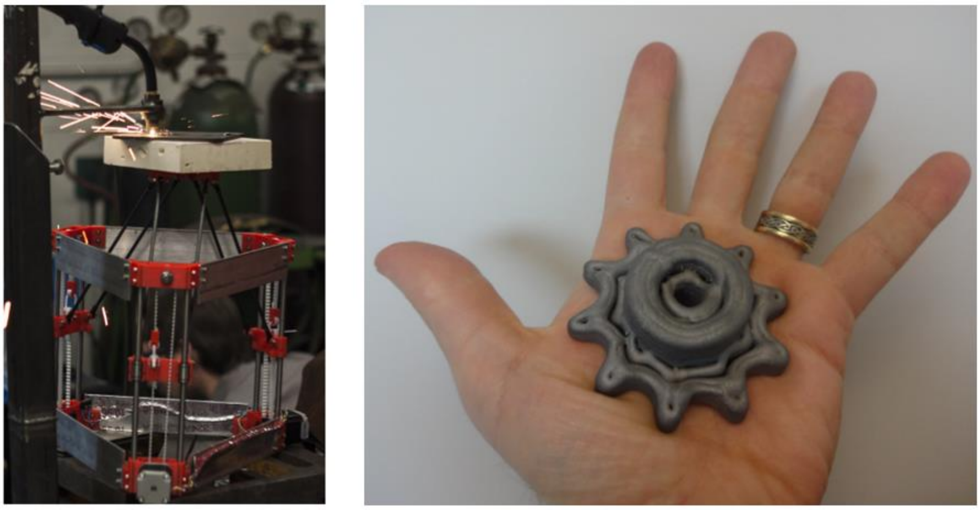

Figure 2.33. The desktop-type, open-source based 3D printer (left), the manufactured metal product (right) (Anzalone et al., (2013))

As it is further discussed in the next sections, the FFF-type printer devices can be evolved into a metal printer if the necessary modifications are done on it was demonstrated in the study. Although the dynamics of metal processing operations require much more effort compared to the polymers, there are a lot in common regarding the process parameters in terms of AM such as –but not limited to-, axial motion, deposition rates, temperature and actuation control and the preperation and the slicing of a CAD model. If the necessary amount of focus with the required level of engineering effort is spent on the customization of the open-source AM devices, it would be a promising technology for the metal industry as a game-changing technology.

3. MATERIAL AND METHODS

In this section, the mechanisms, components used for material deposition operations with their functions are focused. The methods of manufacturing processes are also described both for FFF and MDJ processes.

3.1. The Anatomy of FFF-type Devices

In FFF processes, many operations must be carried out simultaneously and in a controlled manner. These operations are carried out by a number of electro-mechanical components. Although the fundamental elements such as frame (chassis), deposition platform, heating, cooling, axial motion, material extrusion are common for all FFF operations, they may vary in shape, accuracy, operational principle and the way of control. To be able to fully understand the operational principle of these kinds of devices, the comprehensive analysis of the anatomy of the devices needs to be made. An example of FFF-type device is given in the Figure 3.1, and the explanations will be given over the relevant region marked in the demonstration.

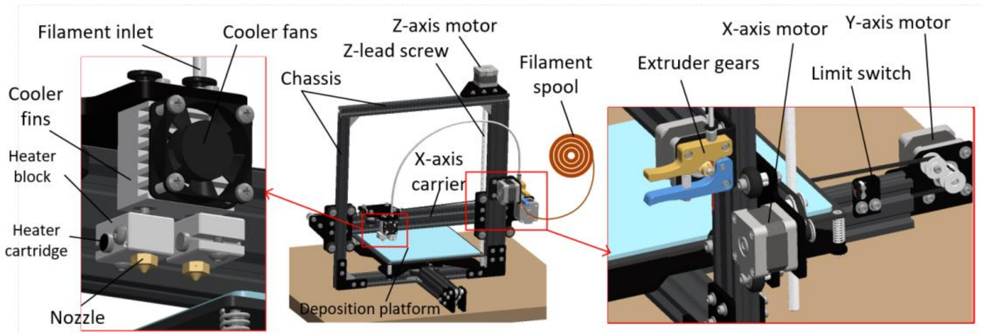

Figure 3.1. The general view of FFF device with its main components

First of all, it is necessary to attach all the fixed and movable components, such as motors, platform, extruder and carrier parts on a suitable chassis (frame).

The assembly of the chassis is mainly responsible for the maximum built size, arrangement and the placement of the components. As a first step to installing such a device, the frame must be assembled in such a way that it can withstand the weight of any part that will be attached to it, whether movable or not. In the open-source environment, there are many variety of assembling options using various components. Part selection in frame assembly, which is one of the most critical steps regarding the almost unlimited combination of hundreds of different parts, is one of the most critical steps. The print bed (deposition platform), extruder mechanism, heaters and sensors then can be installed on to the frame suitable. After assembling all the necessary parts, a suitable control board must be connected to the device with an appropriate power supply. The flow diagram of a standard FFF process is given in the Figure 3.2.

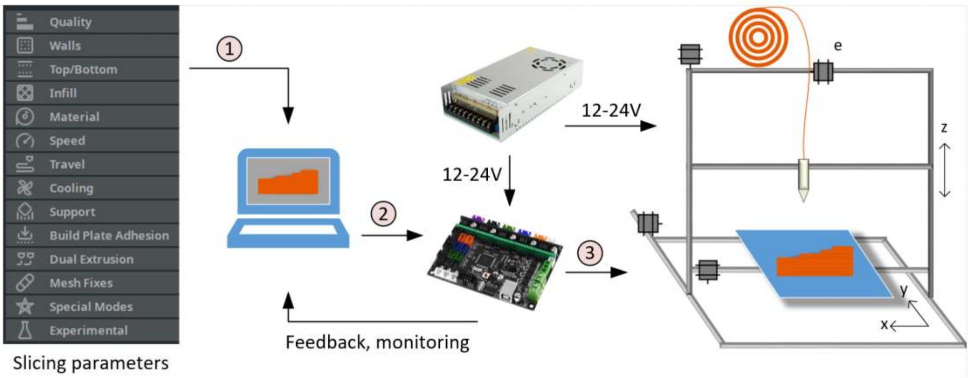

Figure 3.2. A flow diagram of fundamental FFF processing steps.

The method of part printing can be classified as three main steps.

1- *Slicing step*

In this step, the desired CAD model is converted into Stereolithography (.stl) file format and exported into the slicer software. There are many slicer softwares freely available in the open-source ecosystem such as Cura, Slic3r, Repetier and so on. In addition to being free, these softwares are supported by many communities such as Github, where numerous developers and software experts are involved, and they continue to evolve (Website, 2022j). At this point, this factor takes critical importance. This is because, the more accurate results the software gives, the higher the quality of the produced parts. Specifically, the layer height, line width, shell thickness, infill density, infill pattern and orientation, part orientation, the amount of line and layer bonding, printing temperature, platform temperature, printing speed, material flow rate and support options are configured in this step. Since these parameters are the most critical ones affecting the surface quality, the strength and the processing times, this is the most important step of the whole FFF process.

2- Data transfer to the control board

After slicing the digital model suitably, the G-code file is transferred to the control board. The control board is directly responsible from controlling dynamic printing process. That is, the signals are sent to the various loads such as motors, heaters and coolers, and then their feedback is gathered by the sensor simultaneously. At this point, the control board should be selected from those that are compatible with the physical device specifications. This is because, some controller boards are limited by their hardware capabilities, others because of their proprietary design. Fortunately, thanks to the open-source concept, the source codes are open-to-access for everyone and allow configurations within the operating conditions under which the device can operate stably. There are ready-to-use configuration packages available which may be implemented on even the custom-made devices, called *firmware*. One of the most widely used 3D printer firmware is Marlin Firmware (Website, 2022k). This is because, it allows high level of customization and has a high update frequency by the strong community support. As another reason, it uses the Arduino platform as a user interface which is one of the biggest founder and supporter of the open-source concept. This firmware is derived from the traditional control software used in CNC machines and has been developed to be used in FFF devices today effectively.

3- *Actual printing process*

In this step, the actual material depositon process is initiated. According to the data sent by the control board, the material feed, the heating process and the axial movements along three axes are started. During the layering process, there are many variants those effect the quality of the part. To be able to finalize the process succesfully, the first the structure of the device must have been set in order to overcome the number of printing problems. The device should be calibrated from a several point of view to avoid deposition failures such as, under-extrusion, over-extrusion, agglomeration, blobbing, warping and insufficiently bonded lines or layers as shown in the Figure 3.3. The compilation of the most common printing failures, but not limited to these, are reflected.

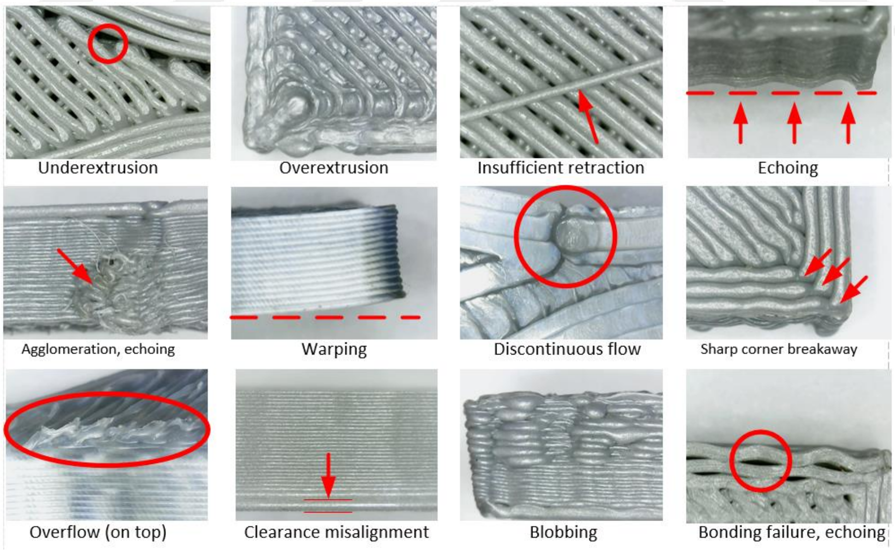

Figure 3.3. The common failure types in FFF processses.

As an examle, the ability of vibration damping due to the dynamic motions must be provided in sufficient level. This is because, the resolution, surface quality and many more part property is negatively affected by the vibrations occur on the device frame. Otherwise, the wavy shapes may occur both inside and the outer regions in the part. Some examples can be seen in the Figure 3.3, called as “echoing”. The terms echoing, ghosting or ringing are used to define this failure formation due to appear as similar to the sound waves echoing from an obstacle. There are many interactive communities addressing these issues also by providing the possible solutions as a guide of troubleshooting (Websites, 2022e-i).

3.2. The Configuration of Material Extruder Mechanisms

The most of the failure types are related to the amount of material extrusion, which determines the actual line width and layer thickness. In fact these parameters are defined in the slicing step. However, the digital values may not match to the actual deposited line properties. To be more specific, the flow rate of the material should be calibrated according to the equipments used in the established. It is then the extruded lines can be equal to the defined parameter in the slicer. Only in this way, the dimensional agreement between the manufactured part and the digital model can be obtained.

In the study of Geng et al., (2018), the effects of material extrusion speed was examined on the microstructure of the extruded lines made of PEEK material. The twin gears were used as an extruder and their rotational speed were varied in the experimets (Figure 3.4.a). The width of the extruded lines was measured via a digital microscope. As a first step, the lines were extruded towards a dimethicone liquid to reduce the influence of the gravitational forces on squeezed material. In this way, the flow rate of the semi-molten (pasty-state) material against the extrusion speed was revealed (Figure 3.4.b). At this point, the conservation of mass equation (Equation 3.1) was used to calculate what the diameter of the material collected in the liquid would correspond to the printing speed in actual deposition process (Figure 3.4.c). In the equation, V_x corresponds the printing speed along the axis, V_a is the extrusion speed, D is the diameter of the inlet filament and the d is nozzle diameter.

$$V_x / V_a = (D / d)^2 \tag{3.1}$$

It was observed that the flow rate increases proportionally to the extrusion speed. It is indicated that the increasing extrusion speed forces the material flow to speed up, thus the length of extruded material increases while its diameter decreases. As a result, the extrusion system was confirmed to be applicable to the actual printing process. This is because; based on the conservation of mass, the amount of entering and exiting material trough the extruder was observed to be equal in the initial tests. In this first step, it was ensured that there are no obvious defects in the nozzle tip or extruder mechanism, such as machining error or electromechanical distortions, which may cause unaccountable errors in later experiments. As second step, the actiual printing process was realised on a steel surface. The distance between the nozzle tip and the surface was measured via laser displacement sensor, so that the deposited material is not over-pressed by the nozzle tip, or not extruded into the air. Then the microstructure of the lines both collected inside the liquid and deposited on the surface was investigated via Scanning Electron Microscopy (SEM).

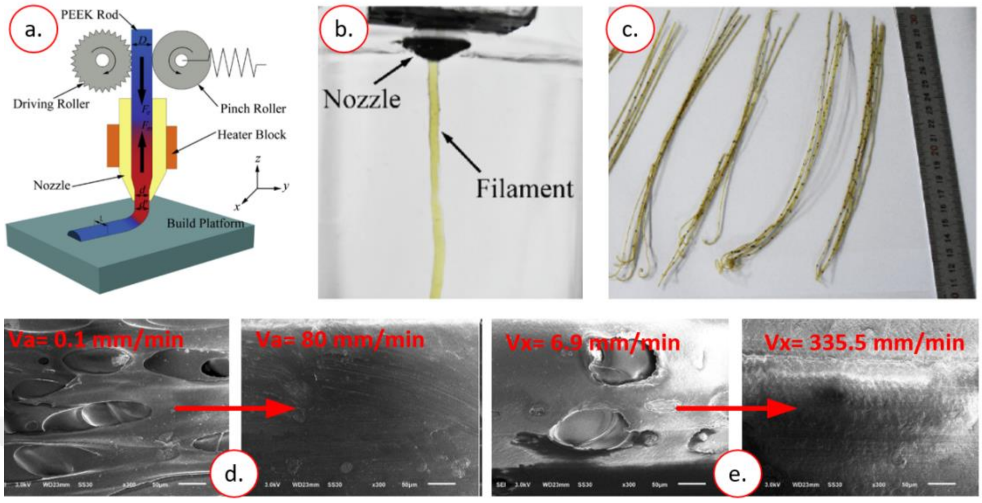

Figure 3.4. a The extruder system, b. Line extrusion into the liquid c.The diameter measurements of the extrudates, d. Surface morphology enhancement by increasing print speed, e. By increasing extrusion speed (Geng et al., 2018)

It is concluded in the study that the extrusion speed is a critical parameter for the dimentional accuracy of the physical part to the digital one. It directly affects the melt pressure proportionally, thus the width and the surface morphology of the deposited lines. The higher melt pressure may prevent the surface defects and the diameter to be deviated as also reported (Figure 3.4.d). Furthermore, the printing speed was stated to be also important parameter which needs to be configured according to the selected extrusion speeds (Figure 3.4.e). This issue was attributed to the thermal interactions between the liquifier, nozzle and the deposition surface. It is understood from this study that; The extrusion speed is required to be configured in between the useful interval taking into account the nozzle diameter and the printing speed; It is then the dimensional accuracy can be achieved in the final part; The extrusion speed can be configured via a parameter of Extrusion Multiplier (Flow Rate) during the slicing step of the digital part.

A nozzle clogging is another process failure which is oftenly caused by excessive material feed through an orifice with a small diameter. The mechanical pressure created by the gears in the extruder mechanism determines the flow force accumulated in the orifice region. It was suggested by Tlegenov et al., (2017) that the amount of force can be measured and customized by an accelerometer attached on the extrusion area as shown in the Figure 3.5.

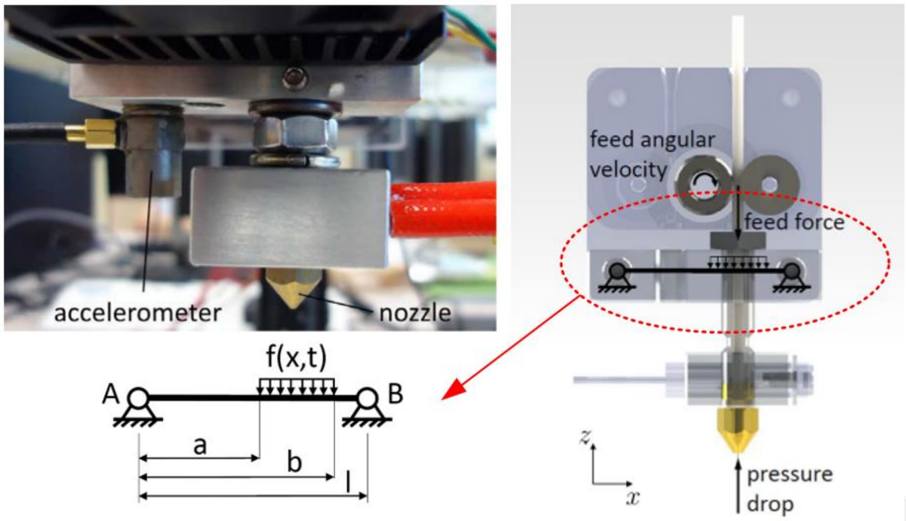

Figure 3.5. An accelerometer attached on the extrusion area for the force measurement (Tlegenov et al., (2017))

The force generatead by the extruded gear was modelled based on a distributed force on a fixed beam from two tips. While modeling, the forces generated during the extrusion process are taken as a basis. The extrusion process starts with the solid filament being pushed into the melting zone by a gear driven by a stepper motor. At this point, the filament acts as a piston and creates a propulsive pressure on the molten material. The amount of thrust released in this region also determines the actual flow rate of the melt. If the force is applied less than it should be, under extrusion, if it is applied too much, over-extrusion errors may occur. Moreover, when excessive force is applied, even buckling of the solid filament can occur, causing the material flow to be interrupted. It should be noted here that the amount of force to be generated is directly related to the angular speed of the gears and the motor power in the extruder mechanism. The fact that these extrusion properties can be adjusted with the flow rate parameter reveals the importance of the need to calibrate this parameter precisely. In the mentioned study, the RepRap Arduino Mega Pololu Shield (RAMPS) control board was employed. Thanks to the open-source community, the way of calibrating the flow rate of the extrusion is provided in the official RepRap calibration guidelines (Website, 2022l). The calibration process independent from knowing the gear diameter, rotation speed or the drive power of the motor, can be made by several repetitive steps using the Equation 3.2.

$$New\ Flow\ Rate = \left(\frac{Input\ Line\ Width\ (in\ sciler)}{\text{Previous}\ Line\ Width\ (extruded)} \right) \chi Current\ Flow\ Rate \qquad (3.2)$$

In order to apply this method, a single lines are first deposited on a surface, with a default line width and default flow rate (generally %100) values in the slicer software. After than the extruded lines' width are measured. If the digital line width value does not match to the digital value, the same equation with the previously measured (deviated) line width value is applied. This way, the new flow rate value required for obtaining the correct width of extruded lines that should be, is achieved. In this way, the correct width size of the deposited lines is reached with the new flow value. If the deposited line width cannot be obtained in the second round, the same process is repeated with the new values. This process is continued until the digital and real measurements exactly match each other (Korkut and Yavuz, 2020). After the flow rate parameter is adjusted appropriately, lines of desired width can be obtained. However, no matter how smooth the lines are, if they cannot be sufficiently bonded to each other, distortions occur both within and between the layers. In addition to the amount of bonding, joint angles and alignment orientations are also critical for the mechanical strength of the part.

3.3. The Material and the Energy Consumption in AM Processes

There are numerous studies available in the way to enhance the mechanical properties of parts printed with AM devices. As mentioned in the previous sections, the strength of the part can be improved by some sort of configurations on the basis of controlling the amount material feed. However, when a printing process is required, the subjects of material and the energy consumption must be considered. Due to the nature of AM processes, only as much material as needed is used in the production of parts. However, as the part size increases, the processing times become longer, and accordingly, both material and energy consumption increase. As mentioned in the previous sections, with some parameters such as flow rate, infill density and wall thickness, the material requirement can be reduced to some extent. However, for a truly eco-friendly production process, more comprehensive examination of AM devices is needed (Wohler, 2018). To do this, the printing processes can be classified due to its operational steps as given in the Table 3.1.

Table 3.1. The operational steps of a printing process

Printing Operation		
Preperation	**Printing Period**	**Post-printing**
Bed heating	Built parameters	Cooling
Nozzle heating	Motorised motion	Idling
Calibration	Extrusion	
Priming	Heating	
Idling	Idling	

Each print session requires some kind of preparation step. During these steps, the nozzle and the deposition bed must be sufficiently heated. Meanwhile, the appropriate distance between the bed and the nozzle tip should generally be calibrated before each print for proper extrusion and adhesion. Also a clean nozzle must be provided by evacuating the residual material left from previous prints (priming). When the printing is initiated, the motors should provide the smooth axial motion in order to extrude the semi-molten polymer into the appropriate coordinates on to the heated bed. After the job is accomplished, it is necessary to wait for the part to be cooled for a sufficient time avoiding the plastic defects. Additionally, an additional time should be accounted for the side components those drain energy such as controllers, sensors, lightening and LCD monitor during the whole process (the idle time). The most important factor for determining the consumed energy in the process is the built parameters. That is, the time, the amount of material and the consumed energy strictly depend on the build parameters defined in the slicer software. It is reported by many sources that the parameters of layer thickness, nozzle temperature, heated bed temperature and the head speed are the most responsible ones from the energy consumption in a printing process (Song et al., 2018; Suarez et al., 2020; McAlister et al., 2014; Baumers et al., 2012). Based on these parameters, the energy consumption was experimentally investigated using an open-source, custom build FFF device in the study of Korkut and Yavuz, (2022c). The device was build based on the cartesian-type motion mechanism and operated with the Makerbase (MKS) control board having an open-source Marlin firmware. The power consumption was measured via online power quality analyser (Fluke 43B). As a sample, standart tensile testing specimens were selected and printed (Figure 3.6).

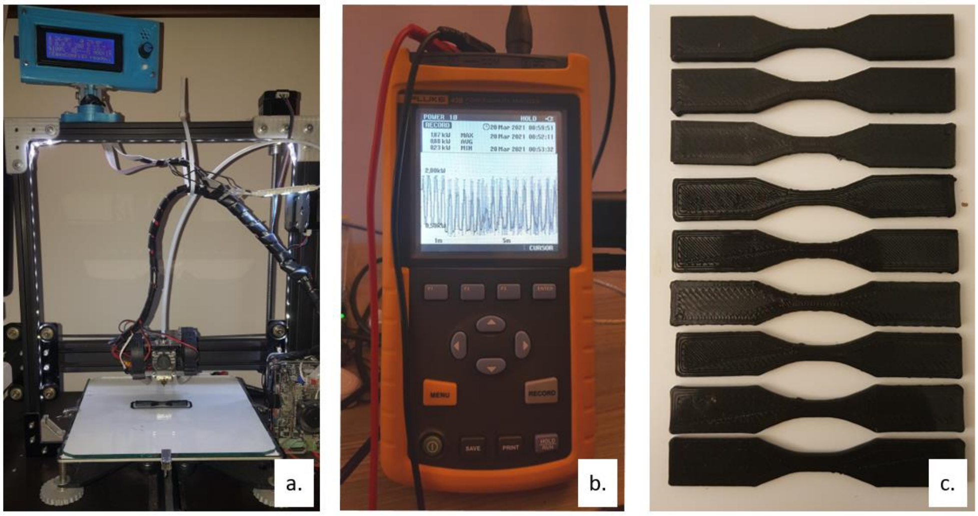

Figure 3. 6. a. Open source FFF device, b. Power quality analyser c. Printed samples

The design of experiments was planned with method of Taguchi Orthogonal Array. The results were evaluated based on Signal-to-Noise Ratio and the Analysis-of-Variance (ANOVA) analysis which are widely accepted and powerful statistical tools in the field of experimental engineering. The Orhogonal Array designs provides finding solid process parameters by minimizing the variance of input parameters over the output responses. By the design, the noise (uncontrollable disturbing factors) on the inputs is aimed to be reduced as much as possible. In this way, the deviation in the desired target is minimized. When the deviation is reduced, the effectiveness of the inputs over the output response become more distinct. The relation between the input and the output is measured by the Signal-to-Noise (S/N) Ratio which corresponds the quantitative measure of the process performance. In the Taguchi analyses, the S/N Ratio is desired to be high since it represents the improved quailty of the job (Roy, 2010). From an engineering point of view, this method provides minimum but sufficient number of experiments while ensuring the validity of the obtained results to be generalised. Effort, test times, and product costs are the most important aspects of engineering.

In ANOVA analysis, the S/N ratios found in the Taguchi analyses are accounted for revealing the percentages of each parameter in accordance with their effectivenesses. In this way, the dominant parameters presenting the contribution of above %5 can be interpreted with their exact amount of the percentages (Roy, 2010). According to the results, it was observed that the layer thickness and platform temperature parameters valid for each printing process have a significant effect on both power consumption and processing time. Because when these parameters are optimally adjusted according to the job, as also recorded in the tests, the energy consumption can be reduced within shorter printing times. The effects of these parameters on the need of energy-time have also been supported by revealing their percentage contributions. As a result, a reduction of 6.91% in energy consumption has been achieved. In addition, the printing time was also reduced significantly (Korkut and Yavuz, 2022c). The mentioned statistical approaches are preferred also in this thesis study due to their features provided in the evaluation of the experimental results.

The material waste is another subject that needs to be further analysed beside the energy consumption. Both the device itself and the user intervention may cause excessive material usage in printing operations due to several issues. The reasons behind the material waste were systematically investigated by collecting data from a number of devices belongs the attendees of an extensive workshop by Song and Telenko, (2017). As the methodology of evaluation, the failure types causing a material waste were classifed as the user error, machine error and desing error. Errors leading to material loss were recorded in a large number of devices under observation and were recorded in the relevant class. After then the findings were tabulated as in Table 3.2

Table 3.2. Failure types ended with the material waste (Song and Telenko, 2017)

	Failure caused by:		
	User	Device	Design
Unused Filament	●	●	
Platform Heating	●	●	
Part Shape	●		●
Layer Shift		●	●
Support Removal	●		●
Printer Stops	●	●	●
Calibration	●	●	
Skip Layers		●	
Non-Physical Defect			●

To be more specific, the print job may be failed due to the several reasons which result in a material waste. That is, the nozzle may block or the operation may be interrupted by a user or by electrical issues. In this case, the filament used up to this point is wasted and the job needs to be repeated. For another case, the operation may fail due to the part due to the wrong calibration of the clearance between the nozzle tip and the platform. That is, if the gap is adjusted too much, the filament is extruded on air and the material cannot be deposited properly. In contrast, the deposited lines are over-compressed by the nozzle if the gap is too small. In both cases, the layers become extremely deformed and do not allow a healty layering process. Most importantly, specifying the wrong parameter during the slicing step can lead to serious material wastage. The slicing process, which is the most critical stage in printing processes, should be determined in accordance with the capacity and the ability of the device. For example, if the material is not located correctly in the built chamber, more support material will have to be used than necessary. Similarly, the heating of both the nozzle and the platform must be handled in suitable levels according to the material's thermal properties. Otherwise, such failures as warping or cracking in the part may occur. In addition, critical parameters such as infill density, shell thickness, line width, layer height should be adjusted to meet expectations such as surface quality, functionality and durability from the part. To date, numerous parametric studies have been carried out to improve the end-product properties. However, more detailed researches, regardless of the part model and the device features in order;

- ✓ -to increase the strength,
- ✓ -not to waste a material,

while,

- ✓ -not sacrificing the functionality or the surface quality
- ✓ -only by optimizing the process parameters,

are still needed. Therefore, the mentioned issues are also focused in this thesis study.

3.4. The Adaptation of FFF Infrastructure to the MDJ Operations

AM devices based on the direct part manufacturing method involve subsystems with many common processes and equipments. That is, a movable system along the three axis driven by a motor, some sort of heating system, a deposition platform, a material extruder, a nozzle, a control board, a monitoring screen, sensors, a power suppy and other miscellaneous hardware are the essential components for such a device. However, the way of deposition determines the details of these subsystems. The main distinction between the different methods is mostly the differences in extrusion and deposition mechanisms. For example, in the FFF devices, the filament type material is extruded towards the heated area by a gear system, the material is softened in that area, then it is forced by the non-heated part of the same material towards the deposition platform through an orifice. The operations for the material deposition in the droplet generators can be said to be similar; the material is driven into a heated region, and forced towards outside through an orifice. However, the methodology of driving the molten material is different. The required thrust pressure needs to be supplied externally via various actuation mechanisms in the droplet generators. In this context, although the FFF and MDJ methods have many common points both in subsystems even thought in their principles, the difference in the actuation system brings the need to examine the MDJ system to be investigated on its own specifications. A conceptual image of the two systems is provided in the Figure 3.7.

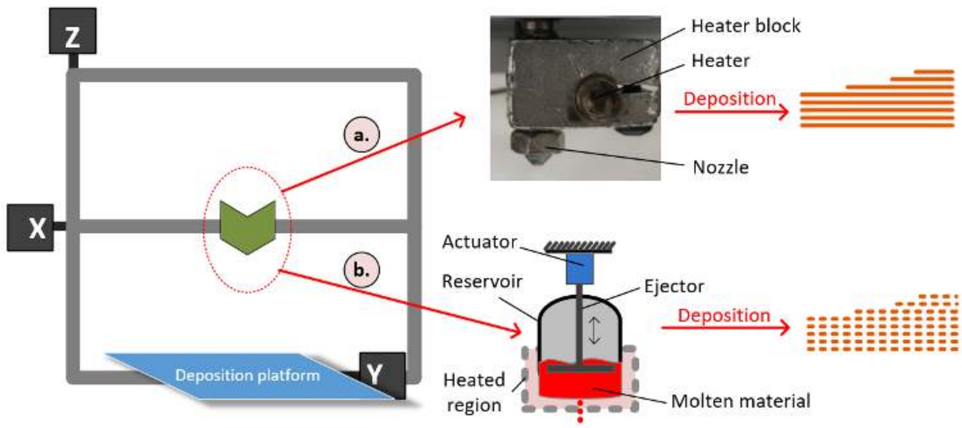

Figure 3.7. The extrusion area of the a. FFF system, b. MDJ system

In addition to the actuation mechanism, the factor of the base material to be melt being metal rather than a polymer complicates the operational conditions. Therefore, many components and sub-processes need to be investigated separately. At the beginning of these are the heating methods, the feeding system to transfer the material to the heating zone and a reservoir design where the melted material can be stored. The reservoir to be used must be in a structure that will allow all the operations listed, even to carry other parts such as actuator parts, heaters, coolers, insulators, sensors. Due to the mentioned, but not limited to, process conditions, details on the MDJ method will be provided separately in the following sections.

3.5. The Methods and Equipment Used in MDJ Systems

The metal droplet generator can be integrated to movable systems that of the FFF type material extrusion devices. However the the body of generator itself needs to be equipped with a special components to be able to create a droplets made of metal. The droplet production process is much more complicated than pushing a filament through a gear and forcing it to flow out of the orifice as in FFF processes. Therefore, in this section, the necessary components for MDJ processes are introduced and some important methods applied in the literature are presented.

First of all, an actuator that can operate in a healthy way at temperatures that will ensure the melting of the material should be selected. When the suitable actuator is mounted on the generator body, it is necessary to attach a sort of transfer mechanism to transmit the vibratory motions towards the ejection zone. The ejection area is one of the most critical body part of the generator. This is because, the melting operation is done in this region. Therefore, the structure of this body parts must act as a reservoir for the storage of the molten material. At the same time, it must resist the elevated temperatures required for the melting operation. Moreover, the design should allow the material inlet, contain the nozzle for the liquid ejection and carry all the necessary components such as heaters and sensors. A serie of studies were conducted by Lee et al., (2005, 2008a, 2008b) on generating neat droplets as a function of generator body design properties. It was developed a solder-based (Bi58Sn, Pb-free) metal droplet generator using a piezoelectric actuator. The setup was equipped with a precise distance adjuster for the gap between the piston tip and the orifice. The most important feature of the system was reported to be a custom machined piston geometry and replaceable nozzle part. The descriptive image for the setup is given the Figure 3.8.

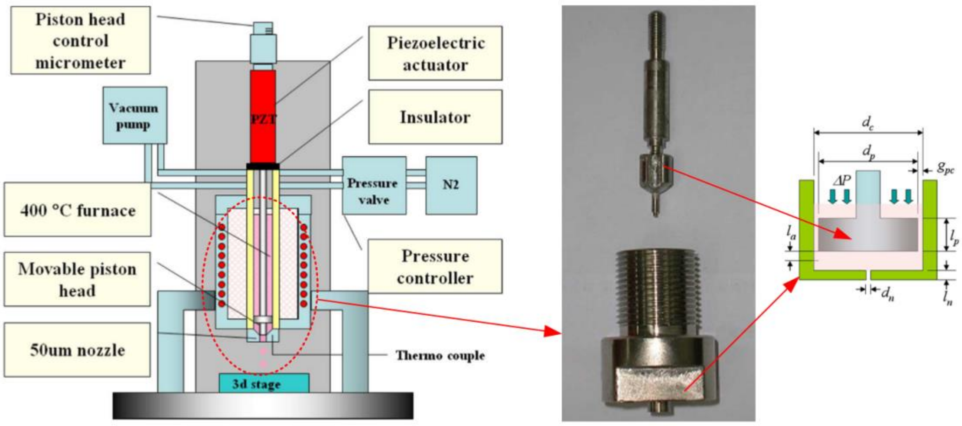

Figure 3.8. The body of the droplet generator, piston-like rod and the ejection area (Lee et al., (2005; 2008a; 2008b))

While assembling the actuator into the body, an insulator was mounted between the piezoelectric actuator and the heated area. This way, the function of the piezoelectric material was prevented to be failed due to its nature. The custom-made piston was connected to the other side of the insulator and the vibration was then transferred into the ejection region. The droplet generation performance was tested by adjusting the distance between the piston and the orifice, the ejection frequency and the amount of backpressure. By establishing such a device, it was reported that the droplet size can be varied on demand owing to the adjustable gap distance in the ejection area. The changeable nozzle was another feature which allows the work with orifice having various diamater. Not only the change in diameters, it was also provided a possibility of quick maintenance when a problem occurs in orifice such as clogging and failed sphericity in shape. It was also stated that the nozzle dimensions are also critical parameters for proper ejection process. In addition to the orifice-to-piston distance, the geometry of both the piston tip and the inner reservoir should allow the fluid flow towards the nozzle as denoted. More specifically, the necessary amount of pressure difference between the upper and bottom surface of the piston tip must be provided, so that the viscous effects are overcome, then the liquid ejection occurs propertly. Thereby, external pressure assistance was also adopted to support the thrust pressure of the mechanical impacts. As a result, succesful vertical towers were deposited by the modulation of the mentioned parameters in design as shown in the Figure 3.9 (Lee et al., 2008a).

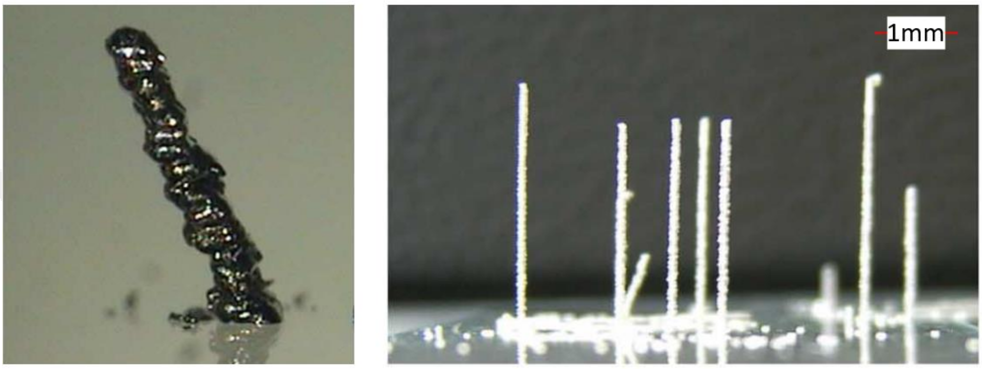

Figure 3.9. Vertical columns deposited by solder droplets (Lee et al., 2008a)

To be able to characterize the droplet generation operation regarding the device itself, an experimental procedure was developed as; filling the solder material into the non-heated container, initiating the heating process, adjusting the gap, setting the backpressure support, setting the actuation parameters and starting the ejection, respectively (Lee et al., 2008b). Although there was given limited information on the process parameters of material feeding into the heated reservoir, these studies are solid guides for consistent droplet generation and design of a functional generator due to the information provided.

Based on DOD method, a droplet generator was developed by Sohn and Yang, (2005) using a solenoid vibrator instead of piezoelectric actuator. This way, the necessity of extensive insulation for the actuator was eliminated. The solenoid actuator was mounted on an adjustable slot which provides an adjustment of the piston positioning versus the nozzle hole. The reservoir, nozzle and the piston rod were machined from a stainless steel. At this point, it should be noted that it required for many high melting point material to be kept in a container that has a non-wetting characteristic. This way, it can be prevented that the liquid material to grip the inner walls of the reservoir excessively and not to be ejected as reported. For this reason, there are many studies available adopting the Silica, Alumina, Zirconium based alloys and glass based ceramics (Berg, 1993). However in the study, it was proved that the stainless steel is also suitable for the Tin alloys for droplet generation. To facilitate the liquid flow, the melting temperature (around 300 ^{o}C) was kept much above the actual melting point (around 190 ^{o}C) of the material. The soldering material (Sn63Pb37) was adopted for the experimental investigation. For the proper ejection of droplets, it is mainly focused on the crucible geometry at the impact region (Figure 3.10).

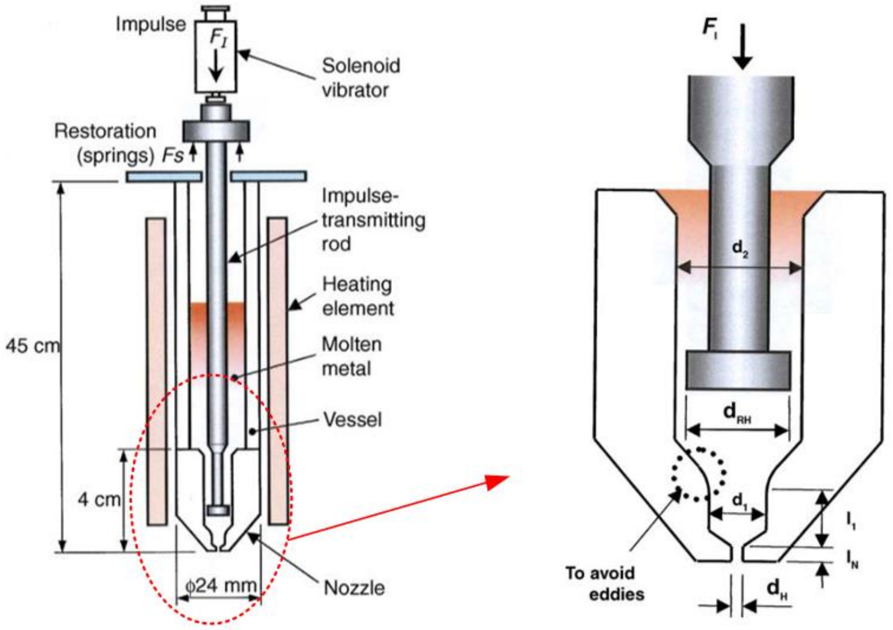

Figure 3.10. The adopted droplet generator system and the dimensions of ejection region (Sohn and Yang, 2005)

Based to the conservation of the mass of liquid between the collected portion inside the reservoir and ejected volume, the droplet sizes were modulated with a serie of experiments. That is, the initial mass, before the impact, between the piston tip and the nozzle must be equal to the sum of liquid left in the same place after the impact and the back-flew liquid through the capillary gap at the lateral piston walls. To be able to prevent the excessive back-flow, it was stated that both vertical and horizontal clearances between the piston tip and the inner walls of the reservoir must be kept suitably in when the high viscosity materials such as metals are ejected. For further, it is noted that the thickness and the diameter of piston tip itself had a critical importance on droplet diameter. By configuring the thickness of the piston tip to 2 mm, the diameter to 5.95 mm and the impact stroke to 0.5 mm, the droplets having less than 5% deviation in diameter were succesfully obtained. It is understood from the study that in the droplet formation processes, not only the particle size but also the amount of fluid exchange in the reservoir is critical. Although there is insufficient information availabe on how much or how the required material should be fed in a reservoir, the study provides a qualified perspective on the structural concept of MDJ processes.

The droplets having a small diameter with a good sphericity was generated via mechanical impacts in a two-step study. As a first step, He et al., (2014) developed a solder based (Sn63Pb37) droplet generator consisting piston-diaphragm couple. As a working principle, the piezoelectric actuator was mounted on the top. As a feature of the device, a flexible and thin sheet, made of beryllium bronze sheet, called diaphragm, was used as a both seperator and insulator between the piezoelectric material and the heated region. The actuator, diaphragm, transfer rod, diaphragm and piston rod were used as motion transmission sequence. In this case, the vibrations were transmitted to the ejection zone without loss through the diaphragms. In addition, water circulation was implemented between the two diaphragms for cooling purposes. In terms of structure, the system was made resistant to deterioration that may result from high temperatures. The general view of the mentioned device is given in the Figure 3.11.

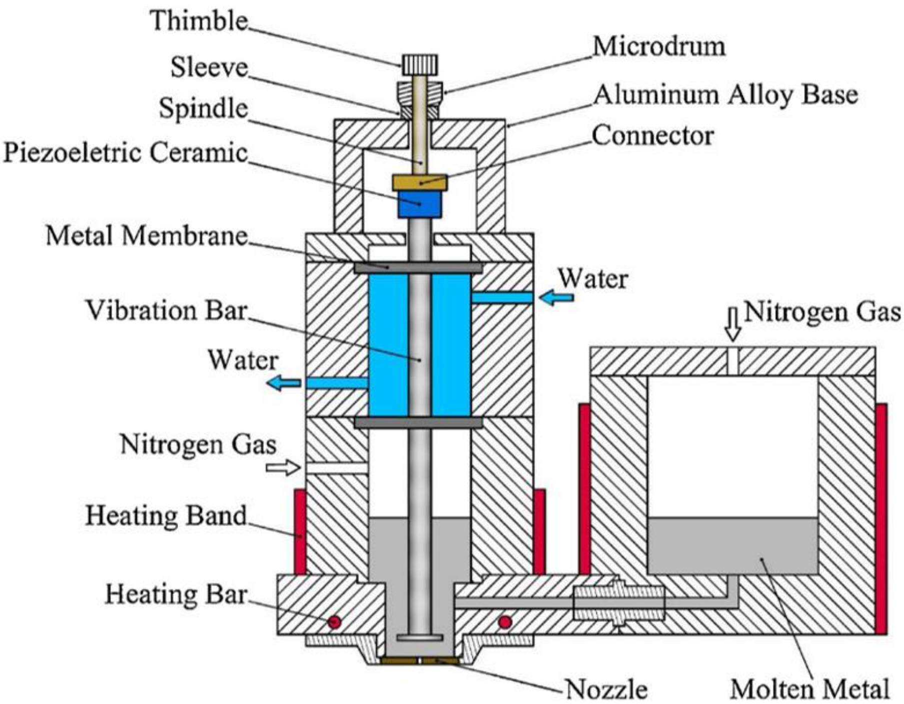

Figure 3.11. A membrane-based metal droplet jetting system (Ma et al., 2019)

According to the initial experiments, the droplets having diameters smaller than 100 um are achieved. However, it was required to characterize the droplet diameter with further investigations. This is because, if the ejection conditions are not adjusted within a useful interval, a satellite droplets or no droplet generation occurs as observed. To do this, it was reported that the three parameters should be investigated as; actuation voltage, the pulse duration and the temperature of the reservoir. The effects of three parameters were then evaluated taking into account the dimensioning of the ejection area. To be able to control the droplet size, it was modelled the flow of the molten metal as incompressible, continuous, homogeneous, Newtonian and laminer since the predicted Reynold number as found to be less than 2320 (Chen et al., 2013). Taking into account the flow characteristic as well as the conservation of mass, it was intended to predict the ejected droplet volume through the flow rate of the molten liquid. The predictions were made based on the total flow rate of the flowing liquid towards both outside from the nozzle and back to the reservoir through the lateral gap. The flow rate of the ejected liquid was defined based on Hagen-Poiseuille equation (Equation 3.3) as given as follows;

$$Q_N = \frac{\pi d_N^4}{128\mu l_N} \Delta P_N \tag{3.3}$$

Similary, the flow rate of the back flowing liquid is;

$$Q_R = \frac{\pi d_p \delta^3}{12\mu l_P} \Delta Pp \tag{3.4}$$

Then the total flow rate was given as;

$$Q = Q_N + Q_R \tag{3.5}$$

Where the Q_n is flow rate of the molten metal through the orifice, Q_r is the flow rate of the back flowing liquid, d_N is the orifis diameter, l_N is the thickness of the orifice plate, d_p is the piston diameter, l_P is the tip thickness, δ is the lateral gap distance, μ is the dynamic viscosity of the liquid, ΔP_N is the pressure difference between the upper and bottom level of the orifice plate, lastly the ΔPp is the pressure difference between the upper and bottom level of the lateral gap region. The dimensional parameters were defined as in the Figure 3.12.

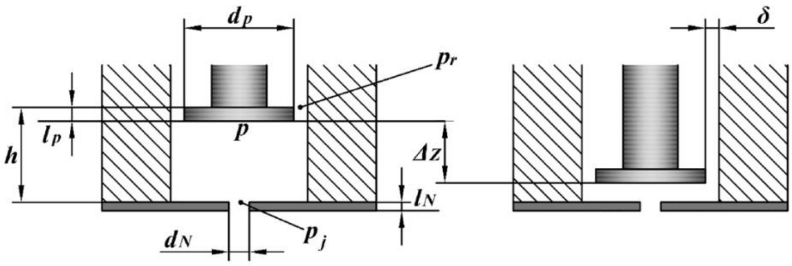

Figure 3.12. The dimensions of the ejection region (Chen et al., 2013).

After the calculation of the total flow rate, the Equation is derived into the pressure balance, then to the volume of the droplets as given in the Equation 3.6.

$$V = \frac{\pi(3\mu l_p d_p^2 d_N^4 \Delta z + 2d_p P_b \delta^3 d_N^4 t)}{\mu(128 d_p I_N \delta^3 + 12 l_p d_N^4}\qquad(3.6)$$

According to the single droplet volume derived from the Equations 3.3-3.5, it was observed that the time duration (*t*) of the pulse signals in the duty cycle was also a critical parameter for the droplet's volume. Besides the *t* and the other dimensional parameters, the melting temperature also was found to be determinant the droplet size due to the fact that it has an effect on the dynamic viscosity of the liquid. Using these equations derived from the flow rate and the pressure balance of the liquid, the stable droplets were finally able to be formed. Regarding the pressure balance, it should be noted the the material was fed from an external reservoir into the ejection are by an external pressure supplement as can be seen Figure 3.11. At this point, some interpretations can be made that negatively affect the process in general. First, the number of components (heaters, containers, sensors, valves, pipelines and others) that must be used in the external storage had to be increased. Consequently, in addition to the cost increase, this situation complicates the controlling issues droplet production process even more. Moreover, the issue of how much material is fed to the ejection zone was not mentioned in the study. At this point, it should be taken into account that the material fed inwards may also create an extra hydrostatic pressure inside. Lastly, the amplitude of the piston stroke, thus the pressure generated by the impacts was another unknown. Therefore, there is a need to investigate in more detail whether this amount of pressure will affect the pressure balance adopted in this thesis study. In this way, droplet size characterization can be done more comprehensively.

In the study of Luo et al., (2016), the amplitudes and the pulse widths of the mechanical impacts were analysed in detail. The main target was obtaining uniform and micro-sized droplets by impact-driven system. The impacts were created by a solenoid actuator and transferred into the ejection area via a two seperate piston rods in seperate processes. (Figure 3.13.a) The first rod was attached on the actuator and was set to hit to the second one to transfer the vibration. The second one was equipped with two types of a stopper: a return spring (Figure 3.13.b) and a solid metal ring (Figure 3.13.c). Then the transferred vibrations on the second rod was mathematically modelled based on a simple a free damped vibration (mass-spring-damper) system (Figure 3.13.d)

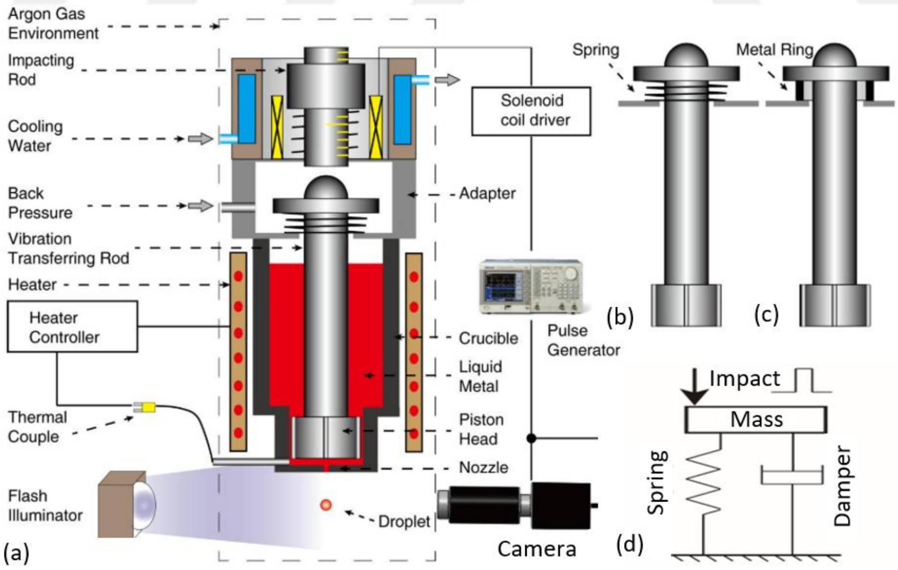

Figure 3.13. a. The proposed setup, b. Spring loaded piston c. Metal ring loaded piston d.The mathematical model of piston rod (Luo et al., (2016))

The droplet sizes and their flight velocities were first simulated via numerical analysis. As an input force, the value calculated from the mathematical model was used. After then, the experiments were initiated with the ejection frequency of 1 Hz, nozzle diameter of 0.1 mm. The sizes and the velocities of individual droplets were measured via the real-time images captured via high-speed camera. According to the test results, as the piston stroke reduces, the size of the droplets also tends to decrease. In contrast, the droplet size increases when the duration of the pulse width increase. The simulation results through vibration analysis were observed to be in a good agreement between with the experimental results. That is, the upper and lower limits of the vibration were determined in order to form a single droplet without dripping or without satellite formation. When the amplitude exceeded the upper limit, the amount of liquid to be ejected increase, the neck formation appears in the nozzle outlet when the impact was at peak-point. When the piston is released, some of liquid flow back towards the reservoir, which result in a break-up of a big drop, instead of droplets. During the break-up, random-sized small droplets also break from the drop. This phenomenon leads a droplet formation having unpredictible diameters, precluding the uniformity in droplets generated. It is also stated that it is necessary to ensure that the pulse-width amount is at a value that will allow the droplet to break. That is, when the half-cycle of the impact is completed, the nozzle becomes blocked by the bottom of the piston. In this period, the flow towards outside is cut and the liquid is forced to break from the reservoir. The surface tension re-forms the detached liquid shape into a sphere. To be able to keep the amount of droplet seperation equal in every impact cycle, it is required to reveal the optimal (minimal) pulse duration. It was proposed that only in this way that a proper droplet formation process can be achieved. The study is important as it is a pioneering investigation for the pulse amplitude, and its electrical inputs such as pulse width and its duration. However, as a limitation of the study, there was no continuous material feed into a melting region established which result in a discontinous ejection process. In other words, it is required to re-fill the material, re-heating it, the re-start the actuation in order to keep the ejection continuously. It is also necessary to disassemble and reassemble the generator to fill the reservoir manually which cause time-taking labour efforts. Therefore, to keep the ejection process as long as it is desired, the further investigations about the continuous material feeding are still required.

The similar deficiency can be seen in the study of Zhang et al., (2017). The feed of material feed was insufficiently explained. However, the droplets were deposited with a quite well precision in a vertical orientation, without a support structure. To do this, one-dimensional heat transfer model was implemented in the subject of droplet's coalescence. The theoretical investigations were correlated with the amount of the fusion and the coalescense between the droplets. The schematical setup of the system can be found in the Figure 3.14.

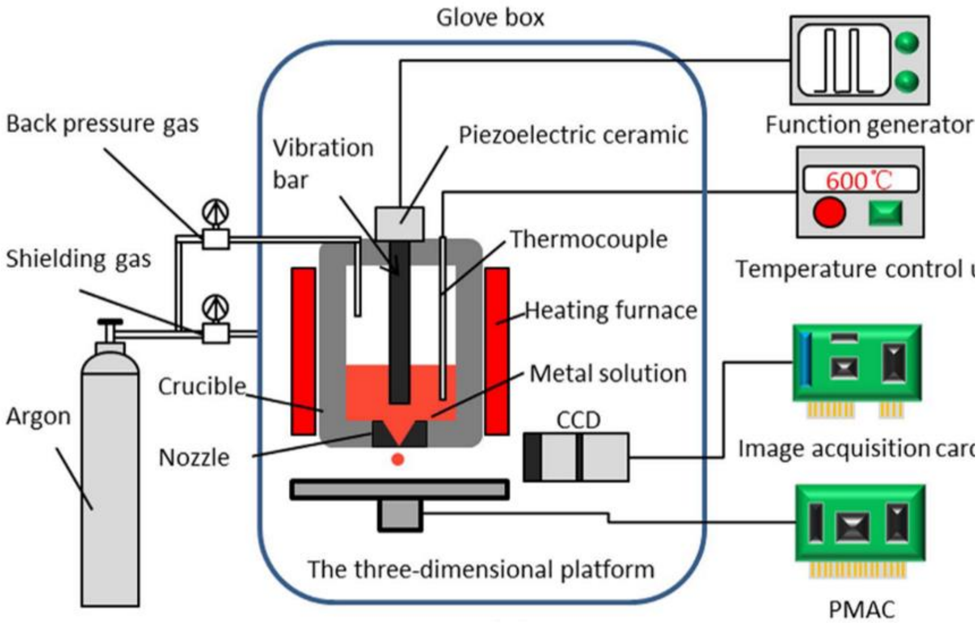

Figure 3.14. The schematical view of the operational flow (Zhang et al., (2017))

This study is one of the first that has examined the droplet's bonding in terms of proper deposition. In the study, the inclanation angle was calculated by taking into account the frequency and the head speed of the ejector. The correlation between them was named as the Offset ratio, which was described as a ratio of the droplets' distance to a diameter of a single droptet's diameter. The relevant Equation 3.7 is given as follows;

$$\xi = \frac{w}{2r} \tag{3.7}$$

where the *w* indicates the distance between the sequential droplets and the *r* for the radius of an individual droplet. In the following, the fusion ratio was described as follows (Equation 3.8);

$$\delta = \frac{h}{2r} \tag{3.8}$$

where the *h* is the droplet's height. Finally the inclanation angle of the column consist of droplets can be calculated based on the Equation 3.9 as given as follows (Gao and Sonin, 1994);

$$\theta = \arccos \frac{\xi}{\delta} \tag{3.9}$$

The quantities given in the formulations were visually described in the Figure 3.15.

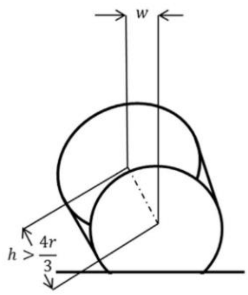

Figure 3.15. The deposition criteria for the droplets with dimentional parameters (Gao and Sonin, 1994);

However the issue of droplet bonding was stated to be a complex phenomena. This was addressed to the aggressive thermal behaviour of the molten liquid. In order to compansate the uncontrollable situations, it was required to apply the flow characteristic in accordance with the low ***We*** numbers as reported. Since the greatness of the *We* can be attributed to the time of droplet landing (impacting (Araki and Moriyama, 1981), spreading (Trapaga et al., 1992), re-melting (Zarzalejo et al., 1994) rebound (Schiaffino and Sonin, 1997) and the permentant solidification (Henry and Stavroz, 1996), it was emphasized as a must to determine the value of ***We*** number. As a requirement of the calculation of *We* value, the frequency and the head speed were taken into account in the study. It was concluded that the capillary effect due to the resistive liquid force can be beaten by configuring the impact velocity. Since the velocity can be configured with the ejection voltage, the spreading amount can be controlled at the low ***We*** numbers. The bonding formations were also classified as “no melting”, “partial melting” and “excessive melting”. These categories were stated to be calculated with the given Offset ratios. As a result, a system capable of depositing inclined microstructure by manipulating the fusion interface with a dynamic control of the impinging droplet was introduced.

The placement of the droplets was investigated in a comprehensive study of Zhang et al., (2019). The deposition types were modelled taking into account the spacing between the droplets, the offset ration and the spread diameter. The droplet ejection was provided via a piston-like rod, connected to the piezoelectric actuator. As a base metal, both the solder alloy (Sn63Pb37) and the Aluminum alloy (AlSi12) were adopted. To be able to provide a melting process of high melting point materials such as Al, the droplet generator setup was equipped with a powerful heater system capable of operation around 750 °C. However, the methodology of heating was not provided. For further, the amount of material collected inside the reservoir, the way of material supplement and the material inlet region were not available. The presented system is given in the Figure 3.16.

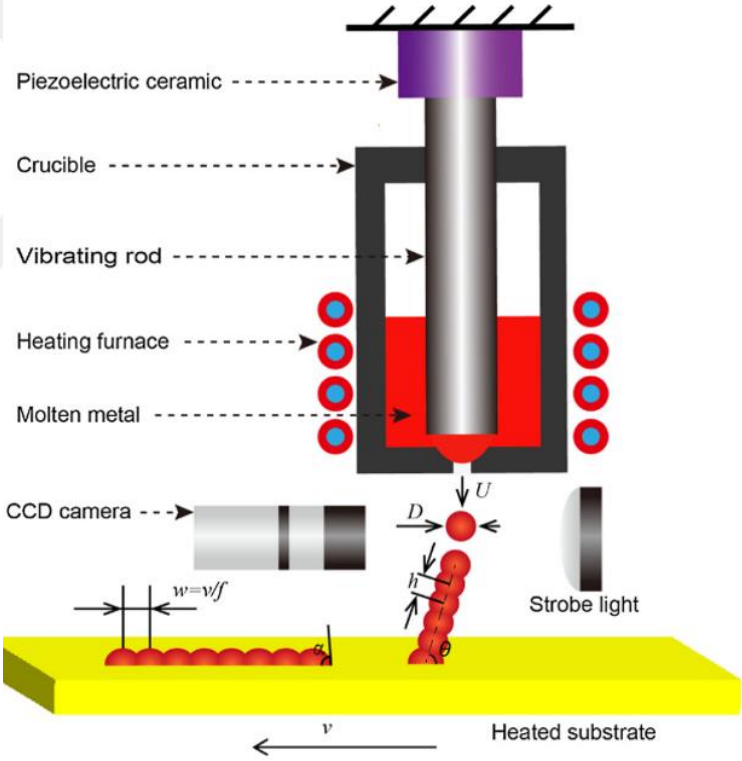

Figure 3.16. The established droplet generator (Zhang et al., 2019)

Although there is insufficient information available about the physical structrure, the qualified visual inspection methodologies was implemented. That is, a single droplet at the time of impact was able to be captured with its all periods during the solidification. The image capturing was the key process to be able to reveal the droplet's impact behavior, thus the solidification and finally the deposition morphology. In the Figure 3.17, the impacting periods of a single droplet is presented.

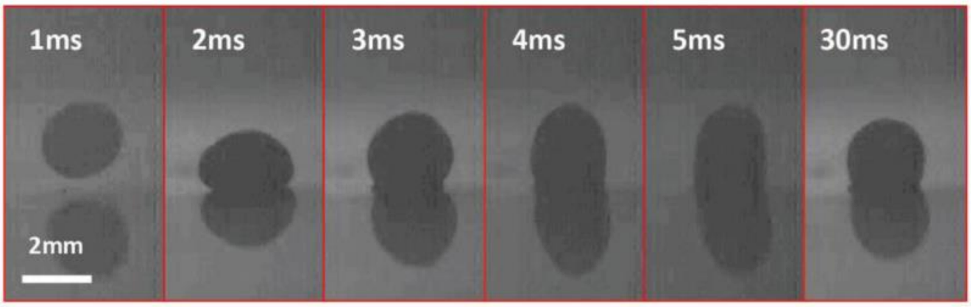

Figure 3.17. The impacting periods of an individual droplet (Zhang et al., 2019)

It can be said that the image capture capacity of the CCD-type camera used was over 1000 FPS. In the figure, the spherical shape of droplet before impact (at 1 ms), the time of the first impact and the spreading (at 2 ms), rebounding (3 to 5 ms) and the final shape of the solidied droplet (at 30 ms), respectively, were clearly captured. Benefiting from the droplets instant shape during the deposition, the deposition characteristic of sequential droplets was able to be identified in details. This study contributes the literature by presenting an actual behaviour of the ejected droplets not only theoretical basis, but also the real-time photoshooting to reveal the droplets conditions during the deposition. This study makes an important contribution to the literature, as it provides not only theoretical but also quality footage showing the actual behavior of the deposited droplets. Furthermore, the wetting characteristic and the droplet size versus the ejection conditions such as frequency, the head speed, platform translation speed and pressure generated during the impact were also examined experimentally. The findings obtained in the study are quite qualified and pave the way for the users to deposite the droplets in the desired morphologies.

In another study, which the previously explained study was also inspired by, a similar device was set up (Zhong et al., 2014). In this study, Al droplets were ejected through a solenoid actuator with a two-segment piston rod attached on it. Although the material feeding issues and the deposition morphology were been studied in detail, the detailed presentation of the piston structure makes this study important. The device and piston structure are shown in the Figure 3.18.

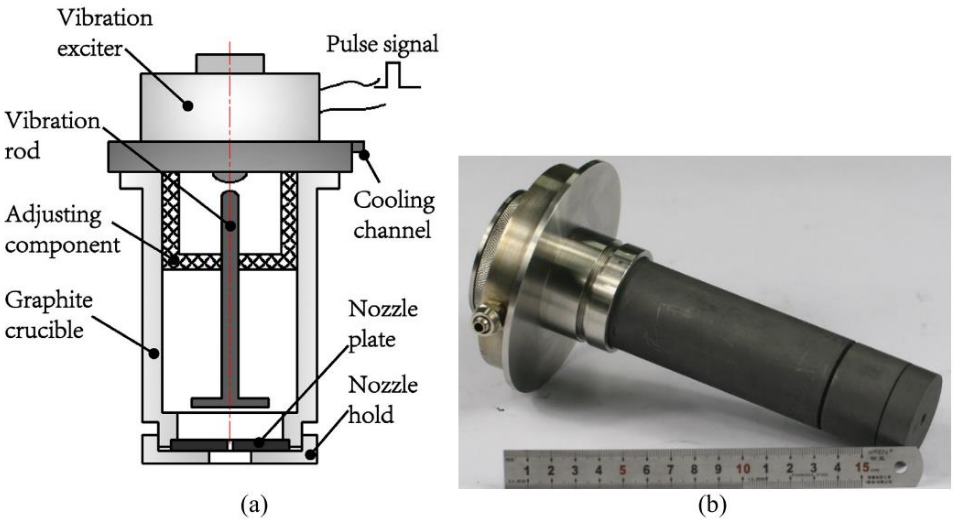

Figure 3.18. a. The structure of the droplet generator b. The custom-machined piston (Zhong et al., 2014)

The first segment fixed to the actuator was made of an iron. However, the second part was machined from Graphite, which may resist the elevated temperatures without failure has a good corrosion resistance. In addition to the piston rod, the reservoir and the nozzle plate were also machined from the Graphite material. In the study, it is seen that the advantage of being easy to process Graphite material is used in general terms. This feature contributes the droplet generators to become more flexible and cost-friend in the droplet generation operations. In the study, the amount of the assistive (back) pressure to the mechanical impact pressure using an inert Argon gas was examined. The various combinations were tested in the experiments. That is, only the back pressure up to 30 kPa was supplied without mechanical impact, but in this way the droplets could not be ejected. At the same pressure levels, the vibratory impacts were activated but still no formation was observed. When the pneumatic pressure was gradually increased up to 45 kPa, only accompanied by the mechanical impacts, the droplets started to be ejected. However, this time, the satellite or multiple droplet formations were observed. As a last case, when the gas support was exceeded the 45 kPa, with the mechanical actuation, the proper droplet generation regime was obtained. By applying various combinations of mechanic and the pneumatic pressure supplements, the operational limits of the appropriate ejection was able to be determined. On the other hand, the need of assistive gas supplement to the mechanical impacts complicates the design of the droplet generator body. For further, extra equipments are required for both supplying a gas and its controlling purposes. These issues can be interpreted as a deficiencies of a droplet generation processes via pneumatic support. In order to provide more cost-effective and more flexible droplet formation operations, the alternative ways for supporting the mechanical impacts are need to be further investigated.

In fact, the issues of achieving continuous metal deposition with pneumatic pressure support are frequently investigated. Because droplets created by pneumatic methods are quite suitable for characterization. Moreover, with this method, it is possible to expel the droplets without contacting the molten area. However, the number of control and application equipment used for the method is quite high. Consequently, the installation costs are also high. When the mechanical impact-based DOD technique is evaluated from this point of view, it is understood that equipment costs and control elements are much more feasible. Moreover, since generator body designs do not require an extra gas inlet, outlet and its control, they are more easily produced, intervened and more practical to operate. Because of these advantages, this method is also preferred in this thesis study.

4. EXPERIMENTAL PROCEDURE

In this section, the experimental procedure is presented. The planning of the experiments are set based on the two main stages. In the first stage, custom-made, open-source and the low-cost FFF-type AM device is establisted. With this device, a serie of samples are printed using the important process parameters. The process parameters are selected among those that affect the bonding conditions of lines and layers, and thus the strength of the part, in the light of literature research. The printed samples with different combinations are exposed the mechanical tests and the results are evaluated using some sort of statistical approaches.

In the second stage, the FFF device is modified and evolved into a metal droplet generator. To do this, the axial motion platform, the deposition substrate, the control board, the computer for the monitorizing purposes and most of the control devices used in the FFF device are either kept as they are, or minor modifications are applied. However, the major modifications are done on the material ejection region. That is, the material extrusion apparatuses for the FFF are replaced with the droplet generator body. For further, a custom made material feeder mechanism into the melting region is developed. After integrating a mechanical impact-based actuation mechanism into the generator body, the material ejection in form of droplets is enabled. The process parametrs in the droplet ejection period are configured suitably in accordance with the material feed rate. The droplets are then able to be ejected and deposited in various morphologies. The deposition morphology is investigated over the placement of the droplets on the platform, either on the cases that they are bonded or not. There are detailed descriptions of how the adopted AM device is modified effectively and the benefits of this advantage, with two-step experimental procedures that are systematically described.

4.1. Overview of the Experimental Procedure in the FFF Process

In this study, the amount of overlap on the shell walls are prioritized while determining the input parameters. Because, it was noted that the bonding of the inner and outer structure of the part plays major role over the mechanical behaviour (Tymrak et al., 2014; Pierson and Chivukula, 2018; Rodriguez et al., 2003). The overlapping occurs at the point where the shell and infill lines coincide. This point is mainly responsible for keeping inner and outer lines together with the sufficient amount of adhesion. In the case of insufficient adhesion, the segregation or the air gaps may lead to lose bonding resulting in part failure (Hossain et al., 2014). Inversely, bubble-like formations may appear around the perimeter of the part due to the excessive overlapping that reduce the surface quality significantly. For these reasons, the proper amount of overlapping appears to play an important role (Korkut and Yavuz, 2020). Simultaneously, line width, shell thickness and infill orientation are also taken into account since they have direct effect over the amount of overlapping. These four parameters with five different setting levels are examined to determine their effect on the Ultimate Tensile Strength (UTS) of the printed samples. While this study is being carried out, the subject of material consumption, which is one of the main interests of engineering, is also focused. Minimizing the material consumed while increasing the part strength is considered as a must, more than being an option in today's manufacturing technology. For this reason, the effect of the same input parameters over the material consumption is also examined in the study. The effect of all parameters, especially the infill overlap, on mass variation is statistically analysed. The parameters that are effective in reducing material consumption are determined and the reasons of this situation are investigated. Considering that the given parameters directly influence the amount of overlap on the shell, the varying overlap areas are examined geometrically. The areas occupied are measured in both CAD software and digital microscope. Due to the significant findings, the optimum parameters are obtained in behalf of increasing the UTS while keeping the material consumption at average levels. As a widespread effect, generalized equations are established and presented in order to calculate the occupied area by an overlap. By implementing these equations, the users are enabled to calculate the area before the printing operation. In this way, it is contributed for the users to configure the device-specific input parameters on behalf of manipulating the area; thus increasing the UTS while controlling the material consumption.

4.1.1. Experimental Planning for the Printing Processes

The experimental planning is set based on the Taguchi's Design of Experiments (DOE) approach using L_{25} Orthogonal Array (OA) table. By doing this, the procedure is able to be implemented with minimum, but sufficient number of samples within order. 25 different samples with three repetitions of each (a total of 75 samples) are fabricated. The printing process is realized via open-source type using a modifiable FFF device. The PolyLactic Acid (PLA) filament used for the study is 1.75 mm in diameter, natural grey in colour and it is manufactured by *Shenzhen Esun Industrial Co. Ltd.* The printed samples are tested for tensile strength. Then, the results are interpreted according to the Signal-to-Noise (S/N) Ratios found by Taguchi analysis. This is done to be able to obtain the optimal parameter combination for the best tensile strength. The Analysis of Variance (ANOVA) is also implemented to see the percentage contribution of the parameters individually over the tensile characteristic. The results obtained are presented with the analytical correlations supporting the arguments. The flow diagram given in Figure 4.1 represents the operational steps of the study.

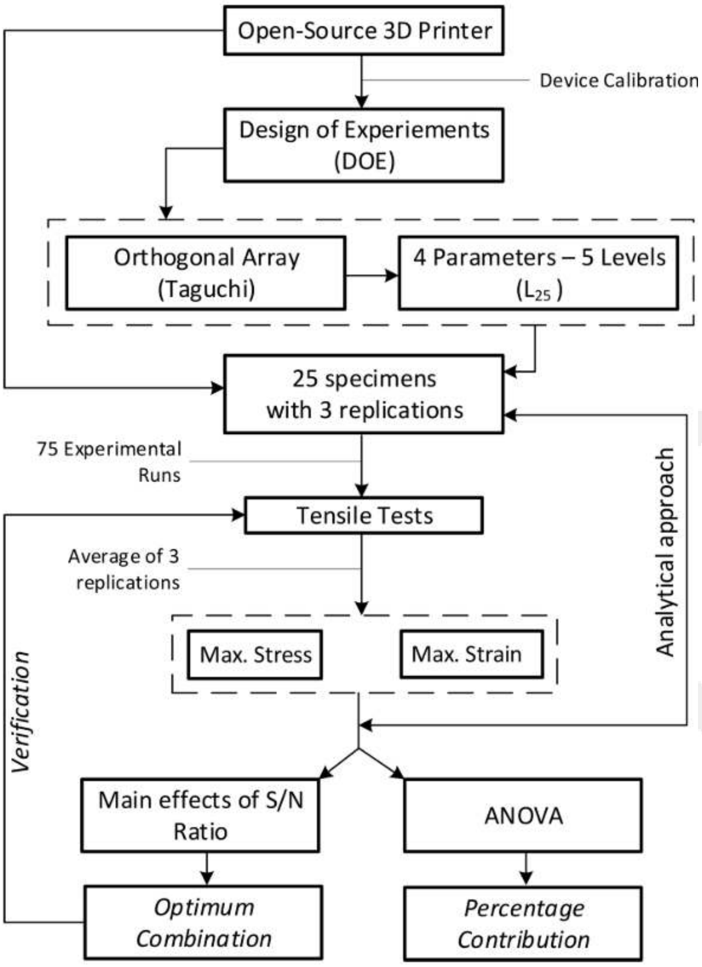

Figure 4.1. The flow diagram of the operational steps

4.1.2. The Configuration of the Printing System

Open-source printing devices have widespread usage in many applications due to the modifiable structure according to the job. The widely used, Cartesian-type FFF device with the open-source Marlin Firmware (v2.0.x) (Website, 2022k) installed on the Makerbase (MKS Gen L v2.0) control board are established for the tensile specimen manufacturing (Figure 4.2).

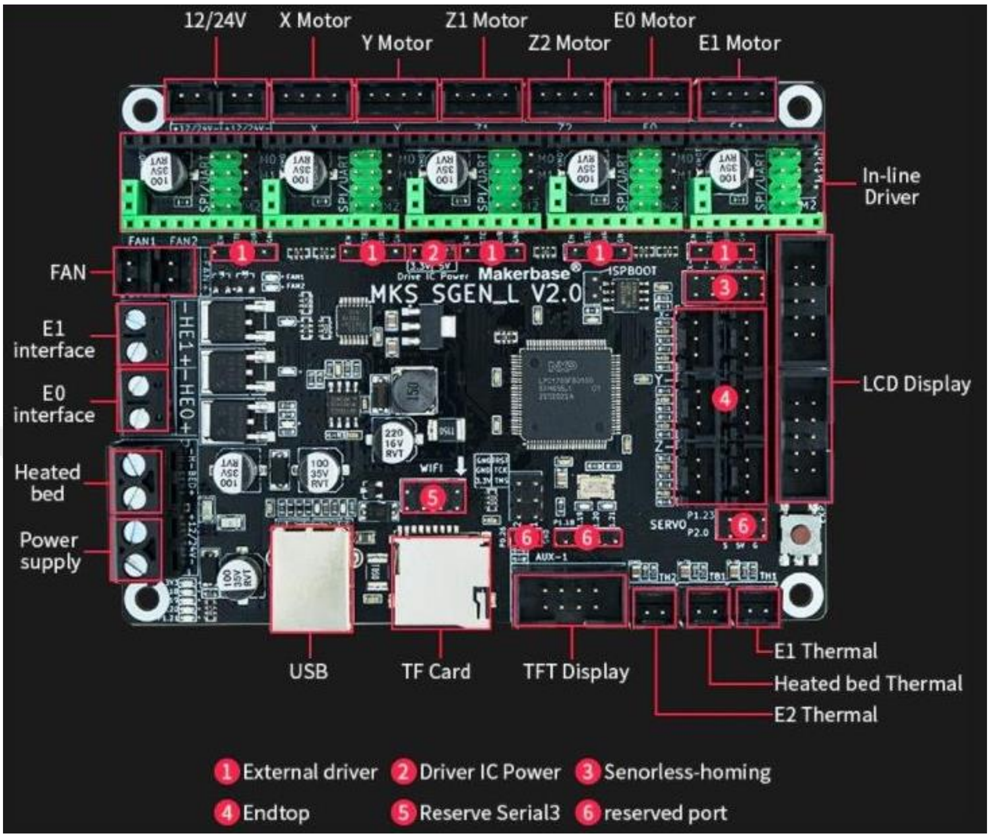

Figure 4.2. The MakerBase (MKS) Gen L v2.0 control board with the connection pins

The slicing operation is done via Cura Slicer (v4.2.1). This software is preferred because it allows very detailed parameter definition owing to its open-source concept. Before the manufacturing, some routine engineering applications were implemented on device to be able to increase the print quality. Conceptually, user-assembled type printers are marketed with minimum equipment in order to lower the initial cost. For this reason, the device is equipped with additional supportive parts as shown in Figure 4.3.

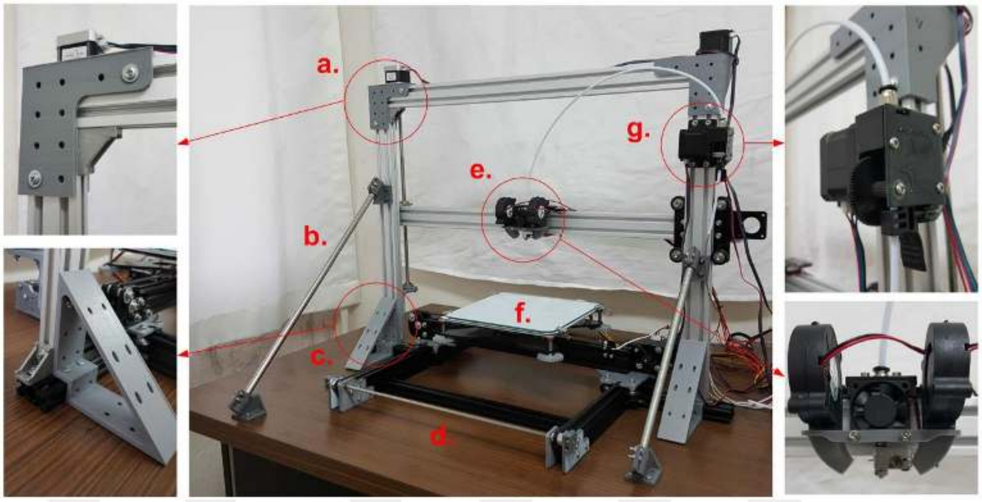

Figure 4.3. The demonstration of the used device with a number of improvements

The layer resolution of 0.1 mm is maintained by two Nema 17 bipolar stepper motors (Figure 4.3.a) having the step angle of 0.9° (400 steps/rev, holding torque of 44 Ncm) which are connected to the lead screws that have a pitch of 2 mm (8 mm in diameter). The Z axis' carrier columns have been fixed from both sides to the stand using the custom-designed fixtures (b, c). The Y axis is also modified to be driven from both sides (d). In order to maintain the quick cooling over the lines already extruded, two external 12 Volt DC fans are attached on the nozzle (e). Here, the nozzle is replaced to stainless steel one rather than brass type since it is more resistant to the corrosion by time at elevated temperatures. As shown in (f), the glass laminate was placed on the heated bed as it was observed that the glass provides smooth adhesion. The elements of PID temperature control for both the nozzle and the heated bed are re-set from the firmware in order to receive the quickest response from the heater system. Regarding the re-setting of the PID elements, it is benefited from the auto-tuning feature of the Marlin firmware. That is, when the initial setup of the device is completed, the default K_p, K_i and K_d values are used those provided with the stock firmware. These values are determined by developers as default settings suitable for most heater models used in printers. In order to provide optimum temperature control performance in the modified device described in the study, PID elements are re-set using the auto-tune feature (M303 command) of the Marlin firmware (Website, 2022n). The tuning based on *Ziegler-Nichols' classic method* was conducted with 8 repetitions of heating process (at 200 ^{o}C for the nozzle, 95 ^{o}C for the heated bed) (Website, 2022m). In fact, the tuning operation is done automatically by the preset firmware codes. However, the necessary coding is presented by RepRap community to be able to adjust the proportional, integral and derivative control for the nozzle and heated platform temperature according to the used component specifications. As a further upgrade, the Titan Extruder (g) with the gear ratio of 3:1 (*Tevo 3D Electronic Tech. Co. Ltd*.) is mounted in order to increase the stability of the extrusion operation. Owing to the gear reduction ratio, the need for high filament drive torque is lowered compared to the conventional extruders having the ratio of 1:1. Besides, the lightweight gear design makes the mechanism more responsive to the sudden retractions. After the improvements done on device, the excessive vibration, dimensional failure and heat-related defects are minimized as observed. It is then the manufacturing process is initiated. In addition, a set of calibration step is conducted over the extruder mechanism. Regarding the calibration, it should be noted that the amount of material extruded is a crucial factor since the end-product is emerged by the deposited single lines. In order to maintain the dimensional accuracy in printed samples, the extruder mechanism is calibrated until the width of the extruded lines matches with the defined value in slicer. This process is done by adjusting the Flow Rate parameter in slicer which indicates the amount of filament extruded in a second (mm/s). The final flow rate was found by adjusting the flow rate parameter repeatedly until the actual value of the extruded line width matches to the defined line width parameter. These calculations are done by using Equation 4.1 as follows.

$$New\ Flow\ Rate = \left(\frac{Input\ Line\ Width\ (in\ sciler)}{\text{Measured}\ Line\ Width\ (extruded)} \right) \chi Current\ Flow\ Rate \tag{4.1}$$

For instance, the parameters of the line width and the flow rate were set in Cura as 0.5 mm and the 100% (default value), respectively. Then, the lines are extruded with these parameters. The average of the measurements of the line width from 12 different points was found as 0.485 mm. When these values are put in Equation 4.1, the new flow rate is calculated as 103.09%. After extruding the single lines once more again with the new flow rate, the average width of lines is measured as 0.501 mm. It is then become possible to proceed with the experiments. This process was repeated in every line width change according to the experimental procedure. The basis of the procedure was also explained in the Section 3.2. Principally, the filament is pressed between the rotating gears then driven into the heated zone and the deposition surface, respectively.

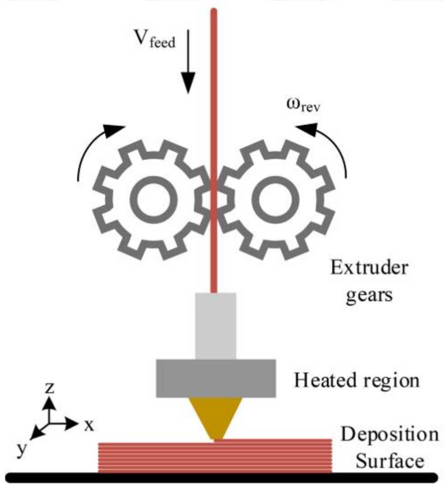

Figure 4.4. The representation of the filament feed (extrusion) mechanism

As shown in Figure 4.4, the rotational speed (ω_{rev}) determines the linear velocity (V_{feed}) of the filament. In the slicer, the flow rate parameter corresponds the ω_{rev}, thus the V_{feed}. In other words, the feed velocity of the filament can optionally be changed by adjusting the flow rate parameter. To be able to confirm that the flow rate defined in the slicer to match the exact values, a serie of preliminary tests are conducted. As a test specimen, single-walled, hollow part geometry is employed as shown in the Figure 4.5.

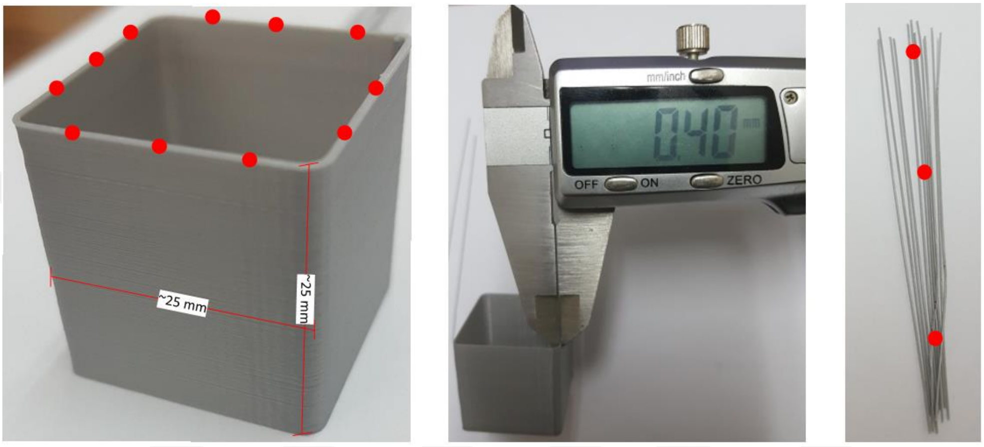

Figure 4.5. The preliminary experiments for the flow rate calibration

Measurement of wall thicknesses in order to eliminate as much as possible flow rate deviations caused; A total of 12 wall thicknesses, 3 from the top points of the walls of the all edges were measured by digital caliper and the mean of the measured values was recorded as the resultant wall thickness. The actual thicknesses obtained and digital flow rate values defined in each experiment are applied into the Equation 4.1, and the same experimental procedure was repeated 3 times. In this way, the line thickness, which was initially determined as 0.4 mm but measured as 0.46 mm, was corrected to be 0.2% deviation, that is, 0.4008 mm, owing to the applied equation. After eliminating flow rate deviation, the test specimens are manufactured within the acceptable dimensional tolerances.

4.1.3. The configuration of the printing parameters

In this stage, some well-accepted statistical approaches are employed in order to standardize the experimental procedure. The design of experiments is established based on Taguchi's L_{25} OA table. The OA design aims to obtain robust process parameters by reducing the variability of the input factors upon the desired output responses. By using the OA design, the inputs are rendered as insensitive as possible against the disturbing factors (noises) those cannot be controlled. This way, the deviation around the targeted point is minimized. As deviation decreases, the effects of inputs over the outputs become more evident. Therefore, when it is desired to obtain the best performance from the output (the highest UTS for this study), this method provides an advantage in terms of determining the optimum input parameters. In fact, there are other solutions those can further reduce the noise factor that may lead less variance over the output. However, the number of experiments may increase dramatically, so the effort, time and cost increase at the same rate. The OA method is frequently preferred especially in engineering applications in order to maintain time-money balance by reducing the number of experiments (Roy, 2010). For the same reason, it is also preferred in this study.

The relation between the input and the output is determined by S/N Ratio value which corresponds the quality characteristic of the process. Since it represents a higher quality, higher S/N values are expected to be obtained. In the study, 4 input parameters (factors) at 5 level settings (Table 4.1) are defined in various combinations using the Taguchi's suggested OA table (Table 4.2).

Table 4.1. Four parameters with five level settings

	Line width (mm)	Shell wall number	Infill orientation (°)	Infill overlap
Symbol	*A*	*B*	*C*	*D*
Levels				
1	0.40	1	[0°]	20%
2	0.45	2	[45°/−45°]	40%
3	0.50	3	[45°/−45°]*	60%
4	0.55	4	[0°/90°]	80%
5	0.60	5	[0°/45°/90°/135°]	100%

Table 4.2. Taguchi's suggested L_{25} Orthogonal Array bable

Parameters	Specimen number																								
	1	*2*	*3*	*4*	*5*	*6*	*7*	*8*	*9*	*10*	*11*	*12*	*13*	*14*	*15*	*16*	*17*	*18*	*19*	*20*	*21*	*22*	*23*	*24*	*25*
A	1	1	1	1	1	2	2	2	2	2	3	3	3	3	3	4	4	4	4	4	5	5	5	5	5
B	1	2	3	4	5	1	2	3	4	5	1	2	3	4	5	1	2	3	4	5	1	2	3	4	5
C	1	2	3	4	5	2	3	4	5	1	3	4	5	1	2	4	5	1	2	3	5	1	2	3	4
D	1	2	3	4	5	3	4	5	1	2	5	1	2	3	4	2	3	4	5	1	4	5	1	2	3

Below, the parameters given in Table 4.1 were described in respect to the subject;

- *Line width (LW):* The width of the line extruded from the nozzle onto the deposition surface. Here, the nozzle diameter is a dominant factor in the LW as much as the flow rate at least. As a rule-of-thumb, the width of the line should be equal to or slightly greater than the nozzle diameter. However, there is a useful width range that could be achieved with only a single nozzle.
- *Shell wall number*: The number of contour lines covering the infill structure. The *Shell Thickness (ST)* of the part is determined by the number of the wall lines. The percentage of the overlapping has been calculated over the total shell thickness.
- *Infill orientation*: The geometrical array of the infill lines. This parameter has been selected as a straight line form but in different directions. In Fig. 4.6, the selected angular directions of the lines have been presented.

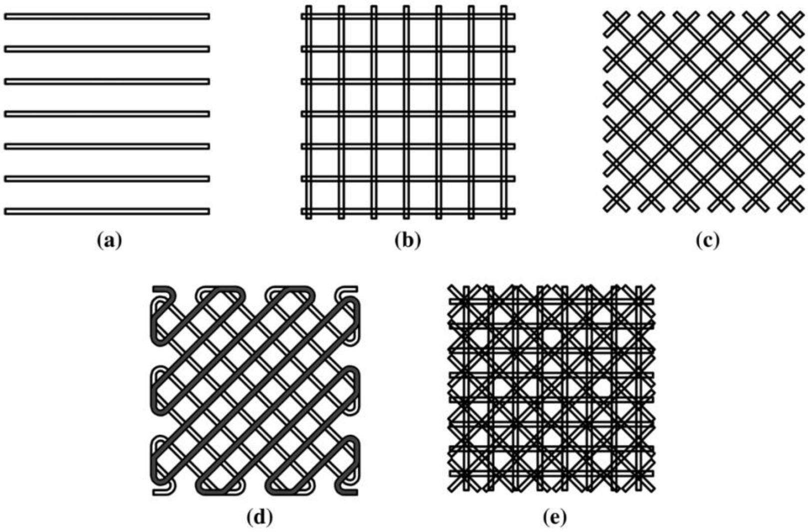

Figure 4.6. Representative infill directions with angles. a. [0°] or [90°], b. [0°/90°], c. [45°/− 45°], d. [45°/− 45°]*, e. [0°/45°/90°/135°].

- *Infill overlap (IO):* The amount of overflow of the infill lines over the shell. It is also responsible from the bonding between the infill pattern and the shell walls. This parameter can be called in both percentage and millimetres as it will be mentioned in the next sections.

In Table 4.1 as well as in the rest of the context, the symbol (*) represents the infill pattern with continuous infill lines (as shown in Figure 4.6.d and 4.7.c). In Figure 4.7, representative layers are provided to illustrate the amount of overlap as well as the structure and area occupied by the intersection geometries. As it is shown in the figure, the percentage of overlapping, the line width and the infill pattern together determines the amount of the coalescence between the inner and outer lines. Here, the investigation of the interaction between the infill and the shell by focusing on the overlapping region is discussed in this study due to lack of interest in this subject.

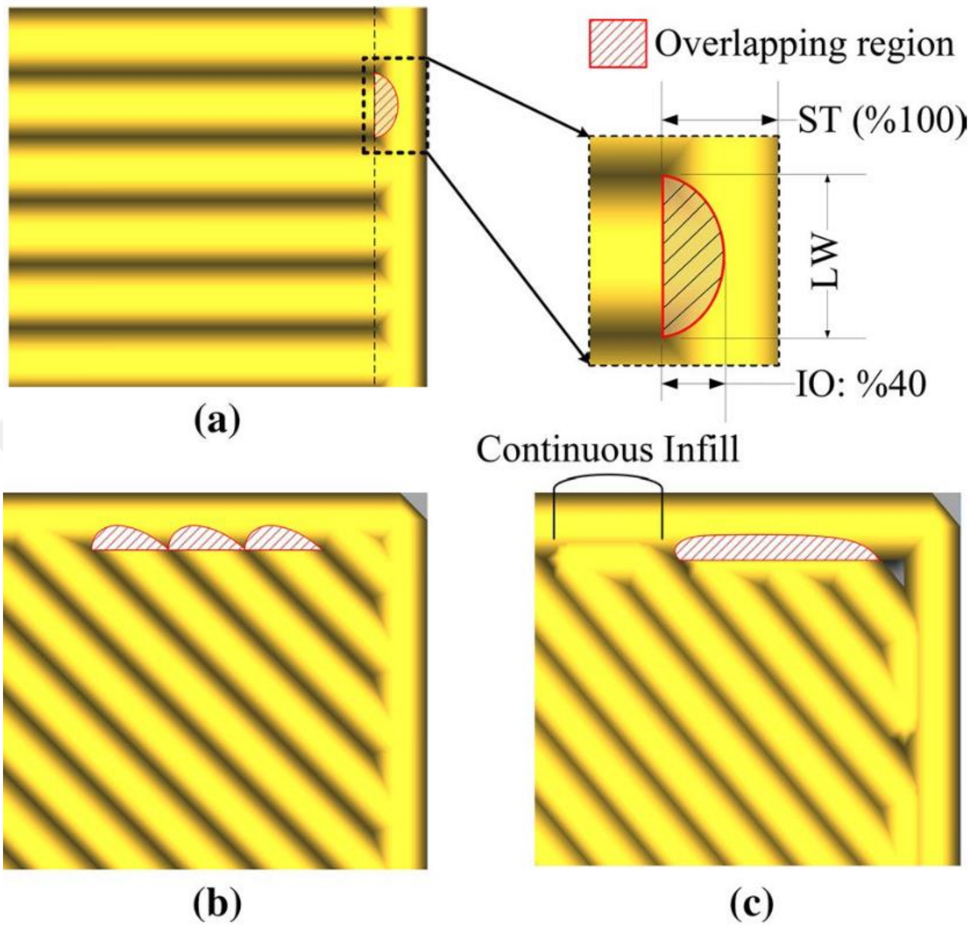

Figure 4.7. Overlapping regions, a. [0°], b. [45°], c. [45°]*, (ST: Shell Thickness, IO: Infill Overlap, LW: Line Width)

4.1.4. Fabrication Process and Tensile Testing

In accordance with the OA table, the set of 25 samples are printed at one go (Figure 4.8.a). The relevant parameter combination belonging the each sample is set individually by using the "Per Model Settings" feature of the Cura software. It is then become possible to print 25 samples with various settings in one printing session. By repeating the mentioned process twice more, the 75 samples in total are manufactured (Figure 4.8.b).

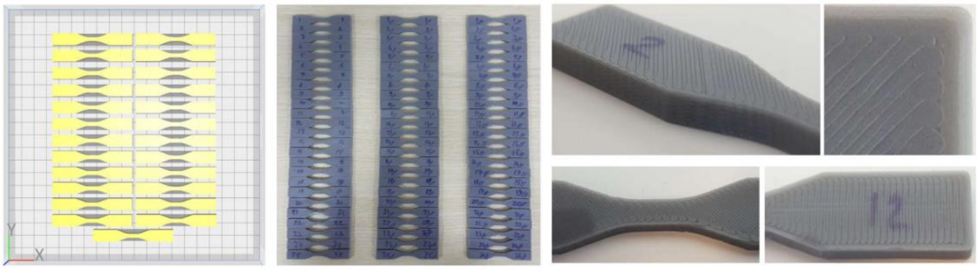

(a) (b) (c)

Figure 4.8. a. Build orientation in slicer, b. Printed samples, c. Randomly captured overlap models

Besides, the fixed parameters valid for all the samples are given in Table 4.3.

Table 4.3. Fixed printing parameters with the test specimen dimensioning

Fixed printing parameters				ASTM D638 (Type V)
Filament material	PLA	Ambient temperature	24 °C	
Filament diameter	1.75 mm	Ambient humidity	40%	
Nozzle material	St. Steel	Layer thickness	0.2 mm	
Nozzle diameter:	0.4 mm	Build orientation	*XY*	
Nozzle temperature	200 °C	Infill density	100%	
Heated bed temperature	65 °C	Print (head) speed	40 mm/s	

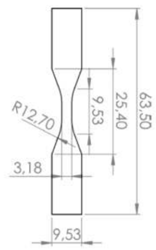

As a test specimen, the model of D638 (Type V), standardized by ASTM for tensile testing of polymer-based materials is employed (ASTM, 2014). The printed samples are subjected to tensile testing with a precision universal tester (Figure 4.9; Shimadzu AGS-X 100 kN, *Shimadzu Corp.*) accompanied by non-contact digital extensometer (*TRViewX, Shimadzu Corp.*) which conforms the ASTM E4 grade (Force Verification of Testing Machines).

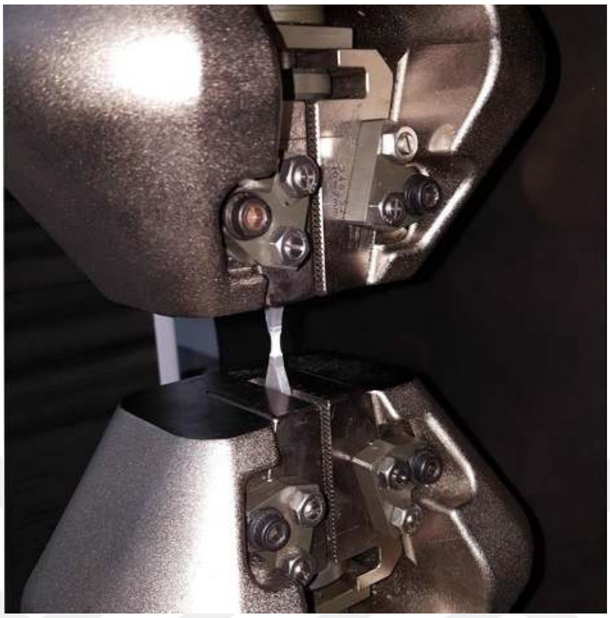

Figure 4.9. Tensile testing process (*Shimadzu AGS-X 100 kN, Shimadzu Corp*.)

The tests are carried out at a tensile speed of 1.25 mm/min, which is within the standard test speed range for this standard model.

4.2. The Transformation of the FFF Device into an MDJ System

So far, in the aforementioned studies, it is noticed that there is a lack of knowledge about necessary amount of feeding that will ensure continuous droplet formation with mechanical impulses with the absence of inert gas assistance. For these purposes, a novel droplet generation system based on the drop-on-demand concept is developed in this thesis study (Korkut and Yavuz, 2022b). The droplets are ejected only by mechanical impacts which are characterized by the mechanical and electrical inputs. The input parameters, such as actuation, heating, and axial translation are controlled using the open-source concept that of FFF processes. The ejection mechanism is substantially equipped with reusable or easily changeable parts which make the system highly favorable. The detailed methodology for changing the material feeding system into the melting region is presented. The required amount of wire-type material feed allowing the proper droplet formation in open-air conditions is achieved through a unique and modifiable feed mechanism. The appropriate feeding parameters obtained by theoretical calculations were also confirmed experimentally. As a result, a stable, cost-competitive droplet generator having a dynamic wire feeding mechanism is introduced with its all aspects. The proposed setup, as well as their electronic substructure, is supplied with their scientific infrastructure based on the Open-Source Hardware definition made by OSHWA. By doing this, it is intended to present the device in a way that can be built, even developed by other users. For further, the droplet generator was attached on the same device used for polymer based material deposition with by applying minor modifications. That is, after the experimental process of the FFF process was completed, the deposition head, in which the softened polymer was ejected, is replaced with a metal droplet generator body. Although many basic components such as the motion mechanism, heated bed and the motion sensors are not intervened, some modifications are made in the slicer software, temperature sensing tools, the material heating system and the material feeding parameters.

The experimental setup of MDJ system involves an induction heating system, a solenoid actuator, a vibration transmitter rod (plunger) connected to the actuator, a mechanical vibration amplitude restrictor (needle type micrometer), and a wire feeder mechanism. The schematical view of the established droplet generator body is presented in the Figure 4.10.

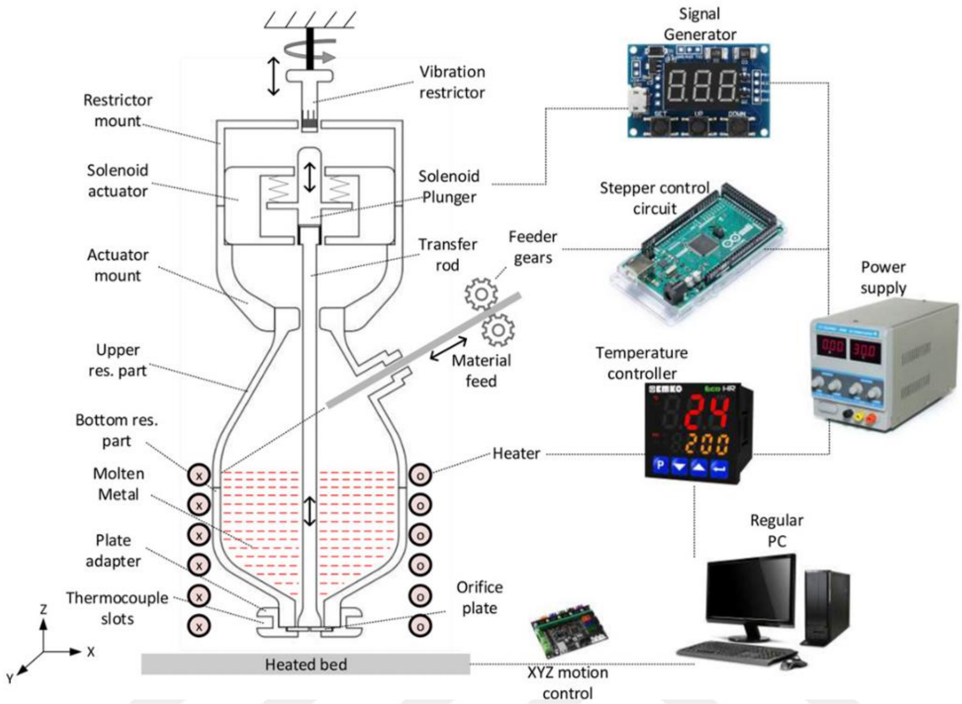

Figure 4.10. The schematical view of the established droplet generator system

As a working principle, the conventional solder wire (Sn60Pb40 (Fluxless), *Soldex inc.*) is fed into the reservoir by stepper motor–based feeder mechanism. The stepper motor is controlled both in direction and rotational speed by Arduino Mega board. The motor control software is implemented with the code available in the Arduino Stepper Library (arduino.cc/en/reference/stepper). The schematic circuit diagram belonging to the feeder system is provided in Figure 4.11.

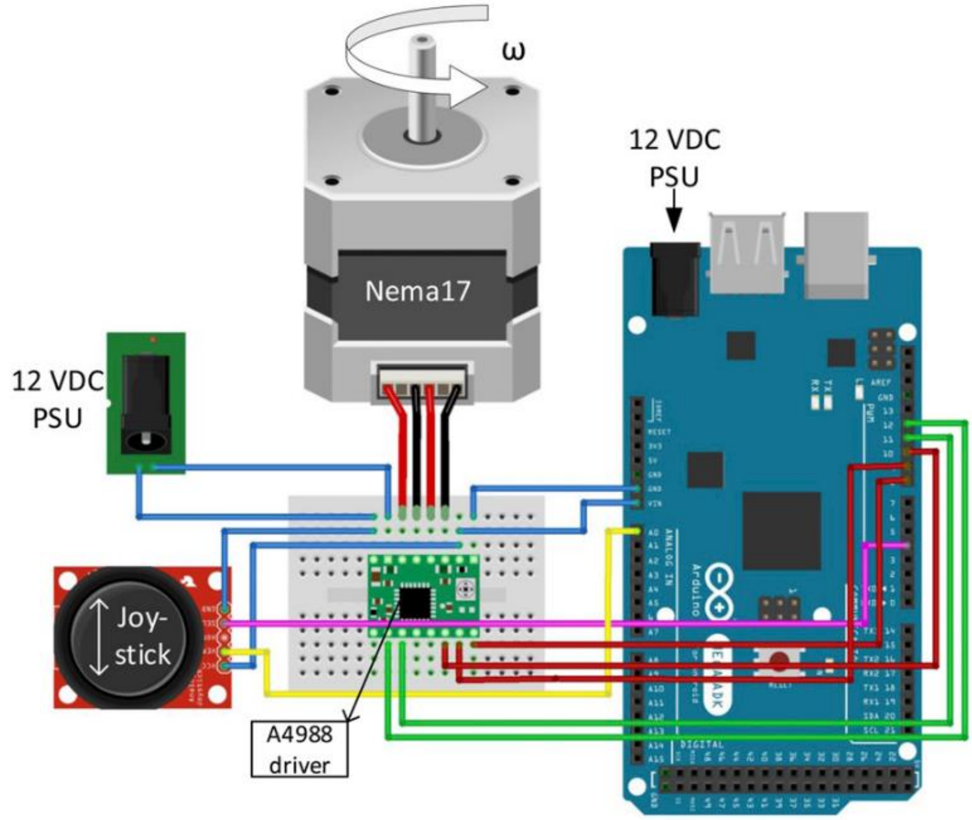

Figure 4.11. Externally-driven wire feeder (extruder) circuit diagram.

During the preparation tests, the motor is driven manually via a regular joystick at a fixed RPM. The temperature is measured by two K-type thermocouples and controlled by a common PID controller (EcoPID, Emko Electronics); those cost around 20 USD as a set. The necessary heating is provided by a low-cost induction heater driven by the Zero-Voltage Switching (ZVS) module capable of providing the power up to 1000 W (12 g of solder wire in one second). The heating module operates on the basis of the Flyback Driver circuit, which can be gathered by a user by connecting the individual elements (Website, 2022o) or be purchased in the ready-to-use form from the online market (costs around 30 USD). The driving circuit of the heating systems is provided in the Figure 4.12.

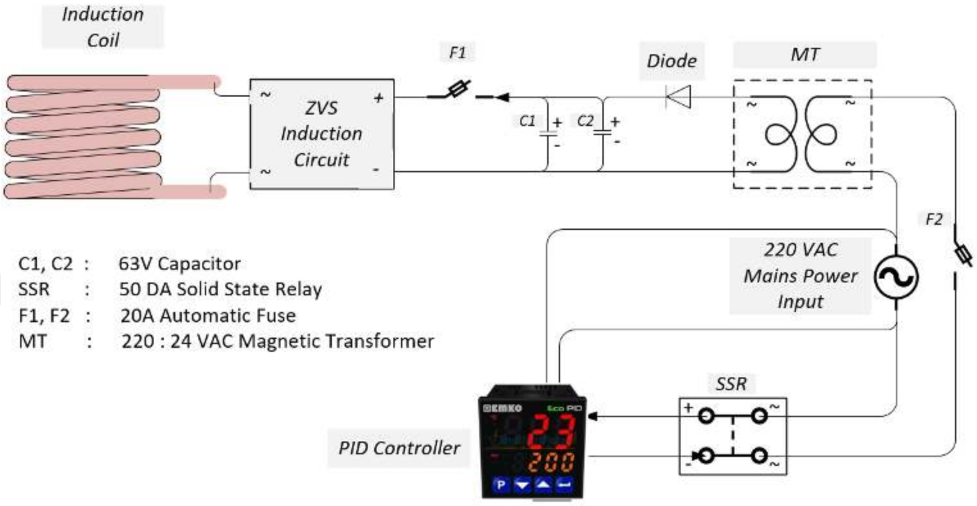

Figure 4.12. The circuit diagram of the induction heating system.

The flow diagram for the power supplement and the control system is provided in the Figure 4.13.

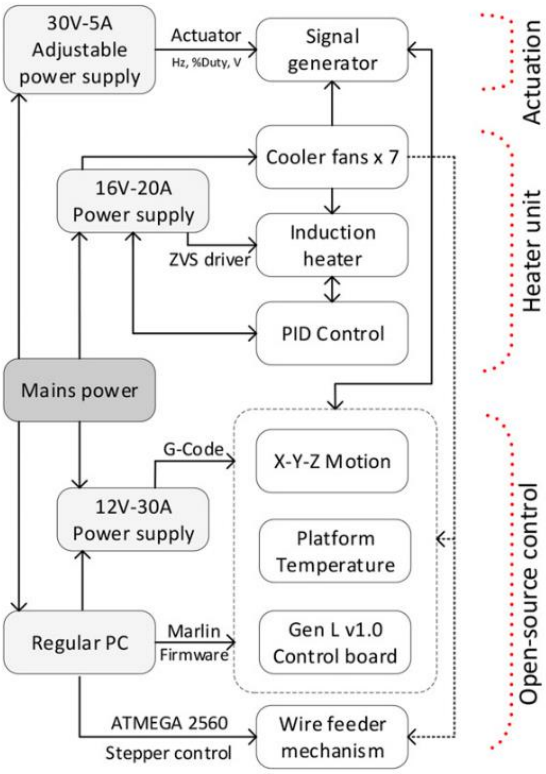

Figure 4.13. The flow diagram of the power supplement with the control system

The solenoid actuator is preferred as an impact source which can operate between 15–22 V. The actuator consists of commonly used push–pull type solenoid coil parts which can vibrate up to 5 mm with the absence of an external restriction. However, the vibration amplitude is mechanically limited by a needle-type micrometer with an accuracy of 0.05 mm mounted on top of the actuator. At the bottom of the actuator, there is a transfer rod that transmits the vibration to the molten pool. The duty cycle and the frequency of the actuator are controlled by a simple, power- independent, two-channel, 12V PWM signal generator (costs below 5 USD). The mechanical parts, such as reservoir, actuator mount, disc plate with an orifice, and disc holder, are machined from a structural steel (EN 10025). Since melting, ejection and the measurements mostly take place in the reservoir area; it is important to be able to intervene in these parts when necessary. Therefore, no permanent connection type is used between the parts. The actual shown of the droplet generator body with its necessary components is given in the Figure 4.14.

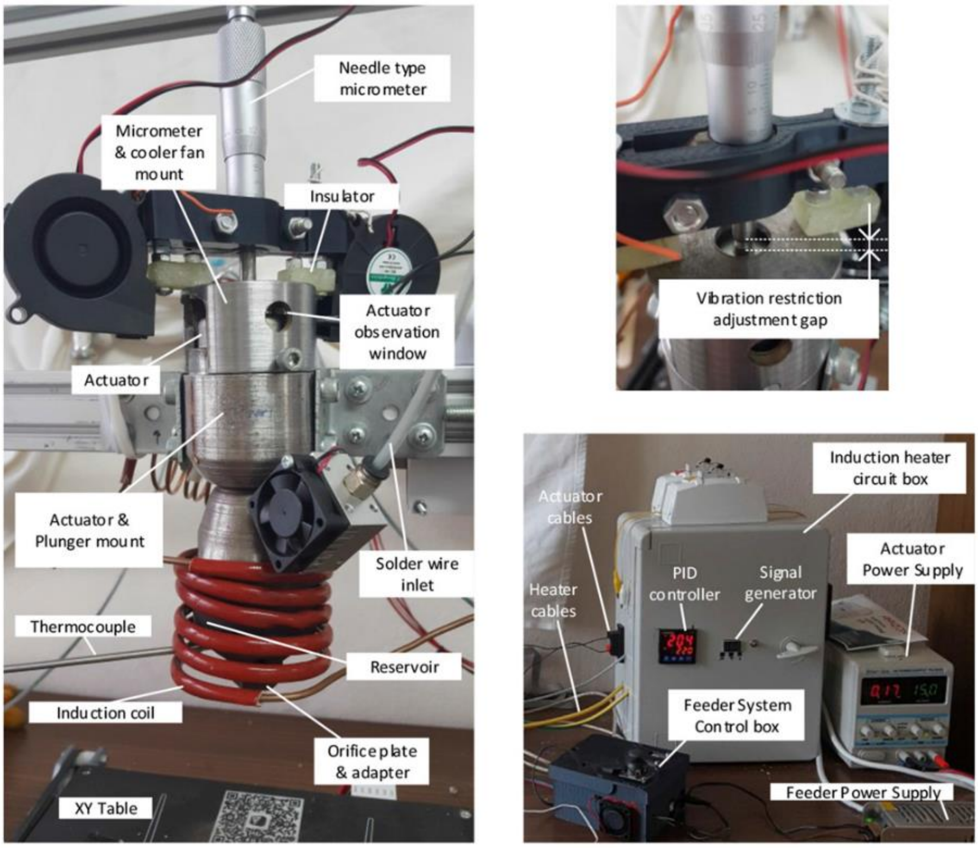

Figure 4.14. The main components of the droplet generator

This feature provides flexibility in the droplet generator when repairing, replacement, or routine maintenance of a part is required. In addition, the mechanism consists of the metal parts as actuator slot, the material inlet, as well as the fixtures does not require a specific manufacturing method or an exact dimensioning. As it is explained in the next sections, the users do not have to follow the similar manufacturing methods by obeying the strict dimensioning. That is, the proposed method is planned to be adoptable to the custom-made droplet generator bodies by applying the developed equations relevant to the material feeding. Lastly, the droplet generator with its all units (temperature, actuator, and sensing equipment) is fixed into the Cartesian based axial motion stage which was also used for the FFF processes previously (Figure 4.15).

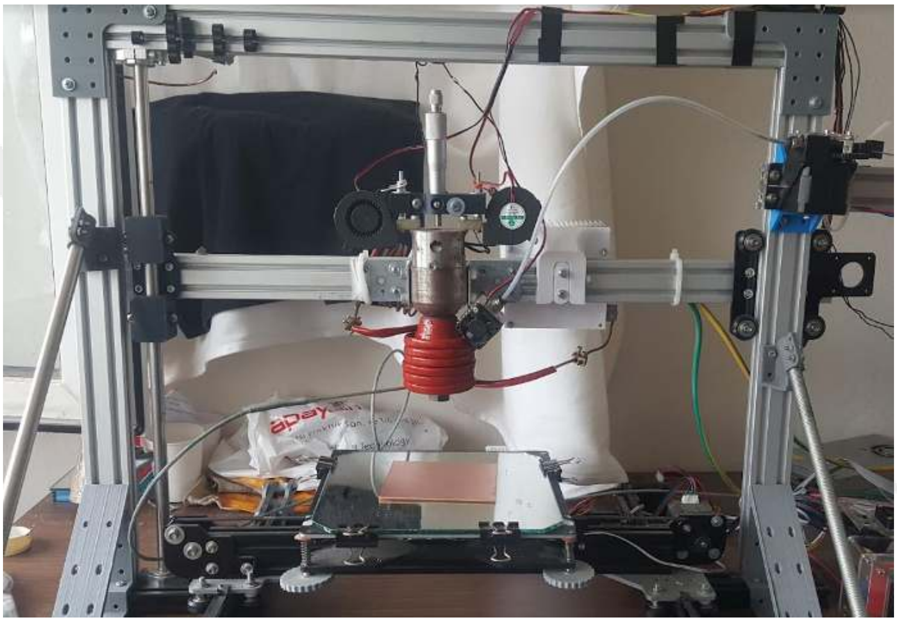

Figure 4.15. The developed droplet generator body mounted into the motion stage

The slicing of the digital model is carried out with Cura slicer. It should be noted that any type of a CNC router could optionally be used for the axial motion since the generator itself is detachable. Finally, a systematic explanation is proposed describing the fundamental component cost to be approximately 700 USD in total as shown in Table 4.4.

Table 4.4. The bill of materials

Components	Cost (USD)	Description
Power supply	180	400W adjustable (V-A) PSU, 600 W heating, 250W printer control board, 250W misc. electronics (at max. capacities)
Generator parts	90	Raw material, machining (turning, milling, and drilling)
The frame and drive mechanism	120	X chassis, feeder mechanism (profiles, brackets, rods, connectors, belts, pulleys, bearings, fixtures, screws, nuts, and washers)
Electronic parts	125	5 Nema17 stepper motor, drivers, extruder control board, cooler fans, thermistors, LCD display cables, and connectors
Restrictor mechanism	20	Micrometer, 3D printed mountings
Actuation	60	Actuator, signal generator, and electronics
Heating	110	ZVS driver, PID controller, K-thermocouples, and electronics
Total	705	

4.2.1. The Droplet Generation Process

In the light of previous studies, it is noted that the state of the ejected droplet depends on the dimensionless number of ***We*** (Equation 4.2). It was stated that droplet characterization can be proposed depending on the diameter, velocity, frequency and ambient conditions of the droplet by means of this number. In other words, it was indicated that the homogeneity of the droplets and the modification of their properties according to the study to be performed are only possible with an appropriate ***We*** interval (Tseng et al., 2006; Schiaffino and Sonin 1997).

$$We = \frac{\rho_g U^2 D}{\sigma_d} \tag{4.2}$$

where ρ_d is for the droplet density, U_d for droplet landing velocity, D_d droplet diameter, and σ_d surface tension of the liquid. The continuity and homogeneity of droplet emission depends on the greatness of the ***We*** number, which is classified as low, medium, and high. At low ***We*** numbers ($We \leq 1$), the droplet state can be sustained without any external stimulus or control. When the number increases, an additional pressure in order to form homogenous droplets is required. Then, in order to determine the ***We*** number, the introduced droplet generator is exposed to the initial tests. As a result, it is recorded that the generator has ***We*** numbers varying between 22 and 30 in all parametric scenarios where it can operate stably. That is, the need of an additional impacting pressure is confirmed to be able to form droplets in a controlled manner. When the system operates, the density (ρ_d) and the surface tension (σ_d) stay unchanged due to the fixed temperatures. Therefore variation in ***We*** numbers are correlated with the values of droplet velocity (U_d) and droplet diameter (D_d). Since the voltage (*V*), duty cycle (%), and the amplitude (mm) of the actuation have a direct effect over the droplet velocity and the diameter, the experiments are set based on these three parameters (Sohn and Yang, 2005; Lee et al., 2006; 2008; Zhang et al., 2019; Yokoyama et al., 2009; Korkut and Yavuz, 2022a). The ejection conditions for the generator are presented in Table 4.5.

Table 4.5. Selected parameters having three different level sets for each

Levels	1	2	3
Amplitude (mm)	0.5	1	1.5
Voltage (V)	15	18	20
Duty cycle (%)	25	50	75

At this point, it should be noted that rather than finding the value of the ***We*** number, examining the effect of the change in these two parameters on the droplet formation is prioritized. The levels of these parameters are selected according to the capability of the solenoid actuator used. All ofthe combinations of parameters with three levels for each are examined. Thus, 27 (3^3) experiments were carried out. Besides, the other fixed parameters are given in Table 4.6.

Table 4.6. The fixed parameters

Fixed parameters	
Solder material	Sn60Pb40 (Fluxless)
Wire diameter	1.2 mm
Melting temperature	220°C
Built platform temp.	75°C
Orifice diameter	0.5 mm
Actuation frequency	1 Hz
Flight distance	5 mm
Reservoir fill duration	5 min
Feeder motor speed	5.56 RPM

As a test procedure, the heating process is initiated until the temperature reaches the melting level. It is noticed that there is 2°C difference between the thermocouple slots and the molten pool when the temperature level reaches equilibrium. Therefore, this difference is taken into account in the actual experiments. After this, the raw wire material is fed into the heated region via Titan Extruder mechanism (*Tevo 3D Electronic Tech. Co. Ltd*) having a high gear ratio. From the software interface, the motor is commanded to rotate at a constant rotational speed. The feeding operation is performed with a constant rotational speed for 5 mins. without interruption. When the feeding terminates, the actuator is switched on and the ejection is started and continued until the reservoir was completely emptied. The ejected droplet samples are collected inside machine oil at room temperature. The flight distance between the orifice outlet and the deposition surface is set to be 5 mm. The procedure was repeated three times for each of the 27 experiments. The diameters of the stored droplets are measured both by digital microscope and image editing software and the *Digital Mitutoyo AOS* caliper. Furthermore, the mass measurements (via *TP-214, Denver Instruments*) are also carried out. The images of the droplets measured are as in Figure 4.16.

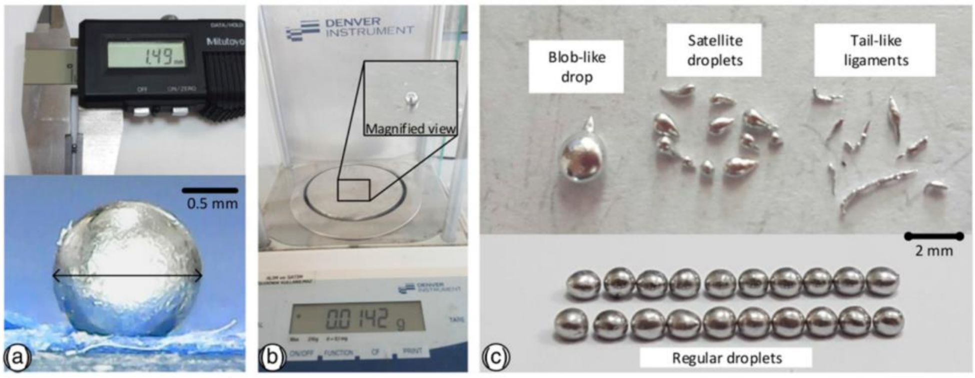

Figure 4.16. a Diameters were double-checked via the digital caliper and image processing software, b. Mass measurement, c. Types of ejected material.

The experiments having the deviations below 5% in both diameters and masses are given in Figure 4.17.

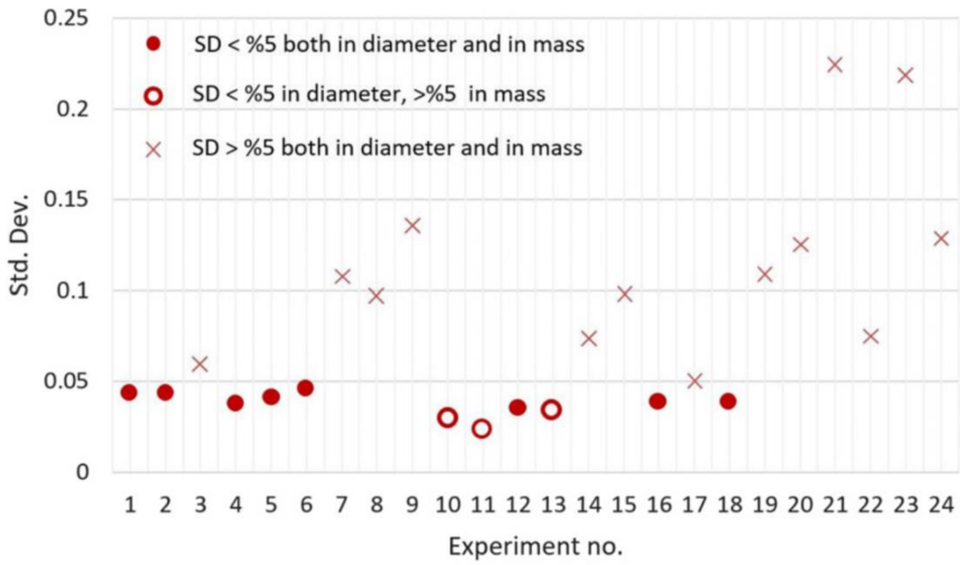

Figure 4.17. Standard deviation of each droplet generation experiment taking into account the three replications in both diameter and mass measurements.

In the graph, the standard deviations of the droplets are shown corresponding to the respective experiment numbers. The standard deviation in diameter was found less than 5% in 11 experiments. However, three of them could not pass the mass deviation threshold of 5%. Therefore, it is finally observed that droplets with homogenous properties could be generated in only eight experiments. In addition, in the last three experiments (25–27), the droplet regime was very unstable and proper droplet formation was not observed; therefore, they are not presented in the graph. In this study, revealing suitable combinations is adopted as a tool rather than a goal. In this way, as the originality of the study, it was possible to proceed to the detailing of the wire-type feeding issue, which is necessary for the sustainable operation of low-cost systems that can operate in open-air conditions without extra gas support. Therefore, only the qualified experiments those result in homogenous droplet production are presented in Table 4.7 with their numbers and parametric combinations.

Table 4.7. Diameter and the mass of the generated droplets in eight experiments

Exp. No.	Amplitude (mm)	Voltage (V)	Duty cycle (%)	*Average*	±[a]	*Average*	±[a]
1	0.5	15	25	1.507432	0.044084	0.019949	0.001899
2	0.5	15	50	1.523817	0.043658	0.022475	0.002913
4	0.5	17.5	25	1.528594	0.03764	0.023424	0.00411
5	0.5	17.5	50	1.489528	0.040661	0.026237	0.004135
6	0.5	17.5	75	1.72885	0.045579	0.031763	0.00411
12	1	15	75	1.646727	0.03532	0.036678	0.004436
16	1	20	25	1.432642	0.038346	0.022763	0.004069
18	1	20	75	1.544211	0.038459	0.021136	0.004015

[a]standard deviation.

During the experiments, within the first and the last 30 second of the each session, unexpectedly big (drip) and/or satellite type droplet formations are observed. The rest of the regime interval is taken as the reference basis for the measurements. Considering that approximately 120–130 droplets are generated in each experiment (except the last three), near 6000 measurements are carried out in total for the obtained results.

Until this point, homogenous droplets with a deviation below 5% are achieved in eight experiments. However, it should be noted that this droplet generation process is not continuous. Because, during the operation, the reservoir is filled first, the feeding is stopped, and the ejection is started, and when the reservoir becomes empty, the droplet formation automatically ends. Moreover, it is observed that there was no proper droplet formation during the first and last 30 mins. of the experiments. In other words, the homogenous droplets can only be generated within a certain period of time. Therefore, the stable droplet formation is associated with the height of the liquid inside. Because the only factor that varies in time is the liquid height, thus the hydrostatic pressure. To express the pressure balance in the reservoir (Equation 4.3);

$$\cancel{P_{atm}} + P_{hs} + P_p = \cancel{P_{atm}} + P_{rf} + P_{st} \quad (4.3)$$

Given that the droplet forming process is conducted under the open-air conditions, P_{atm} is equally effective for both inside the reservoir and the outer zone. Besides, the mechanical pressure (P_p) applied to the fluid from the rod tip is also equal in every cycle of the impact. Considering the terms in the equation, it can be concluded that the consistent droplet formation is observed only when the hydrostatic pressure (P_{hs}) starts to overcome the surface tension (P_{st}) and the re-flow pressure (P_{rf}) sufficiently. Here, it is denoted that P_{rf} refers to the capillary reflow around the lateral piston to the upward during the impact (Lee et al., 2008). Taking into account, the P_p, P_{st}, and P_{rf} also remains constant, which are shortly indicated with P_c; the droplet formation stages can be narrowed into three states as observed in the experiments;

- State I. $P_{hs} >> P_c$: Irregular droplet generation (blob, satellite)
- State II. $P_{hs} > P_c$: Homogenous droplet generation
- State III. $P_{hs} \leq P_c$: Satellite or discontinuous droplet generation.

Therefore, in order to maintain the homogenous droplet formation regime, the height of the liquid inside must be kept constant at a certain point (State II). In the next step, the factors affecting the melt height inside are investigated. In this way, it becomes possible to generate homogenous droplets without any time limitation.

4.2.2. The Relationship between the Molten Height and the Droplet Ejection

An additional and more detailed experiment is conducted in order to analyze the homogenous droplet formation process depending on the height of the liquid. Therefore, droplet formation in eight experiments is repeated, and the periods are recorded more precisely. The experimental procedure is kept under the same fixed conditions given previously. However this time, instead of feeding the wire non-stop for 5 mins as in preliminary experiments, the feeding system is controlled dynamically. The details about the feeding operation can be followed from Figure 4.18 involving the droplet formation States, Cases, time durations, and the liquid volume (V_{molten}) depending on the feed amount.

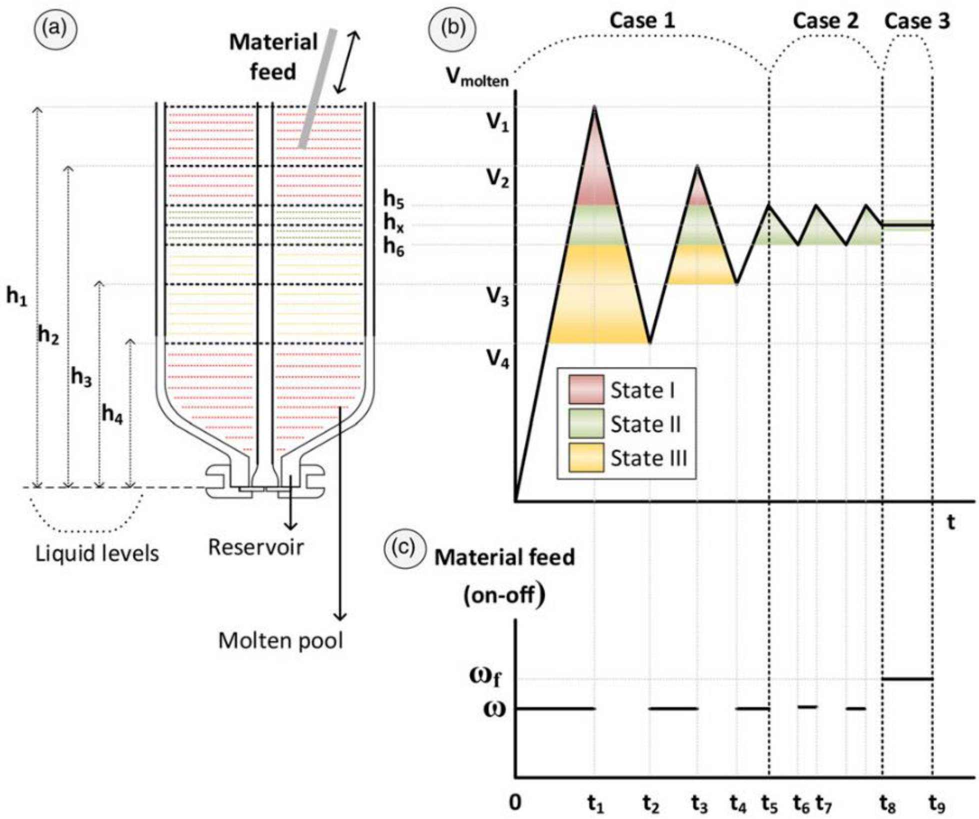

Figure 4.18. a. Varying molten pool levels inside the reservoir, b. Representative State intervals corresponding to varying molten metal volume, c. Time intervals for the gear extrusion operation for wire feeding.

In the previous section, the States were defined, and it was declared that the ultimate goal was to reach State II. Now, the amount of wire that needs to be fed in order to maintain the droplet generation process in State II stably is studied in detail under different Cases. In these Cases, the feeding is performed at different speeds and intervals dynamically. As a result, sustainable droplets are ejected in Case 3 by finding the most suitable wire feed amount. Detailed observations and explanations of the feeding operations in the cases are presented under the titles of Case 1, Case 2, and Case 3, respectively. It should be noted that the cases indicate the separate and multiple experimental sessions, but given together in the graphs representatively.

4.2.2.1. Case 1

As soon as the desired temperature is reached, the actuation and material feeding processes are initiated at the same time (0-t_1). When the droplets start to form (t_1), the feed is cut and the regime is monitored (t_1–t_2) until the droplets cannot be formed. This period includes all of the states defined previously (State I, II, and II). In order to determine the useful time period (State II), the feed is restarted and continued until the droplet generation starts again (t_2–t_3). By repeating this procedure, it is intended to narrate the time duration in order to achieve more precise intervals for proper droplet formation. The ejection is monitored again (t_3–t_4). This process was repeated until the time interval for the droplet regime without blob or satellite formation is obtained (t_5–t_8). In Case I, the required range of the molten pool level is able to be revealed even though the feeding was still performed manually.

4.2.2.2. Case 2

As the blob-like and the satellite droplet formations are eliminated, the useful interval is achieved for generating spherical droplets having a standard deviation in the mean diameters below 5%. In Case 2, more experiments are performed to further narrow the upper and lower fluid height limits found in Case 1. The range is narrowed further in each experiment consecutively. In this way, instead of a certain height range, a single and precise liquid height required for homogenous droplet formation is found. Within the on–off period of the material feed, the level of the molten liquid varies between the h_5 and h_6. By means of comparing incoming and leaving material amount, a correlation for the necessary time of wire feeding to eject one (unit) droplet in a unit time is established. In other words, it is aimed to restore the descending volume height of the liquid within one second which was to keep the droplet generation stable. Therefore, the mathematical calculation for keeping the liquid height fixed at an effective level (h_x) is established. First, the amount of wire driven is the determinant factor for the hydrostatic fluid pressure inside (P_{hs}), depending on the fluid height (h_f) that can be expressed by Equation 4.4;

$$P_{hs} = h_f . d_s . g \qquad (4.4)$$

where the term d_s stands for the density of the solder material and g for the gravitational acceleration. In order to obtain the relation between the feed amount and the height inside, a series of calculations are made based on the unit droplet mass (m_u) generated per unit time. To do this, the total mass of the droplets (M_t) depending on the frequency (f) within the homogenous regime interval, that is, t_5–t_6, was taken as a starting point (Equation 4.5), which is;

$$M_t = m_u . f \qquad (4.5)$$

The total volume (V_{out}) of the material ejected through M_t can be expressed as (Equation 4.6);

$$V_{out} = \frac{M_t}{d_s} \qquad (4.6)$$

Thus, the unit volume of a droplet ejected in every impulse ($V_{out,\ unit}$), (Equation 4.7);

$$V_{out,unit} = \frac{M_{t/f}}{d_s} \qquad (4.7)$$

As shown in Figure 4.19, the necessary volume of wire (V_{wire}) in order to compensate the decreasing liquid level for a unit droplet ejected that needs to be fed must be $V_{wire}=V_{out,unit}$. (Equation 4.8).

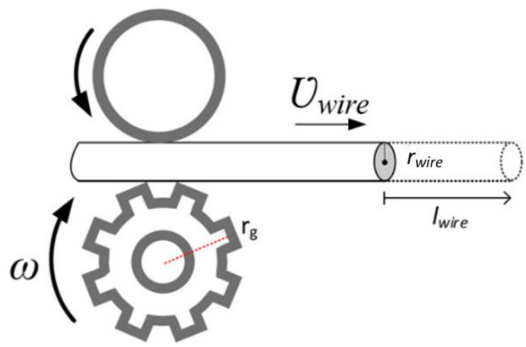

Figure 4.19. Amount of wire fed by the extruder gears

and,

$$V_{wire} = \pi r_{wire}^2 . l_{wire} \tag{4.8}$$

r_{wire}

where r_{wire} is the radius of the solder wire and l_{wire} is the length of the wire that is fed into the reservoir within t_{feed} seconds for one droplet. That is, the length of the wire fed toward inside with a linear velocity of (υ_{wire}) during the t_{feed}, can be obtained as (Equation 4.9);

$$l_{wire} = U_{wire} . t_{feed} \tag{4.9}$$

Since the linear velocity of the wire directly depends on the rotational speed (ω) and the radius (r_g) of the feeder gear, the linear velocity can also be expressed as follows (Equation 4.10);

$$\upsilon_{wire} = \omega . r_g \tag{4.10}$$

To combine Equations (4.9) and (4.10) into the (4.8), V_{wire} is found as (Equation 4.11);

$$V_{wire} = \pi r_{wire}^2 . \omega . r_g . t_{feed} \tag{4.11}$$

When the equation is compiled as to be $V_{wire} = V_{out,\ unit}$ (Equation 4.12);

$$\frac{M_t / f}{d_s} = \pi r_{wire}^2 . \omega . r_g . t_{feed} \tag{4.12}$$

By re-arranging the equation, the necessary feeding time for a single droplet while keeping the liquid level same is achieved as (Equation 4.13);

$$t_{feed} = \frac{M_t}{f . d_s . \pi . r_{wire}^2 . \omega . r_g} \tag{4.13}$$

In summary, the necessary feeding time for generating a single droplet is revealed taking into account the known operational inputs (wire, feeding, and actuation properties). It was performed by monitoring the eligible intervals providing a homogenous ejection and also by measuring the mass of droplets. To summarize, the height of the melt inside will not change if the wire is fed with a certain rotational speed (ω) and duration (t_{feed}). Therefore, the effective hydrostatic pressure will not change which leads a homogenous droplet generation.

4.2.2.3. Case 3

After this stage, the work is taken a step further, and the manual wire feeding mechanism is automated. The automation process is set in order to achieve a fixed liquid level inside reservoir while the ejection process keeps continuing. Thus, the software is modified to refill the reservoir to compensate for the volume of each discarded droplet. To do this, the new found rotational speed (ω_f) is defined for the extruder gears through the Arduino software by using Equation 4.13. Owing to the modifications, the reservoir can now be refilled just in 1 second under the defined actuation inputs. The ω_f is obtained with the inverse proportion of the previous rotational speed (ω) within the t_{feed} time interval (Equation 4.14).

$$\omega_f = \omega . t_{feed} \tag{4.14}$$

Through the correlation, it is observed that the liquid height can be kept constant if the extruder gear is re-set to rotate with 0.582 rad/s rotational speed for 0.9050 s for a single droplet. Thereby, the final rotational speed for re-filling the reservoir continuously during the ejection within 1 second can be found as 0.527 rad/s due to Equation 4.14. The results of calculations according to the developed correlations are summarized in Table 4.8.

Table 4.8. Operational conditions and the found results of the subjected correlations

	Value	Unit
t_5-t_6	20	S
f	1	Hz
N	20	Droplet count
M_t	0.4	g/mm^3
d_s	0.0086	g/mm^3
r_{wire}	0.6	Mm
w	0.582	rad/s
r_g	0.6	mm
t_{feed}	*0.9050*	*s (for a unit droplet)*
ω_f	*0.5272*	*rad/s (for continuous feed)*

N: total droplet number ejected within the homogenous regime interval of t_5-t_6.

According to the experimental results, the liquid height, and thus the hydrostatic pressure, can be kept constant if the feeder gear is operated under the rotational speed of ω_f. Until this point, the gradual enhancement by taking into account the three cases is realized. The experimentations are continued by creating a solder droplet array in a certain pattern using the new found operating parameters.

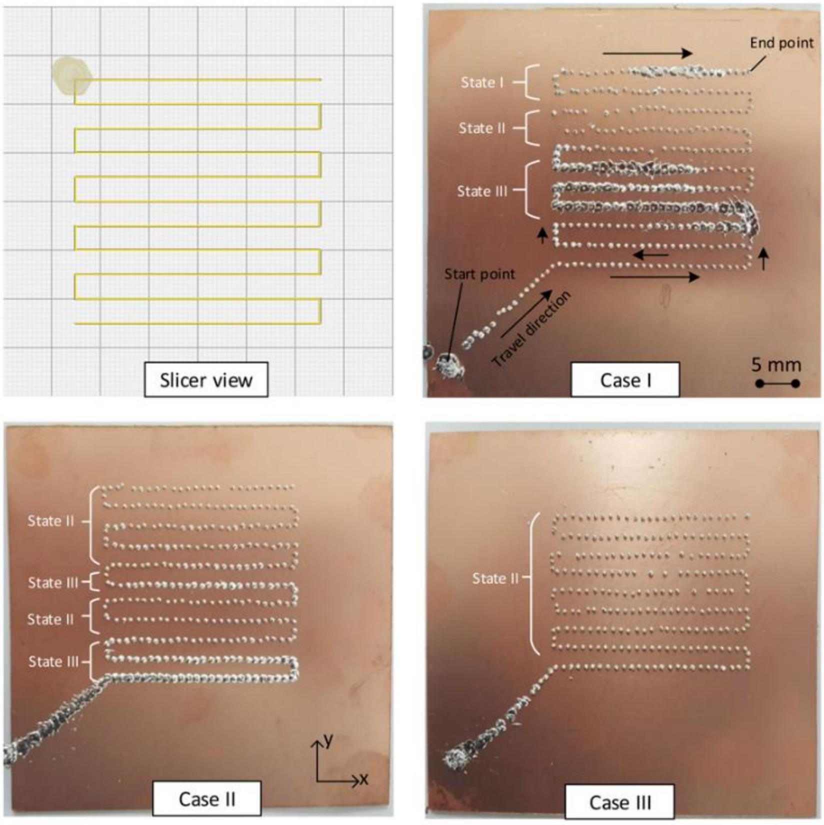

Figure 4.20. Gradual droplet generation steps belonging to the Cases and the view from the Cura Slicer

In Figure 4.20, the real-time implementation of the State's and Case's defined in Figure 4.18 are presented. During these printing operations, the fixed parameters are kept the same. After achieving a proper pattern consisting homogenous droplets, the built parameters on the slicer were rearranged in order to examine the system capability for printing a functional circuit. The printed circuit having a certain pattern is demonstrated in Figure 4.21.

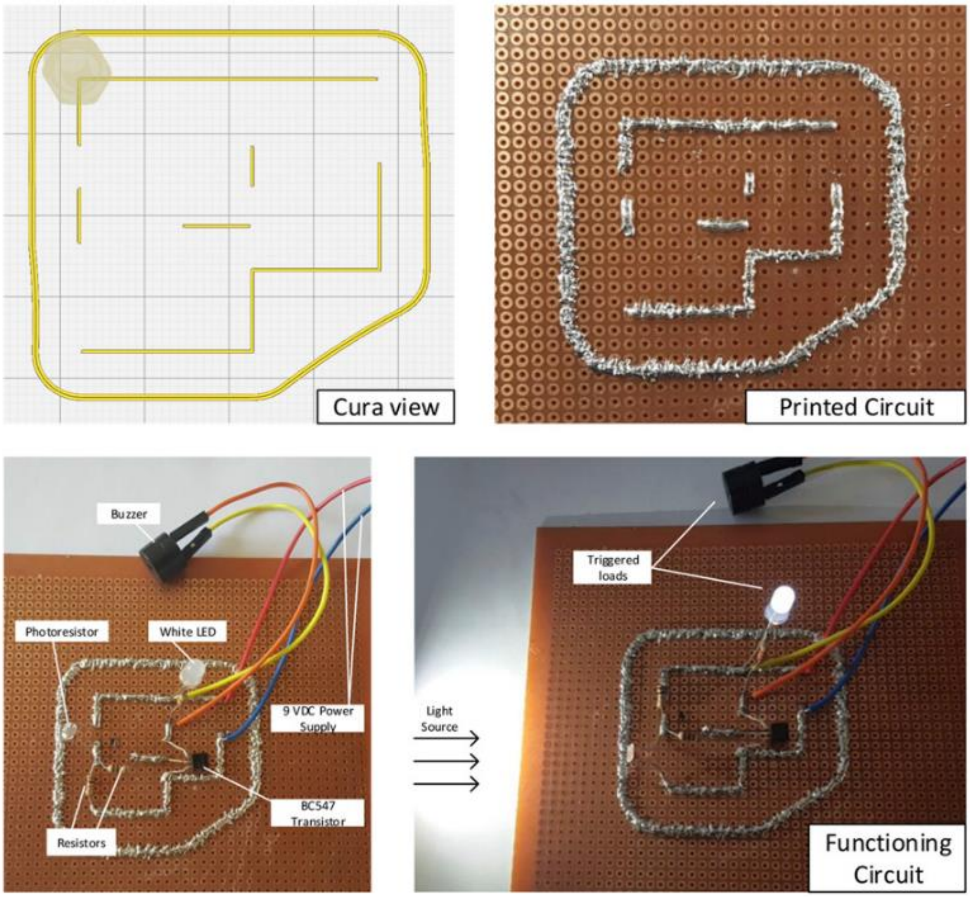

Figure 4.21. Light-dependent resistor (LDR) circuit manufacturing steps.

The light-dependent resistor (LDR) circuit is chosen in order to test the functionality of the consistent droplets obtained in the experiments. The light-sensitive circuit triggers the connected load depending on the amount of light it detects by using a photoresistor (Website, 2021j). Both a white LED light and a buzzer are used as a load in the circuit. The circuit diagram is first designed as a CAD model then exported to the slicer software. The pattern pathway is passed three times in order to prevent possible disconnections on the circuit. After the printing process completed and the electronic components are placed on, the functionality is tested by empowering the circuit which results in no problem on duty.

5. RESULTS AND DISCUSSION

In this section, the results are presented in a systematic way, first as FFF and then MDJ, as adopted in the experimental narratives. Although the findings obtained in polymer and metal-based processes vary widely in characteristics, there is also a lot in common due to the nature of AM processes. The foremost of these is that the open-source concept can be used in a practical way in terms of industrially effective processes such as metal deposition. Then, owing to the modifiable infrastructure, it becomes possible to produce multi-purpose and multi-material parts. Studies that started with polymer deposition have been made suitable for metal deposition operations thanks to low-cost, routine engineering applications that are applied in a minor but effective way. In this thesis study, both problems are evaluated on the same ground and the novel solution methods are discussed as specific as their background requires.

5.1. The Statistical Analysis of the Tensile Test Results

In this section, with the help of some statistical tools, it is aimed to reveal the effects of the parameters on the UTS of the FFF-printed part. In order to achieve the highest tensile behaviour, Main Effects plots for the S/N ratios are generated via Minitab® (with trial licence ID: 1evXYgxIRwcBO93OAJaQ) software. These plots are used for determining the best combination of the parameters with their suitable levels. Afterwards, the validation of the obtained results has been done by printing new specimens with the newly found optimal parameters. Finally, ANOVA analysis was performed to see the percentage contribution of each parameter on the tensile response. Tensile test results have been shown with related parameter combination in Table 5.1.

Table 5.1. Tensile test results

Print order	Parameters				*Test order*	Responses (at max.)		*Print order*	Parameters				*Test order*	Responses (at max.)	
	A	*B*	*C*	*D*		Stress	Strain		*A*	*B*	*C*	*D*		Stress	Strain
1	1	1	1	1	*1*	45.68	5.22	*14*	3	4	1	3	*14*	50.08	6.86
2	1	2	2	2	*2*	55.67	7.43	*15*	3	5	2	4	*15*	53.59	7.94
3	1	3	3	3	*3*	56.03	**7.98**	*16*	4	1	4	2	*16*	51.29	6.78
4	1	4	4	4	*4*	48.73	6.45	*17*	4	2	5	3	*17*	52.04	7.43
5	1	5	5	5	*5*	49.92	6.25	*18*	4	3	1	4	*18*	49.38	6.53
6	2	1	2	3	*6*	52.78	6.69	*19*	4	4	2	5	*19*	48.20	6.55
7	2	2	3	4	*7*	55.48	7.68	*20*	4	5	3	1	*20*	55.04	7.86
8	2	3	4	5	*8*	49.42	6.24	*21*	5	1	5	4	*21*	47.60	7.24
9	2	4	5	1	*9*	**56.74**	7.52	*22*	5	2	1	5	*22*	45.95	5.93
10	2	5	1	2	*10*	55.48	7.25	*23*	5	3	2	1	*23*	54.17	7.49
11	3	1	3	5	*11*	52.12	7.11	*24*	5	4	3	2	*24*	56.17	7.93
12	3	2	4	1	*12*	52.78	7.05	*25*	5	5	4	3	*25*	55.80	7.51
13	3	3	5	2	*13*	54.17	7.58								

The bolded values show the highest responses among the 25 specimens. These responses represent the average of three replications for each. (Max. Stress in MPa, Max. Strain in % units.)

The printed specimens have been tested with the same order after printing was completed

5.1.1. The Analysis of S/N Ratio

The value of the S/N ratio indicates the interaction between input and output. Higher values are desired, which means reduced variability of the input parameter on the output quality. In other words, the optimum combination can be revealed according to the highest S/N ratios of the levels for each parameter. In Table 5.2, the S/N ratios of the levels are presented using the main effects plots.

Table 5.2. The rankings of S/N ratios with main effects plot

Level	*A*	*B*	*C*	*D*
1	19.32	19.28	18.95	19.78
2	19.90	19.92	20.08	20.30
3	20.19	19.99	20.66	20.17
4	19.84	19.88	19.57	20.00
5	20.05	20.24	20.06	19.07
Delta	0.87	0.96	1.71	1.23
Rank	4	3	1	2

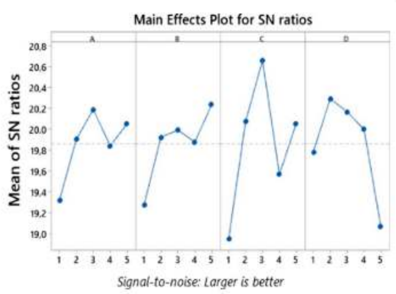

Taking into account the magnitudes of the S/N ratios, the best combination was obtained for the highest tensile strength using the same software. As mentioned, the S/N ratio is expected to be high in Taguchi analysis. However, the method of calculating the ratio varies according to the level of quantity expected from the output. This quantity can be determined as to be minimum, average or maximum according to the expectations from the output (Roy, 2010). In this study, the Larger-the-Better approach is applied since the output, i.e. UTS, is expected to be at the highest levels. Therefore, the calculation of the ratios is conducted based on Equation 5.1.

$$S/N = -10\log\left(\sum_{i=1}^{n}\frac{1/Y_i^2}{n}\right) \tag{5.1}$$

In the equation, n represents the number of the tensile test responses and Y_i is the individual result of the level combination of the related sample. It should be noted that the equation is based on the averaged tensile results of three repetitions of each sample. Therefore, n corresponds to 25. For the same reason, individual results (Y_i) also indicate the averaged values of each. In Table 5.2, the tensile responses were found to be more sensitive to the infill pattern (C), infill overlap (D), the shell wall number (B) and the line width (A) taking into account their rankings, respectively. On the other hand, the best combination for the highest UTS was revealed as A at 0.50 mm, B at 5, C at [45°/− 45°]* and D at 40% ($A_3B_5C_3D_2$). In the next section, new specimens with the suggested combination are manufactured then exposed to the verification test runs.

5.1.2. Verification Tests

Additional tests have been performed in order to validate the results of statistical analysis. The specimen with the combination of $A_3B_5C_3D_2$ (with five replications) are printed and average results are presented in Table 5.3.

Table 5.3. Test result for the validation sample $A_3B_5C_3D_2$

$A_3B_5C_3D_2$		
Runs	Max. stress (MPa)	Max. strain (%)
1	66.17	8.78
2	65.66	7.18
3	68.20	8.85
4	69.77	8.64
5	68.51	8.64
SD	1.71	0.70
Average	67.66	8.42

It should be noted that the numbers in the found combination indicate the suitable level of the related parameter. The fixed printing parameters are kept the same that of previously fabricated ones as well as the environmental conditions such as ambient temperature and humidity. When the $A_3B_5C_3D_2$ combination obtained in accordance with the Taguchi approach was subjected to tensile tests, it was observed that the tensile strength-strain values were higher than the previous samples. It is noted that an improvement of about 11 MPa (Sample 9) for the strength value and 0.44% (Sample 3) for the strain value is achieved. In summary, it is concluded that the statistical approach was consistent with the experimental results. It is then become possible to apply the same tensile test results into the ANOVA analysis in order to observe the contributions of the parameters to the tensile strength.

5.1.3. ANOVA Analysis

Besides the optimum combination, the percentage contribution of the selected parameters is revealed by applying the ANOVA to the tensile test results. ANOVA is a statistical method in order to determine the significancy of the input factors' influence over the variation on the response (Roy, 2010). In the analysis, it was accepted that the parameters having p-value less than 0.05 (5%) had a statistically significant effect on the output characteristics. Table 5.4 presents the percentage contribution of the parameters to the maximum tensile stress and the strain that material can withstand.

Table 5.4. The ANOVA tables for maximum stress (above) and strain (below)

Maximum stress

Paramter	DoF	Adj SS	Adj MS	*F* value	*P* value	Contrib. (%)
A	4	26.80	6.700	2.00	0.187	9.82
B	4	43.44	10.861	3.24	0.074	15.92
C	4	84.03	21.008	6.28	0.014	**30.80**
D	4	91.81	22.954	6.86	0.011	**33.65**
Error (Pooled)	8	70.24				
Total	24	272.88				100.00

Maximum strain

Paramter	DoF	Adj SS	Adj MS	*F* value	*P* value	Contrib. (%)
A	4	1.222	0.3055	2.69	0.109	10.39
B	4	1.539	0.3846	3.39	0.067	13.08
C	4	5.143	1.2856	11.32	0.002	**43.70**
D	4	2.955	0.7387	6.50	0.012	**25.11**
Error (Pooled)	8	2.761				
Total	24	11.77				100.00

The bold values represent the percentage contributions of the significant parameters

In addition, PLA material is referred as a brittle material according to the most of commercial resources (Website, 2020a, b, c). Therefore, the limited plastic elongation after the elastic region indicates that UTS and elongation should be evaluated according to the task to be performed. Hereby, ANOVA tests are conducted for both of them. Regarding the upper side of Table 5.4, the infill overlap (D) and the infill pattern (C) parameters stand for dominant factors with 33.65% and 30.80% contribution to the maximum stress of the material, respectively. For the maximum strain, the importance grade of the parameters has swapped as infill pattern of 43.70% and 25.11% of infill overlap. In order to examine determinant level over the significant contribution of these parameters, the post-hoc tests are performed. Based on Tukey Method, the multiple comparisons between the mean responses of 5 levels for each parameter are made. The levels are compared in pairs and the differences between the means is obtained. As a testing procedure, the p-values for each pair are re-adjusted. It is then become possible to interpret the effect of levels on the response of significant parameters (Rocha et al., 2016). In Figure 5.1, the difference of means of the level pairs for parameters C and D with their corresponding *p-values* are presented both for the stress and the strain.

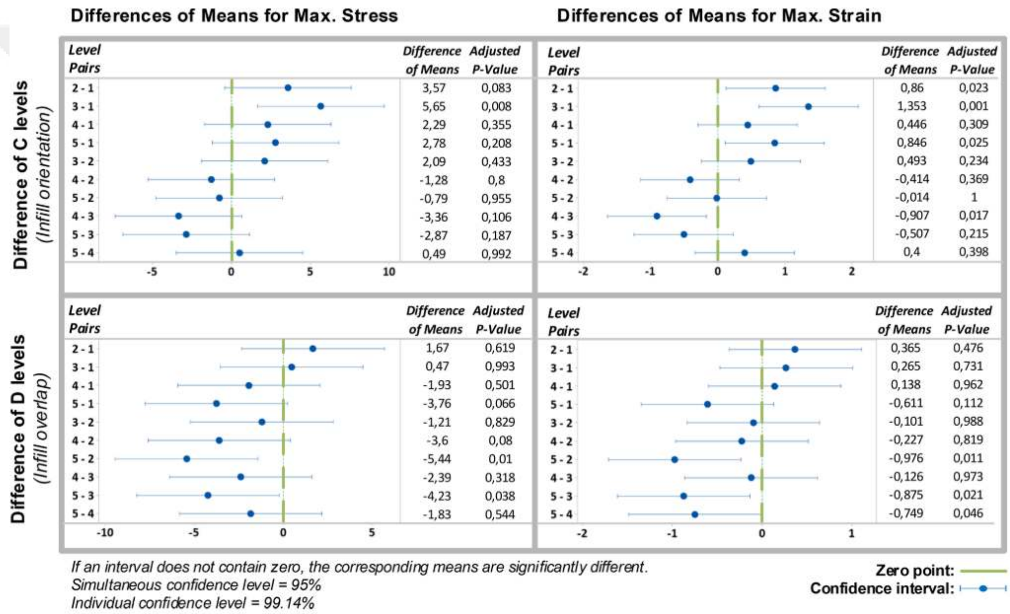

Level Pairs (C)	Stress: Difference of Means	Stress: Adjusted P-Value	Strain: Difference of Means	Strain: Adjusted P-Value
2 - 1	3,57	0,083	0,86	0,023
3 - 1	5,65	0,008	1,353	0,001
4 - 1	2,29	0,355	0,446	0,309
5 - 1	2,78	0,208	0,846	0,025
3 - 2	2,09	0,433	0,493	0,234
4 - 2	-1,28	0,8	-0,414	0,369
5 - 2	-0,79	0,955	-0,014	1
4 - 3	-3,36	0,106	-0,907	0,017
5 - 3	-2,87	0,187	-0,507	0,215
5 - 4	0,49	0,992	0,4	0,398

Level Pairs (D)	Stress: Difference of Means	Stress: Adjusted P-Value	Strain: Difference of Means	Strain: Adjusted P-Value
2 - 1	1,67	0,619	0,365	0,476
3 - 1	0,47	0,993	0,265	0,731
4 - 1	-1,93	0,501	0,138	0,962
5 - 1	-3,76	0,066	-0,611	0,112
3 - 2	-1,21	0,829	-0,101	0,988
4 - 2	-3,6	0,08	-0,227	0,819
5 - 2	-5,44	0,01	-0,976	0,011
4 - 3	-2,39	0,318	-0,126	0,973
5 - 3	-4,23	0,038	-0,875	0,021
5 - 4	-1,83	0,544	-0,749	0,046

Figure 5.1. The difference between the levels of significant parameters strain

In the graphs, if the confidence interval (the blue line) do not intersect with the point zero (the green line), it means that a significant difference in the means exists between the paired levels. In this way, a reliable information about the relevant level(s) contributing to the parameter becoming significant is obtained.

It is found that there is a significant difference between the level 3 and 1 of the parameter C, for the maximum stress as shown in the first quarter of Figure 5.1. In more detail, the parameter C has found to have a significant effect on the stress response as presented previously in ANOVA table. At this point, the reason for this significance may be associated with the significant differentiation between the [45°/− 45°]* and [0°] oriented infills on the mean stress response. For further, the amount of the percentile contribution found in ANOVA may also be related to the amount of the differences of means between the pair of {3-1}. In the second quarter, the mean differences between the pairs {3-1}, {2-1}, {5-1} and {4-3} has been obtained significantly different for maximum strain, from large to small, respectively. It should be noted that the highest difference of means appears in the pair {3-1} as for the maximum stress.

Regarding the D parameter, it has been observed that the mean difference in pairs {5-2} and {5-3} is significantly different in the stress response, as shown in the third quarter. In other words, it is possible to expect a significant impact occurs on tensile stress; if the infill overlap settings of 20%, 40% and 100% are chanced within themselves, taking into account both the ANOVA and the comparative tests. The similar interpretation can be made for the pairs {5-2}, {5-3} and {5-4} of the infill overlap parameter, for the mean differences on the strain response. So far, the differences between the levels have been revealed by means of these analyses. However, the relevant levels that make up the difference between the levels need to be examined in more detail. It is then the real-world effects of significant parameters and their levels on the mass and strength of the part can be clearly explained. In the following sections, measurements made to determine the effects of the levels obtained as a result of the above comparisons on mass and strength are presented.

5.1.4. Evaluating the mass variation in the specimens

From another perspective, the amount of material consumed is an important concern in FFF. While enhancing the tensile properties, it is also important to keep the material consumption at an optimum level. Therefore, the mass measurements of the specimens are done in order to reveal the mass variation according to the combinations. The measurements are conducted within same conditions in series using a precision scale (TP-214, *Denver Instruments*) with the readability of 0.1 mg (Figure 5.2).

Figure 5.2. The precision scale (*Denver Instruments*)

The average values of three replication parts for 1 to 25 and the average of five replication parts for the Sample no:26 are listed in Table 5.5.

Table 5.5. Measured masses of samples

No	Mass	No	Mass	No	Mass	No	Mass	No	Mass
1	2.06	6	2.36	11	2.68	16	2.77	21	3.16
2	2.15	7	2.59	12	2.42	17	2.95	22	3.55
3	2.36	8	2.92	13	2.65	18	3.37	23	2.68
4	2.65	9	2.27	14	2.80	19	3.70	24	2.86
5	2.92	10	2.48	15	3.25	20	2.42	25	3.25
								26	2.62

All mass measurements (in unit of grams) have been done before the tensile testing
Average mass of 25 samples in total: 2.77
Standard deviation of the averages (for the samples 1 to 25): 0.42

Considering that the average mass of 25 samples is 2.77 grams with a standard deviation of 0.42 grams as shown in table, it is observed that the mass of the validation sample (Sample no: 26) was at average levels as also presented in Figure 5.3.a.

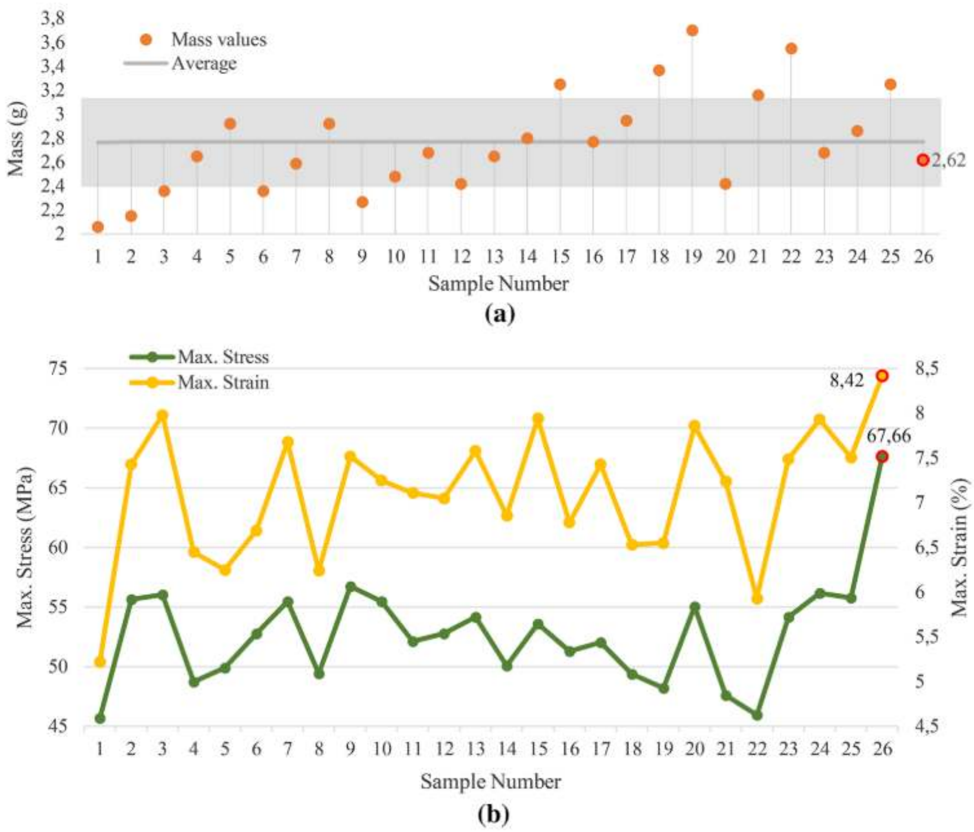

Figure 5.3. a. The mass distribution of the all samples (The grey zone represents the range of standard deviation from the average), b. The maximum stress and the maximum strain values of the samples

In the same figure, the grey zone corresponds the boundaries of the standard deviation from the average. It should also be noted that in the following Figure 5.3.b that the Sample 26 presents maximum values among other samples in both stress and strain values. To express the findings numerically, the improvement of 19.24% in maximum strength and 5.51% in maximum strain is provided while keeping the mass close to the average. As a result, UTS, as it supports the hypothesis, is increased only by configuring the parameters without increasing the material consumption. In other words, UTS could be improved while keeping the mass in optimum level without doing major modifications on the model geometry.

The variation of the mass is also evaluated using the S/N ratios by applying the "Smaller-is-Better" approach. In Figure 5.4, the variation in S/N ratios is given in order to unveil the influence of the parameters over the material consumption.

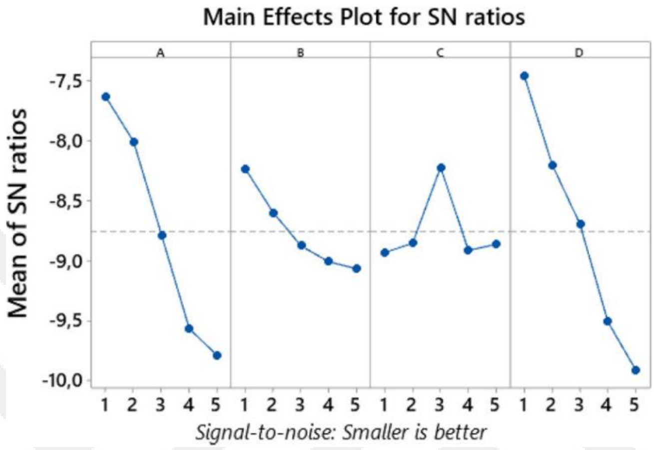

Figure 5.4. Main effects plot for S/N Ratios of the measured masses.

The main effects graph indicates the linear proportionality between the consumption and the level of parameters of line width (A), shell thickness (B) and the infill overlap (D). The consumption decreases when the levels of three parameters decrease as expected. However, there is an irregular variation in the infill orientation. In details, the orientation with [45°/− 45°]* at level 3 has the most powerful effect over the minimizing the material consumption. In other words, continuous infill lines result in enhanced UTS by also providing the significant effect in reducing the material consumed. It should be noted that the unique difference between the continuous and discrete infill lines is associated to the variation in the amount of occupied area by an overlap over the shell. In order to clarify the reasons sourced by the differentiation, the further investigations has been conducted. By doing this, it has been aimed to relate the material consumption, UTS and quantity of area occupied together.

5.1.5. Investigation on Relationship between Overlap Area and UTS

In order to reveal the effect of the continuity in the infill lines over the shell, the area occupied by the overlapping patterns is investigated geometrically. Firstly, the calculations are established on determining the boundaries of the areas using the CAD software. In Figure 5.5, three different overlapping geometries and the dimensions are given with their symbols;

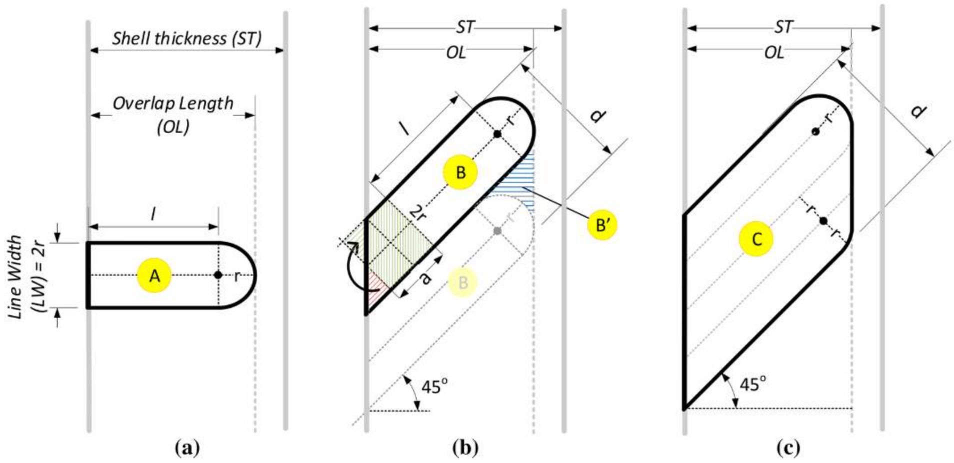

Figure 5.5. Areas occupied by overlappings with different angles a. [0°], b. [45°], c. [45°]*

The corresponding equations for yellow marked areas are presented as follows, respectively.

$$A = l.2r + \frac{\pi r^2}{2} \tag{5.2}$$

$$B = A + 2r.a \tag{5.3}$$

$$C = 2B + B^{'} \tag{5.4}$$

According to the ANOVA analysis, the value of UTS depends on both the infill orientation and the amount of overlapping. Overlaps with the line angle of 0° (also valid for 90°), 45° and 45°* are investigated geometrically. It is focused on these angles because, as discussed in this study, these angular orientations are the most widely used filler arrays in the printing industry. The general correlation is generated between the areas by using the overlap length (*OL*) and the line width (*LW*). The transition between the areas has been done by using the common dimensions among the three overlap models as shown in Figure 5.5. This is to say, the structure of the relation is set based on the linear proportionality between the length of straight edge (*l*) and the length (*a*). In order to relate the dimensions of "*l*" and "*a*", it is necessary to determine the actual size of the overlap covering the shell in millimetres. Since the amount of overlap determined for the samples is in percentile form at the slicer interface, the necessary conversion is made using the relevant parameters presented in Table 5.6.a.

Table 5.6. Overlap conversion table and obtained dimensional relations between "*l*" and "*a*"

(a) *Overlap percentage conversion into length*

LW (mm)	#	20%	40%	60%	80%	100%	Wall Line Count
0.40	1	**0.08**	0.16	0.24	0.32	0.40	1
0.40	2	0.16	**0.32**	0.48	0.64	0.80	2
0.40	3	0.24	0.48	**0.72**	0.96	1.20	3
0.40	4	0.32	0.64	0.96	**1.28**	1.60	4
0.40	5	0.40	0.80	1.20	1.60	**2.00**	5
0.45	6	0.09	0.18	**0.27**	0.36	0.45	1
0.45	7	0.18	0.36	0.54	**0.72**	0.90	2
0.45	8	0.27	0.54	0.81	1.08	**1.35**	3
0.45	9	**0.36**	0.72	1.08	1.44	1.80	4
0.45	10	0.45	**0.90**	1.35	1.80	2.25	5
0.50	11	0.10	0.20	0.30	0.40	**0.50**	1
0.50	12	**0.20**	0.40	1.00	0.80	1.00	2
0.50	13	0.30	**0.60**	0.90	1.20	1.50	3
0.50	14	0.40	0.80	**1.20**	1.60	2.00	4
0.50	15	0.50	1.00	1.50	**2.00**	2.50	5
0.55	16	0.11	**0.22**	0.33	0.44	0.55	1
0.55	17	0.22	0.44	**0.66**	0.88	1.10	2
0.55	18	0.33	0.66	0.99	**1.32**	1.65	3
0.55	19	0.44	0.88	1.32	1.76	**2.20**	4
0.55	20	**0.55**	1.10	1.65	2.20	2.75	5
0.60	21	0.12	0.24	0.36	**0.48**	0.60	1
0.60	22	0.24	0.48	0.72	0.96	**1.20**	2
0.60	23	**0.36**	0.72	1.08	1.44	1.80	3
0.60	24	0.48	**0.96**	1.44	1.92	2.40	4
0.60	25	0.60	1.20	**1.80**	2.40	3.00	5
		OL (mm)					

(b) *Corresponding lengths and areas to OL and LW*

#	OL	LW	Lengths (mm) *l*	*a*	Areas (mm²) A	B
20	0.55	0.55	0.275	0.114	0.270	0.335
13	0.60	0.50	0.350	0.145	0.275	0.345
17	0.66	0.55	0.385	0.159	0.330	0.420
3	0.72	0.40	0.520	0.215	0.270	0.355
7	0.72	0.45	0.495	0.205	0.300	0.395
10	0.90	0.45	0.675	0.280	0.385	0.510
24	0.96	0.60	0.660	0.273	0.535	0.700
26	1.00	0.50	0.750	0.311	0.475	0.630
14	1.20	0.50	0.950	0.393	0.575	0.770
22	1.20	0.60	0.900	0.373	0.680	0.905
4	1.28	0.40	1.080	0.447	0.495	0.675
18	1.32	0.55	1.045	0.433	0.695	0.930
8	1.35	0.45	1.125	0.466	0.585	0.795
25	1.80	0.60	1.500	0.621	1.040	1.415
5	2.00	0.40	1.800	0.746	0.785	1.080
15	2.00	0.50	1.750	0.725	0.975	1.335
19	2.20	0.55	1.925	0.797	1.180	1.615

(c) *The relationship between "l" and "a"*

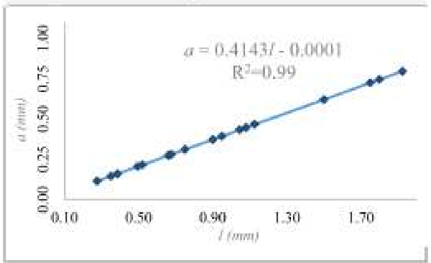

The bold values correspond the OLs (overlap lengths) for the samples 1 to 25. The regions highlighted in yellow indicate the relevant values belonging to the validation sample (No:26)

#: Sample number

R^2: Determination coefficient of regression

In the conversion table, OLs over the shell are calculated one by one through the CAD environment. The OL values (indicated by bolded numbers on each line) for 1 to 25 samples, including validation Sample no: 26 (highlighted in yellow), have been located suitably in table. In Table 5.6, this time the OLs are shown in ascending order with their respective sample numbers (#). As well as the lengths, calculated areas occupied by overlaps of each sample is added into the list. By doing this, the relation between the lengths of "*l*" and "*a*" has been revealed as it is presented in the graph in Table 5.6.c. During the measurements, some overlapping models were not added to the table due to the negligibly small or irregular geometric shape. In Figure 5.5, disturbed areas by overlapping are represented. Noting that "*LW = 2r*" and the "*OL = l + r*" as shown in the figure, the area "*A*" (Equation 5.2) can be written as defined by Equation 5.5 below.

$$A = LW\left(OL - \frac{LW}{2} + \frac{\pi.LW}{8}\right) \tag{5.5}$$

For the area "*B"*, the length "*a*" are expressed in form of "*l*" using the equation taken from the graph given in Table 5.6.c;

$$a = 0.4143l \tag{5.6}$$

Then, the area "*B*" becomes as below (Equation 5.7) combining the Equations of (5.3), (5.5) and (5.6), ignoring the 0.01% deviation;

$$B = A + 0.4143\left(OL - {}^{LW}\!/_{2}\right)LW \tag{5.7}$$

At this stage, the printed samples are examined with a digital microscope in order to ensure consistency of the study and to proceed safely to the next step. In this way, theoretical CAD calculations have also been verified. For verification, the sample with *LW* of 0.5 mm, *OL* of 1 mm (related conversion is available in Table 5.6.a and wall count of 5 is selected. Then, the relevant parameters as well as the area occupied by overlap as shown in Figure. 5.5.b (the area "*B*") are observed under the microscope. In Figure 5.6.a, the section taken from the digital view of the selected sample in the slicer is shown.

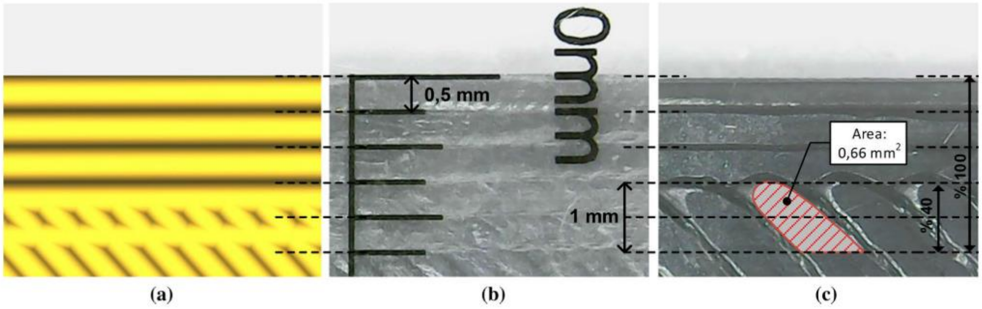

Figure 5.6. Verification of the CAD calculations, a. The screenshot of the sliced part taken from the slicer, b. Microscope image of the printed part, scaled by using a microscope calibration ruler. The image was taken from the shell region of top layer, c. The image of the bottom layer showing the measurement of overlap area on the shell (in the same part)

In Figure 5.6.b, the image of the sample under the microscope is given. This image was taken by placing a transparent calibration ruler on the printed sample. As can be seen from the scale of the ruler, the actual *LW* on the sample was confirmed to be 0.5 mm. In Figure 5.6.c, the length of the overlap was measured as 1 mm (40% of the total shell thickness). In the same image, the edges of the area covered by the overlap on the shell are traced through the image processing utility of the CAD software and the area in between is calculated. The theoretical area value of 0.63 mm^2 (can be found in Table 5.6.b or calculated by using Equation 5.7), showed only a 3% deviation from the measured actual area value of 0.66 mm^2. After observing that *LW*, *OL* and area measurements are highly compatible with digital and theoretical values, formulation processes are continued. In Figure 5.5.c, the area could be expressed as "$C = 2B + B''$", as mentioned in Equation 5.4. Here the area B′ arose from the continuity of the infill line, rather than discrete lines like in others (see Figure 4.6, 4.7 and 5.5). Based on the observations presented in previous sections, the additional area B′ tends to increase the tensile strength of part. To carry the investigation further, the variation in this area depending on the *LW* and *OL* parameters is examined. Considering Equation 5.4, it can be concluded that the difference between the areas *C* and *2B* gives the area *B'*. Thereby the areas of *C* and *2B* are calculated digitally in order to obtain the area "*B′* " and to observe the variation according to *LW* and *OL*. When the results obtained were tabulated, it is revealed that the area *B′* varies linear with the *LW* with a small deviation. The mentioned relationship is presented in Table 5.7.a with the ascending order of the *LW* parameter.

Table 5.7. The relationship between *B′* and *LW*.

(a) *Relationship between B′ and LW*

			Areas (mm^2)		
#	LW↑	OL	*2B*	*C*	*B′*
3	0.4	0.72	0.71	0.76	0.05
4	0.4	1.28	1.35	1.4	0.05
5	0.4	2	2.16	2.21	0.05
7	0.45	0.72	0.79	0.85	0.06
10	0.45	0.90	1.02	1.08	0.06
8	0.45	1.35	1.59	1.65	0.06
13	0.5	0.60	0.69	0.77	0.08
26	0.5	1.00	1.26	1.34	0.08
14	0.5	1.20	1.54	1.62	0.08
15	0.5	2.00	2.67	2.75	0.08
20	0.55	0.55	0.67	0.76	0.09
17	0.55	0.66	0.84	0.93	0.09
18	0.55	1.32	1.86	1.96	0.1
19	0.55	2.20	3.23	3.33	0.1
24	0.6	0.96	1.4	1.52	0.12
22	0.6	1.20	1.81	1.93	0.12
25	0.6	1.80	2.83	2.95	0.12

(b) *The graph of the correlation*

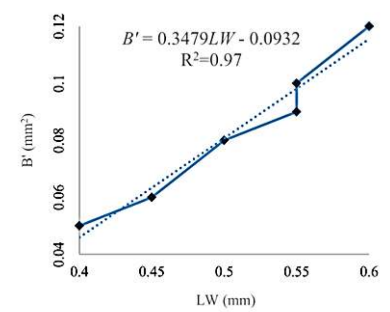

#: Sample number
R^2: Determination coefficient of regression

In the following, the correlation is derived from the graph as shown in Table 5.7.b. Based on the graph in table, the relationship between *B′* and *LW* could be established as (Equation 5.8);

$$B^{'} = 0.3479LW - 0.0932 \quad (5.8)$$

By combining Equations (5.4) and (5.8), the area "*C*" becomes (Equation 5.9);

$$C = 2B + 0.3479LW - 0.0932 \tag{5.9}$$

As an extended form of "C" by putting "B" (Equation 5.6) in Equation 5.8;

$$C = \left[LW\left(2.OL - LW + \frac{\pi LW}{4}\right) + \left(0.8286\left(OL - {LW}/{2}\right)\right)\right] + 0.3479LW - 0.0932 \tag{5.10}$$

Using the Equation 5.10, the generalized solution for the area occupied by [45°/− 45°]* oriented overlapping could be obtained. To summarize, the sample with [45°/− 45°]* oriented continuous infill lines tend to provide higher UTS than [45°/− 45°] oriented discrete infill lines as observed (Table 5.2 and 5.3). It should be noted that the only difference between the two orientation models is the extra area coming from area B' (Figure 5.5.b). Therefore, the reason of UTS increment has been associated to the increased overlap area. Due to the fact that there exist an apparent relation between UTS and the overlap area, the above equations are developed. In this manner, the user can apply the equations in order to obtain quantitative information about the area occupied by a unit overlap. Then, the parameters of *LW* and *OL* can be configured suitably in order to increase the overlap area. By doing this, the UTS value can be improved while keeping the material consumption in average levels. Moreover, the generalized equations for the areas of *A*, *B* and *C* could be applicable to the most of printing process since the orientation angles of 0° (or 90°), 45° and 45°* are suitable for many part structures.

5.2. Droplet Deposition Performance of the Modified MDJ Device

In the study, a novel, low-cost, and open-source droplet generator capable of forming consistent metallic droplets in open-air conditions is presented. The proposed device enables the users to generate neat droplets only by conducting a short series of preliminary experiments and determining their own operational parameters by suggested correlations. The necessary conditions for the droplet deposition process were set based on the dimensionless ***We*** number. In this way, a starting point is determined for the selection ofparameters that should be examined theoretically. In the first stage, the variables of the droplet velocities and the diameters in the equation were measured experimentally. By doing this, the limits of the proposed device were able to be determined. During these initial tests, it was noted that the droplets were formed in various regimes as a result of the observations. When the reasons ofthe variation were investigated, it was determined that the droplet regimes changed according to the amount of material feeding. That is, it is revealed that the melt height, and thus the hydrostatic pressure inside the reservoir, which varies with the feed rate, has a distinct effect on droplet formation.

In order to determine the effective regime in which the uniform droplets can be ejected, the droplet generation operation is analyzed in more detail by classifying the process into States (Figure 4.18). An equation is developed in order to control the amount of feed (Equation 4.14) since the classification of the States was made based on the amount of the material feed. Owing to this equation, the necessary State condition (State II) is achieved. That is, it is verified that the developed equation provides the stable droplet ejection process in the experiments as intended. At this point, it should be noted that the dimensions of the reservoir or the height of the liquid inside is not provided anywhere intentionally because it is dangerous and impractical to intervene in a device operating at high temperature for reasons such as size or liquid level measurement during operation. Instead, a more practical method is presented to provide the necessary pressure balance inside only by controlling the amount of the material fed. As the output of the experimentation, it has been proven that the required ejection conditions can be achieved regardless of the inner chamber geometry or the melt level inside. In other words, the users can manufacture a custom droplet generator for a variety of purposes, with the flexibility to change the dimensions of the generator parts, especially the melt container. In addition to the dimensional design, it has been proved by producing a working printed circuit (Figure 4.21) that if the parameters in the developed equation are adjusted appropriately, droplets suitable for the job can be obtained. As a limitation ofthis study, it can be interpreted that the droplets formed were relatively too large for precise MEMs applications. This fact can also be understood from the relatively large diameter of the droplets produced or the rough lines of the printed circuit board. However, all the features and all the process steps presented in detail with the device are explained in a systematic way. In this way, the proposed device is in a structure suitable for improvement to be used in studies, such as circuit printing production. Considering all the features discussed, this work is adaptable to mechanical impact-based droplet generators through commonly used extruder mechanisms. Moreover, it is possible to obtain homogenous droplet series based on the ejected droplet properties without the need to know the internal volume or liquid height of the reservoir used.

6. CONCLUSION AND FUTURE WORKS

In this thesis study, the AM processes based on direct material deposition method are examined and some of the identified problems are solved. In this context, in the first place, it is seen that there are many studies on increasing the strength of the parts produced with FFF. The most important of these are also given in detail in the relevant sections. However, it is found that material consumption has not been sufficiently taken into account in those studies where examinations aim at improving produced parts strengths. Therefore, in this study, series of experiments are conducted in order to reveal the effects of four interdependent parameters over the tensile behavior of the produced parts. The material consumption issue is also taken into account in determination of the configuration for the process parameters. The presented study is also supported by both statistical and analytical approaches. The commonly used type low-cost and open-source 3D printer is developed and necessary modifications are performed to conduct the experimental study. The 3D printer device is also improved and calibrated in order to maintain the compliance between the digital model and the real part. The obtained results are summarized below;

- The highest UTS of the part is achieved with the parameters of $A_3B_5C_3D_2$ revealed by Taguchi analysis; (Line Width: 0.5 mm, Shell Wall Number: 5, Infill Orientation: [45°/−45°]*, Infill Overlap: 40%). The improvement of 19.24% in maximum stress and 5.51% in maximum strain in the specimen printed with new levels of parameters are observed. Additional validation tests results provide a high degree of agreement between experimental data and statistical approaches.
- The infill overlap and infill orientation parameters have a significant effect on the ultimate tensile strength, given the close percentage contributions presented by the ANOVA analysis. The differences between the levels of

the significant parameters are determined using post-hoc tests. By this means, reliable information about the responsible levels in order to increase the tensile strength while controlling the material consumption are obtained. The details provided guidance to the users when tensile behaviour and overall mass of the printed part issues are a main design concern. Hence, a verified method is proposed that allows achiving the target parameters that need to be examined.

- The material consumption is considered during the design of experiments and also throughout the study. It has been seen that the [45°/− 45°]* infill lines with the 40% infill overlap have provided the highest UTS and the optimal material consumption at the same time. The results are obtained using main effects plots of the S/N ratios. The increase in the UTS of the combination found is given in both the mass and stress–strain distribution graphs. If the parameters are configured according to these settings, the users will be able to increase the UTS of the part while controlling the material consumption.
- In order to relate the interaction between infill orientation and infill overlap, generalized analytical formulations have been developed which supports the data obtained by the digital calculations. Finally, it has been observed that the larger occupied area by overlapping with [45°/− 45°]* orientation yields the higher UTS while keeping the mass in an average level. Furthermore, these equations are applicable to all operations in which the orientation angles of 0°, 45°, 45°* and 90° are used. It is highlighted that the equations are compatible with wide range of printing processes since these angles are widely preferred by the users. Details about the calculations have been presented by providing also the images of mentioned infill models.

As a result of the verified measurements, the UTS increase is achieved in the part, without the need to make major changes in the raw material content or part design. Owing to these user-defined parameters, UTS increase in the part is possible with minor adjustments as observed. It is aimed at contributing to the development and standardization of printing processes by focusing on the process parameters that are not been studied sufficiently looking for a means of tensile strength optimization. This way, it has been revealed and confirmed that the UTS can be improved with minimal mass variation by configuring the responsible parameters (infill overlapping and orienta- tion as revealed) accordingly. In other words, a user can configure the line width and overlap length parameters in the way to maximize the overlapping area using the developed formulations. In addition, the material waste is avoided since these configurations do not cause the mass to variate excessively as observed. A different point of view about the performance of the parts has been provided with this study, which is open for development, to the fast-growing AM industry. In future studies, it is planned to examine overlap increase and mass change by employing more advanced statistical tools as well as the metallurgical observations. This way, more detailed data on UTS increase can be obtained. By expanding the scope of study, the FFF processes can be used to serve many more fields by involving the compressive and flexural properties besides the UTS.

After this stage, the study is taken one step further and some modifications are made on the 3D printer device used in FFF processes. As a part of the modification, a custom-made droplet generator body is designed, manufactured and mounted on the relevant region of the FFF device. Hence a metal-based droplets are produced by the droplet generator. The drop-on-demand–based droplet formation performance is examined in detail with the experiments performed for the proposed 3D printer device. As a result of the theoretical calculations and the measurements, a steady progress is achieved in the droplet generation processes.

Finally, an effective method is presented to be able to meet the necessary conditions for creating qualified droplets. To point out the innovative aspects;

- Cost-effective device with easy access to its mechanical and electronic resources is introduced as an alternative to high-cost metal AM devices.
- The open source features of the system makes it a strong candidate for its use in scientific research and related development works.
- The device is capable of forming stable droplets in open-air conditions without strict pressure requirement. In this way, the difficulty of control applications and the equipment requirement are significantly reduced.
- The system is built on the ***We*** equation, which is a powerful factor in droplet generation. This way, researchers and manufacturers are promised an effective device where they can work on droplet formation and deposition techniques accordingly.
- In line with the findings obtained in the preliminary experiments, the classifications such as States and Cases are used throughout the study. These classifications allowed the experiments to be carried out in a sustainable and systematical in the way to achieve the ultimate goal. By means of classifications, an equation is developed to provide the appropriate wire feed amount. The obtained equation is then adapted to the experiments and it is observed that the theoretical equation is in good agreement with the experimental results.
- The fact that the methods and equations used in the experimental process can be easily adapted to mechanical impact-based droplet generating devices increases the widespread effect of the study.

The developed 3D printer is an open-source, cost-effective, highly modifiable device that can operate in open-air conditions using common type solder wire material and this makes this system an important valuable tool for metal printer related research. It should be noted that not only homogenous droplets are generated, but the presented system itself is highly adaptable for various droplet-based deposition processes according to the need. The presented study fairly contributes the droplet deposition operations by offering a flexible and modifiable system to the specialist for more precise operations.

However, there is still need further investigations on behalf of modulating the droplet properties. That is, the more precise solder arrays and more detailed circuit lines can be achieved by decreasing the droplets in diameter. Moreover, the frequency, thus the deposition rates can be increased which result in shortened production periods. This can be achieved by replacing the solenoid actuators with the piezoelectric actuators which also provides more precise actuation control. To be able to achieve all of the mentioned features, a deeper understanding of the droplet generator structure is still required. In particular, the geometric dimensioning of the generator itself including the reservoir, orifice, inlets, outlets and the other crucial parts need to be configured appropriately for the futureworks. The inclusion of thermal and metallurgical investigations are also expected to make significant contributions to the adoption of the droplet-based production processes into the manufacturing industry.

REFERENCES

Abdulhameed, O., Al-Ahmari, A., Ameen, W., and Mian, S. H., 2019. Additive Manufacturing: Challenges, Trends, and Applications, *Advances in Mechanical Engineering*, 11, 2.

Abtewa, M., and Selvaduray, G., 2000. Lead-free Solders in Microelectronics, *Materials Science and Engineering*, 27, 95-141.

Ahn, D., Kweon, J.H., Kwon, S., Song, J. and Lee, S., 2009. Representation of Surface Roughness in Fused Deposition Modeling, *Journal of Materials Processing Technology*, Vol. 209 Nos 15/16, 5593-5600.

Anzalone, G. C., Zhang, C., Wijnen, B., Sanders, P. G., and Pearce, J. M., 2013. A Low-cost Open-source Metal 3-D Printer, *IEEE Access,* 1, 803–810.

Araki, K., and Moriyama, A., 1981. Theory on Deformation Behavior of a Liquid Droplet Impinging onto Hot Metal Surface, *Trans. Iron Steel Inst.,* 583–590.

Arun Kumar, N., and Ting, C., 2006. A Method for Improved VCSEL Packaging Using MEMS and Ink-Jet Technologies, *Journal Of Lightwave Technology*, 24, 3, 1504-1512.

Astarita, A., Campatelli, G., Corigliano, P., Epasto, G., Montevecchi, F., Scherillo, F., and Venturini, G., 2021. Microstructure and Mechanical Properties of Specimens Produced using the Wire-arc Additive Manufacturing Process, *Proceedings of the Institution of Mechanical Engineers, Part C: Journal of Mechanical Engineering Science*, 235, 10, 1788–1798.

ASTM International, 2012. Standard Terminology for Additive Manufacturing Technologies, West Conshohocken.

ASTM International, 2013. F2792, Standard Terminology for Additive Manufacturing Technologies, West Conshohocken.

ASTM International, 2014. Standard Test Method for Tensile Properties of Plastics, West Conshohocken.

Badrinarayan, B., and Barlow, J. W., 1992. Metal Parts From Selective Laser Sintering of Metal-Polymer Powders, *Solid Freeform Fabrication Symposium,* 141–146.

Baumers, M., Tuck, C., Wildman, R., Ashcroft, I., Rosamond, E., and Hague, R., 2012. Combined Build-time, Energy Consumption and Cost Estimation for Direct Metal Laser Sintering, *Proc of the Solid Freeform Fabrication Symposium*, 278–288.

Beer, S. Z., 1972. Liquid Metals: Chemistry and Physics, Marcel Dekker, New York.

Berg, J. C., 1993. Wettability, Marcel Dekker, New York.

Beuth, J., and Klingbeil, N., 2001. The Role of Process Variables in Laser Based Direct Metal Solid Freeform Fabrication, *J Met,* 9, 36–39.

Bhola, R., and Chandra, S., 1999. Parameters Controlling Solidification of Molten Wax Droplets Falling on a Solid Surface, *Journal of Materials Science,* 34, 19, 4883–4894.

Bogy, D. B., and Talke, F. E., 1984. Experımental and Theoretical Study of Wave Propagatıon Phenomena in Drop-On-Demand Ink Jet Devıces, *IBM Journal of Research and Development*, 28, 3, 314–321.

Bourell, D. L., Leu, M. C., and Rosen, D. W., 2009. Roadmap for additive manufacturing: identifying the future of freeform processing, *The University of Texas at Austin, Austin, TX.*

Brunahl, J., and Grishin, A. M., 2002. Piezoelectric Shear-mode Drop-on-demand Inkjet Actuator, *Sens. Actuator A: Phys*, 101, 371–382.

Campbell, P. G., and Weiss, L. E., 2007. Tissue engineering with the aid of inkjet printers, *Expert Opin. Biol. Ther.,* 7, 1123-1127.

Castrejón-Pita, J. R., Martin, G. D., Hoath, S. D., and Hutchings, I. M., 2008. A simple large-scale droplet generator for studies of inkjet printing, *Review of Scientific Instruments,* 79, 7.

Chandra, S., and Jivraj, R., 2002. Apparatus and method for generating uniform sized droplets, *US Patent,* 6, 446-878.

Chen, Z. R., Wang, H. J., Liu, Q. Z., and Cai, W. H., 2013. Engineering Fluid Mechanics, *third ed. Higher Education Press,* Beijing, 234–284.

Cheng, S. X., Li, T., and Chandra, S., 2005. Producing molten metal droplets with a pneumatic droplet-on-demand generator, *Journal of Materials Processing Technology*, 159, 3, 295–302.

Chun, J. H., 1997. Proceess-Structure Relationships in the Uniform-Droplet Spray Process, *Proceedings of the 1997 NSF Manufacturing and Design Grantees Conference*, 327-328.

Chun, J. H., and Hsiao, W., 2003. Effects of surface roughness on solder bump formation by direct droplet deposition, *CIRP Annals–Manuf Technol*, 52, 1, 161–164.

Cooper, K., Crocket, R., and Roberts, F., 2004. Free Form Fabrication in Space, *American Institute of Aeronautics and Astronautics Inc.,* Reno, NV, United states, 10524–10530.

Dey, A., and Yodo, N., 2019. A systematic survey of FDM process parameter optimization and their influence on part characteristics, *Journal of Manufacturing and Materials Processing.* MDPI Multidisciplinary Digital Publishing Institute.

Es-Said, O. S., Foyos, J., Noorani, R., Mendelson, M., Marloth, R., and Pregger, B. A., 2000. Effect of Layer Orientation on Mechanical Properties of Rapid Prototyped Samples, *Materials and Manufacturing Processes,* 15, 1, 107–122.

F. Savart, 1833. Mémoire sur la constitution des veines liquides lancées par des orifices circulaires en mince paroi, *Ann. de Chim,* vol.53, pp.337-386

Fan, K. C., Chen, J. Y., Wang, C. H., and Pan, W. C., 2008. Development of a drop-on-demand droplet generator for one-drop-fill technology, *Sensors and Actuators, A: Physical,* 147, 2, 649–655.

Fang, M., Chandra, S., and Park, C. B., 2008. Building three-dimensional objects by deposition of molten metal droplets, *Rapid Prototyping Journal,* 14, 1, 44–52.

Fischer, A. C., Mäntysalo, M., and Niklaus, F., 2020. Inkjet printing, laser-based micromachining, and micro–3D printing technologies for MEMS, *Handbook of Silicon Based MEMS Materials and Technologies*, 531–545.

Gallagher, C., Hughes, P. J., Tassie, P., Rodgers, K., Barton, J., Justice, J., and Casey, D. P., 2005. Solder jet technology for advanced packaging, Opto-Ireland 2005: optoelectronics, photonic devices, and optical networks, *Proc of SPIE* 5825, 615–621.

Gao, W., Zhang, Y., Ramanujan, D., Ramani, K., Chen, Y., Williams, C. B., and Zavattieri, P. D., 2015. The status, challenges, and future of additive manufacturing in engineering, *CAD Computer Aided Design,* 69, 65–89.

Gausemeier, J., Echterhoff, N., Kokoschka, M., and Wall, M., 2011. *Thinking Ahead the Future of Additive Manufacturing – Analysis of Promising Industries*, Heinz Nixdorf Institute, Germany.

Geng, P., Zhao, J., Wu, W., Ye, W., Wang, Y., Wang, S., and Zhang, S., 2019. Effects of extrusion speed and printing speed on the 3D printing stability of extruded PEEK filament, *Journal of Manufacturing Processes*, 37, 266–273.

Gibson, I., Rosen, D., and Stucker, B., 2010. Additive Manufacturing Technologies: Rapid Prototyping to Direct Digital Manufacturing, Springer, New York, NY.

Gibson, I., Rosen, D., and Stucker, B., 2010a. Additive Manufacturing Technologies: Rapid Prototyping to Direct Digital Manufacturing, 101-102, SE, Springer, New York, NY.

Gibson, I., Rosen, D., and Stucker, B., 2010b. Additive Manufacturing Technologies: Rapid Prototyping to Direct Digital Manufacturing, 1-498, SE, Springer, New York, NY.

Gibson, I., Rosen, D., and Stucker, B., 2010c, Additive Manufacturing Technologies, 3D Printing, Rapid Prototyping, and Direct Digital Manufacturing, 107-112, SE, Springer, New York, NY

Gibson, I., Rosen, D., and Stucker, B., 2010d. Additive Manufacturing Technologies, 3D Printing, Rapid Prototyping, and Direct Digital Manufacturing, 206, SE, Springer, New York, NY.

Ham, Y. B., Seo, W. S., Oh, S. J., Park, J. H., and Yun, S. N., 2010. A piezoelectric-driven single-nozzle dispenser for liquid droplet jetting, *Journal of the Korean Physical Society,* 57, 41, 877–881.

Harris, D. M., Liu, T., and Bush, J. W. M., 2015. A low-cost, precise piezoelectric droplet-on-demand generator, *Experiments in Fluids,* 56, 4.

Hayes, D. J., Wallace, D. B., and Cox, W. R., 1999. Microjet printing of solder and polymers for multi-chip modules and chip-scale packages, *Proceedings of IMAPS International Conference on High Density Packaging and MCMs*, Denver.

He, L., Wei, X., Zhang, H., Chen, P., Luo, H., Ma, M., and Shu, X., 2014. Drop-on-demand jetting of piezoelectric diaphragm-piston for fabricating precision solder bumps. *Electronic Packaging Technology Conference, EPTC* 10–13, Institute of Electrical and Electronics Engineers Inc, New Jersey, USA.

Henry, H., and Stavros, A. A., 1996. Mathematical modelling of solidification and melting: a review, *Model. Simul. Mater. Sci. Eng.,* 4, 371.

Himmel, B., Rumschoettel, D., and Volk, W., 2019. Tensile properties of aluminium 4047A built in droplet-based metal printing, *Rapid Prototyping Journal*, 25, 2, 427–432.

Hossain, M. S., Espalin, D., Ramos, J., Perez, M., and Wicker, R., 2014. Improved Mechanical Properties of Fused Deposition Modeling-Manufactured Parts Through Build Parameter Modifications, *Journal of Manufacturing Science and Engineering, Transactions of the ASME,* 136, 6.

Huang, S., Liu, P., Mokasdar, A., and Hou, L., 2013. Additive manu- facturing and its societal impact: a literature review, *Int J Adv Manuf Technol*, 67, 1191–1203.

ISO-ASTM, 2015. 52900, Additive manufacturing - general principles – terminology, West Conshohocken.

ISO-DIS, 2015. 17296-2, Additive Manufacturing – General Principles – Part 2: Overview of Process Categories and Feedstock

Ivanova, O., Williams, C., and Campbell, T., 2013. Additive manufacturing (AM) and nanotechnology: promises and challenges, *Rapid Prototyp J*, 19, 5, 353–364.

Jiang, X. S., Qi, L. H., Luo, J., Huang, H., and Zhou, J. M., 2010. Research on accurate droplet generation for micro-droplet deposition manufacture, *International Journal of Advanced Manufacturing Technology*, 49, 5–8, 535–541.

Jiao, Z., Li, F., Xie, L., Liu, X., Chi, B., and Yang, W., 2018. Experimental research of drop-on-demand droplet jetting 3D printing with molten polymer, *Journal of Applied Polymer Science,* 135, 9.

Johnson, W. L., Murr, L. E., Halpin, M., and Frantz, P., 2016. Additive manufacturing systems and methods, *U.S. Provisional Patent Application Number: 62308821*, March 15.

Kentzer, J., Koch, B., Thiim, M., Jones R. J., and Villumsen, E., 2011. An Open Source Hardware-Based Mechatronics Project: The Replicating Rapid 3-D Printer, *IEEE 4th Int Conf on Mechatronics*, 1–8.

Kim, E., Shin, Y. J. and Ahn, S. H., 2016. The effects of moisture and temperature on the mechanical properties of additive manufacturing components: fused deposition modelling, *Rapid Prototyping Journal*, 22, 6, 887-894.

Kim, H., Cherng, J., and Chun, J. H., 2002. Recent Progress in Droplet-Based Manufacturing Research, *Innovation in Manufacturing*, MIT Libraries

Koli, Y., Yuvaraj, N., Sivanandam, A., and Vipin. 2021. Control of humping phenomenon and analyzing mechanical properties of Al–Si wire-arc additive manufacturing fabricated samples using cold metal transfer process, *Journal of Mechanical Engineering Science*, 203-210.

Korkut, V., and Yavuz, H., 2020. Enhancing the tensile properties with minimal mass variation by revealing the effects of parameters in fused filament fabrication process, *Journal of the Brazilian Society of Mechanical Sciences and Engineering*, 42, 10.

Korkut, V., and Yavuz, H., 2022. Examining the Influential Parameters on Reducing both Energy and Time Requirements in Open-Source 3D Printers, *Journal of the Institute of Science and Technology*, 12, 1, 403-411.

Korkut, V., and Yavuz, H., 2022a. In-space Additive Manufacturing based on Metal Droplet Generation Using Drop-on-Demand Technique, *Journal of Materials Engineering and Performance,* In Production (10.1007/s11665-022-06865-7)

Korkut, V., and Yavuz, H., 2022b. Sustainable Metal Droplet Formation via Open-Source, Cost-Effective, and Modifiable Droplet Generator, *Proceedings of the Institution of Mechanical Engineers, Part C: Journal of Mechanical Engineering Science*, OnlineFirst Publication: https://doi.org/10.1177/09544062211065347

Laurell, T., Wallman, L., and Nilsson, J., 1999. Design and development of a silicon micro-fabricated flow-through dispenser for on-line picolitre sample handling, *J. Micromech. Microeng*, 9, 369–376.

Lee, T. M., Jo, J. D., Kim, H. S., Ham, Y. B., Yoon, S. N., and Kim, K. Y., 2005. Design of a gap-adjustable inkjet printing system for dense and high-temperature-melting materials, *In Semiconductor and Organic Optoelectronic Materials and Devices* 5624, 666.

Lee, T. M., Kang, T. G., Yang, J. S., Jo, J., Kim, K. Y., Choi, B. O., and Kim, D. S., 2008. Gap adjustable molten metal DoD inkjet system with cone-shaped piston head, *Journal of Manufacturing Science and Engineering, Transactions of the ASME*, 130, 3, 0311131–0311136.

Lee, T. M., Kang, T. G., Yang, J. S., Jo, J., Kim, K. Y., Choi, B. O., and Kim, D. S., 2008. Drop-on-demand solder droplet jetting system for fabricating microstructure, *IEEE Transactions on Electronics Packaging Manufacturing*, 31, 3, 202–210.

Li, B., Fan, J., Li, J., Chu, J., and Pan, T., 2015. Piezoelectric-driven droplet impact printing with an interchangeable microfluidic cartridge, *Biomicrofluidics,* 9, 5.

Li, L., Sun, Q., Bellehumeur, C., and Gu, P., 2002. Composite modeling and analysis for fabrication of FDM prototypes with locally controlled properties, *J Manuf Process,* 4, 2, 129–41.

Liao, D., Su, D., Liu, S., Li, X., and Zhang, H., 2016. Effects of drive air pressure, exhaust pipe length and deposition height on the morphology of Sn99.3Cu0.7 solder ball, *In 2016 17th International Conference on Electronic Packaging Technology,* ICEPT, 1508–1511, Institute of Electrical and Electronics Engineers Inc.

Lin, H. J., Wu, H. C., Shan, T. R., and Hwang, W. S., 2006. The effects of operating parameters on micro-droplet formation in a piezoelectric inkjet printhead using a double pulse voltage pattern, Materials Transactions, 47, 2, 375–382.

Liu, Q., and Orme, M., 2001. High precision solder droplet printing technology and the state-of-the-art, *Journal of Materials Processing Technology*, 115, 3, 271–283.

Liu, T., 2014. A reproducible and low-cost piezoelectric droplet generator, *Department of Mechanical Engineering, Massachusetts Institute of Technology.*

Liu, W., DuPont, J. N., 2003. Fabrication of functionally graded TiC/Ti composites by Laser Engineered Net Shaping, *Scripta Materialia,* 48, 1337-1342.

Liu, X., Zhang, M., Li, S., Si, L., Peng, J., and Hu, Y., 2016. Mechanical property parametric appraisal of fused deposition modeling parts based on the gray Taguchi method, *The International Journal of Advanced Manufacturing Technology*, 89, 5-8, 2387–2397.

Lu, W., Lin, F., Han, J., Qi, H., and Yan, N., 2009. Scan Strategy in Electron Beam Selective Melting, *Tsinghua Science & Technology,* 14, 120-126.

Luo, J., Qi, L., Tao, Y., Ma, Q., and Visser, C. W., 2016. Impact-driven ejection of micro metal droplets on-demand, *International Journal of Machine Tools and Manufacture,* 106, 67–74.

Luo, J., Qi, L.H., Zhong, S.Y., Zhou, J.M., and Li, H.J., 2012. Printing solder droplets for micro devices packages using pneumatic drop-on-demand (DOD) technique, *J. Mater, Process. Technol*., 212, 2066–2073.

Luo, W. C., and Liu, D. Q., 2009. Area array package-BGA, lCSP & flip chip, *China Integrated Circuit,* 2009.

Ma, M., Wei, X., Shu, X., and Zhang, H., 2019. Producing solder droplets using piezoelectric membrane-piston-based jetting technology, *Journal of Materials Processing Technology,* 263, 233–240.

McAlister, C., and Wood, J., 2014. The potential of 3D printing to reduce the environmental impacts of production, *Summer Study Energy Effic Retool a Compet Sustain Ind*, 1, 213– 221.

Meteyer, S., Xu, X., Perry, N., Zhao, Y. F., 2014. Energy and material flow analysis of binder-jetting additive manufacturing processes, *Proc CIRP*, 15, 19–25.

MIT, 2021. MIT Center for Additive and Digital Advanced Production Technologies (APT) (Retrieved from: http://apt.mit.edu/am-process-comparisons)

Molitch-Hou M., 2016. Optomec Introduces Hybrid Metal 3D Printing at Half the Cost. Fabbaloo.

Molitch-Hou, M., 2018. Overview of additive manufacturing process. *Additive manufacturing,* 3-5, Butterworth-Heinemann.

Molitch-Hou, M., 2018a. Overview of additive manufacturing process. *Additive manufacturing,* 6, Butterworth-Heinemann.

Muntz, E. P., and Dixon, M., 1986. Applications to space operations of free-flying, controlled streams of liquids*, J. Spacecraft,* 23, 4, 411–419.

Muntz, E. P., Orme, M., Pham-Van-Diep, G., and Godin, R., 1997. An Analysis of Precision, Fly-through Solder Jet Printing for DCA Components, *Microelectronics Packaging Soc*, 671–680.

Murr, L. E., and Johnson, W. L., 2017. 3D metal droplet printing development and advanced materials additive manufacturing, *Journal of Materials Research and Technology*, 6, 1, 77-89.

Northrup, W. F., and Sonsini, A. J., 1972. Pulse jet solder deposition, *IBM Tech. Discl. Bull.,* 14, 8, 2354–2355.

Orme, M., and Huang, C., 1997. Advanced Materials Synthesis and Manufacturing Using Controlled Droplet Deposition, *Proceedings of 1997 NSF Manufacturing and Design Grantees.*

Orme, M., and Muntz, E. P., 1987. New technique for producing highly uniform droplet streams over an extended range of disturbance wavenumbers, *Review of Scientific Instruments,* 58, 2, 279–284.

Orme, M., and Muntz, E. P., 1990. Method and Apparatus for droplet stream manufacturing, Publication No. US5226948A; United States Patent Office

Orme, M., and Muntz, E. P., 1992. United States Patent Number 5, 171, 360, United States Patent Office

Orme, M., and Smith, R. F., 2000, Enhanced Aluminum Properties by Means of Precise Droplet Deposition, *ASME. J. Manuf. Sci. Eng. August 2000*, 122, 3, 484–493.

Palmero E.M. and Bollero, A., 2021. 3D and 4D Printing of Functional and Smart Composite Materials, *Encyclopedia of Materials: Composites*, 402-419, Elsevier

Park, J., Moon, J., Shin, H., Wang, D., and Park, M., 2006. Direct-write fabrication of colloidal photonic crystal microarrays by ink-jet printing, *J Colloid Interface Sci,* 298:713–719.

Pasandideh-Fard M., Qiao, Y. M., Chandra, S. and Mostaghimi, J., 1996. *Physics of Fluids,* 8, 650–659.

Pearce, J. M., 2012. Building research equipment with free, open-source hardware, *Science*, 337, 6100, 1303–1304.

Pearce, J. M., 2014. Open-Source Lab: How to Build Your Own Hardware and Reduce Research Costs, *Elsevier*, New York, USA.

Pierson, H. A., and Chivukula, B., 2018. Process–Property Relationships for Fused Filament Fabrication on Preexisting Polymer Substrates, *Journal of Manufacturing Science and Engineering,* 140, 8, 084501-084501-084506.

Priest, J. W., Smith, C., and DuBois, P., 1997. Liquid Metal Jetting for Printing Metal Parts, *Proceedings of the 8th Solid Freeform Fabrication Symposium*, 1–9.

Qi, L. H., Chao, Y. P., Luo, J., Zhou, J. M., Hou, X. H., and Li, H. J., 2012. A novel selection method of scanning step for fabricating metal components based on micro-droplet deposition manufacture, *International Journal of Machine Tools and Manufacture*, 56, 50–58.

Rayleigh, L., 1879. *Proc. London Math. Soc*. 10, 4.

Rayna, T., and Striukova, L., 2016. From rapid prototyping to home fabrication: how 3D printing is changing business model innovation, *Technol Forecast Soc*, 102, 214–224.

Ries, M. D., Banks, D. R., Watson, D. P., and Hoebener, K.G., 1993. Attachment of Solder Ball Connect (SBC) packages to circuit cards, *I3M Journal*, 37, 5, 597-608.

Rinne, G. A., 1997. Solder bumping methods for flip chip packaging, *Electronic Components & Technology Conference, IEEE*, 240-247.

Rocha, J. C., 1997. Control of the UDS Process for the Production of Solder Balls for BGA Electronics Packaging, *S.M. thesis, Massachusetts Institute of Technology*, Cambridge, MA.

Rocha, L. C. S., Paiva, A. P., Paiva, E. J., and Balestrassi., P. P., 2016. Comparing DEA and principal component analysis in the multiobjec- tive optimization of P-GMAW process, *J Braz Soc Mech Sci Eng*, 38, 8, 2513–2526.

Rodriguez, J. F., Thomas, J. P., and Renard, J. E., 2003. Design of fused-deposition ABS components for stiffness and strength, *J Mech Des*, 125, 3, 545–51.

Roy, R. K., 2010. A primer on the Taguchi method, 2nd ed., *Society of manufacturing engineers,* 2nd ed.

Rumschoettel, D., Kunzel, F., Irlinger, F., and Lueth, T. C., 2016. A novel piezoelectric printhead for high melting point liquid metals, *Pan Pacific Microelectronics Symposium, Pan Pacific 2016*, Institute of Electrical and Electronics Engineers Inc.

Sachs, E. M., Cima, M. J., Williams, P., Brancazio, D., and Cornie, J., 1992. Three-dimensional printing: rapid tooling and prototypes directly from a CAD model, *J Eng Ind*, 114, 481–488.

Schuhmacher, D., Niekrawietz, R., Scheithauer, H., Heti, B., Alavi, M., Zengerle, R., and Koltay, P., 2007. Production of solder microdroplets using a highly parallel and contact-free printing method, *IEEE International Conference on Micro Electro Mechanical Systems,* 357-360.

Short, D., and Daniel, B., 2015. Use of 3D printing by museums: educational exhibits, artifact education, and artifact restoration, *3D Print Addit Manuf,* 2, 209–215.

Sin, L. T., 2012. Polylactic Acid: PLA Biopolymer Technology and Applications, William Andrew, Boston, MA, USA.

Sing, S.L., Tey, C. F., Tan, J.H.K., Huang S., Yeong W.Y., 2020. 3D printing of metals in rapid prototyping of biomaterials: Techniques in additive manufacturing, *Woodhead Publishing Series in Biomaterials*, 17-40.

Sohn, H., and Yang, D. Y., 2005. Drop-on-demand deposition of superheated metal droplets for selective infiltration manufacturing, *Materials Science and Engineering A*, 392, 1–2, 415–421.

Song, R., Clemon, L., and Telenko, C., 2018. Uncertainty and variability of energy and material use by fused deposition modeling printers in makerspaces, *J Indl Ecol Wiley/Blackwell,* 10, 1111.

Sood, A. K., Ohdar, R. K., and Mahapatra, S. S., 2010. Parametric appraisal of mechanical property of fused deposition modelling processed parts, *Materials and Design,* 31, 1, 287–295.

Suárez, L., and Domínguez, M., 2020. Sustainability and environmental impact of fused deposition modelling (FDM) technologies, *International Journal of Advanced Manufacturing Technology*, 106, 3–4, 1267–1279.

Sweet, R. G., 1965. High frequency recording with electrostatically deflected ink-jets, *Rev. Sci. Instrum.* 36, 131.

Takahashi, S., Kitagawa, H., Tomikawa, S., Kitagawa, H., and Tomikawa, Y., 2002. A study of liquid dispensing head using fluidic inertia, *Jpn. J. Appl. Phys*, 41, 3442–3445.

Tlegenov, Y., Wong, Y. S., and Hong, G. S., 2017. A dynamic model for nozzle clog monitoring in fused deposition modelling, *Rapid Prototyping Journal,* 23, 2, 391–400.

Tomaszewski, G., and Potencki, J., 2017. Drops forming in inkjet printing of flexible electronic circuits, *Circuit World* 43, 13–18.

Trapaga, G., Matthys, E. F., Valencia, J. J., and Szekely, J., 1992. Fluid flow, heat transfer, and solidification of molten metal droplets impinging on substrates: comparison of numerical and experimental results, *Metall. Mater. Trans. B*, 23, 701–718.

Tseng, A. A., Lee, M. H., and Zhao, B., 2001. Design and operation of a droplet deposition system for freeform fabrication of metal parts, *Journal of Engineering Materials and Technology*, Transactions of the ASME, 123, 1, 74–84.

Tseng, A. A., Lee, M. H., and Zhao, B., 2001. Design and operation of a droplet deposition system for freeform fabrication of metal parts, *Journal of Engineering Materials and Technology, Transactions of the ASME,* 123, 1, 74–84.

Tymrak, B. M., Kreiger, M., and Pearce, J. M., 2014. Mechanical properties of components fabricated with open-source 3-D printers under realistic environmental conditions, *Materials and Design*, 58, 242–246.

Uddin, M. S., Sidek, M. F. R., Faizal, M. A., Ghomashchi, R., and Pramanik, A., 2017. Evaluating Mechanical Properties and Failure Mechanisms of Fused Deposition Modeling Acrylonitrile Butadiene Styrene Parts, *Journal of Manufacturing Science and Engineering*, Transactions of the ASME, 139, 8.

Vaught, J. L., Cloutier, F. L. Donald, D. K., Meyer, J. D., Tacklind, C. A., and Taub, H. H., 1984. Thermal inkjet printer, *US Patent* no. 4, 490-728, Hewlett-Packard, United States Patent Office

Vega, E. J., Cabezas, M. G., Muñoz-Sánchez, B. N., Montanero, J. M., and Gañán-Calvo, A. M., 2014. A novel technique to produce metallic microdrops for additive manufacturing, *International Journal of Advanced Manufacturing Technology,* 70, 5–8, 1395–1402.

Vyavahare, S., Teraiya, S., Panghal, D., and Kumar, S., 2020. Fused deposition modelling: a review, *Rapid Prototyping Journal,* Emerald Group Holdings Ltd.

Wallace, D. B., 1989. Automated Electronic Circuit Manufacturing Using Ink-Jet Technology, *ASME J. Electron. Packag*., 111, 108–111.

Wang, H., Cheng, C., Zhang, L., Liu, H., Zhao, Y., Guo, Y., Hu, W., Yu, G., and Liu, Y., 2014. Inkjet printing short-channel polymer transistors with high-performance and ultrahigh photoresponsivity, *Adv. Mater.* 26, 4683–4689.

Wang, T., Kwok, T. H., and Zhou, C., 2017. In-situ Droplet Inspection and Control System for Liquid Metal Jet 3D Printing Process, In *Procedia Manufacturing,* 10, 968–981, Elsevier.

Weber, C., 1931. The Decomposition of a Liquid Jet, Z. Angew, *Math. Mech*., 11, 136–154

Website, 2020a. Filament properties table, https ://www.simplify3d.com/support/materials guide/properties-table.

Website, 2020b. 3D printer filament buyer's guide, https ://all3dp.com/1/3d-printer-filament-types-3d-printing-3d-filament.

Website, 2020c. 3D Matter (2019) FDM 3D printing materials compared. https://www.3dhubs.com/knowledge-base/fdm-3d-printing-materials-compared.

Website, 2021a. https://www.hubs.com/knowledge-base/types-of-3d-printing/#1.-vat-photopolymerization.

Website, 2021b. https://all3dp.com/1/types-of-3d-printers-3d-printing-technology/.

Website, 2021c. 3D Printer Filament Comparison Guide. Available online: https://www.matterhackers.com/3d-printer- filament-compare (accessed on 17 July 2019).

Website, 2021d. 3D Printer Filament Guide All You Need to Know in 2019. Available online: https://all3dp.com/1/3d-printer-filament-types-3d-printing-3d-filament/ (accessed on 17 July 2019).

Website, 2021e. Printing Materials Compared. Available online: https://www.3dhubs.com/knowledge-base/fdm-3d-printing-materials compared (accessed on 17 July 2019).

Website, 2021f. https://www.engineersgarage.com/3d-printing-processes-powder-bed-fusion-part-5-8/.

Website, 2021g. Arcam. Electron Beam Melting. http://www.arcam.com.

Website, 2021h. https://www.hubs.com/knowledge-base/types-of-3d-printing/#7.-sheet-lamination3.

Website, 2021i. https://www.manufacturingguide.com/en/laminated-object-manufacturing-lom.

Website, 2021j. Electronics Notes. Light DependentResistor LDR: Photoresistor, www.electronics-notes.com/articles/electronic_components/ resistors/light-dependent-resistor-ldr.php.

Website, 2022a. https://support.ultimaker.com/hc/en-us/sections/360003548619-Print-settings.

Website, 2022b, https://all3dp.com/2/3d-printing-shells-all-you-need-to-know/

Website, 2022c, https://www.oshwa.org/open-source-quick-reference-guide.

Website, 2022d, https://opensource.org/docs/osd.

Website, 2022e. https://all3dp.com/1/common-3d-printing-problems-troubleshooting-3d-printer-issues/.

Website, 2022f. https://wikifactory.com/+bitfab/stories/fdm-3d-printing-common-problems-and-how-to-solve-them.

Website, 2022g. https://www.geeetech.com/blog/2016/12/troubleshooting-guide-to-19-common-3d-printing-problemspart-one/.

Website, 2022h. https://www.matterhackers.com/articles/3d-printer-troubleshooting-guide.

Website, 2022i. https://www.simplify3d.com/support/print-quality-troubleshooting/.

Website, 2022j. https://github.com/.

Website, 2022k. https://marlinfw.org/.

Website, 2022l. https://reprap.org/wiki/Triffid_Hunter's_Calibration_Guide

Website, 2022n. https://reprap.org/wiki/PID_Tuning.

Website, 2022o. https://marlinfw.org/docs/gcode/M303.html.

Website, 2022p. Instructables. How to Build a Simple but Powerful Flyback Driver, https://www.instructables.com/ZVS-Driver/.

Wendel, B., Rietzel, D., Kühnlein, F., Feulner, R., Hülder, G., and Schmachtenberg, E., 2008. Additive processing of polymers, *Macromol Mater Eng*, 293, 799–809.

Wijshoff, H., 2010. The dynamics of the piezo inkjet printhead operation, Physics Reports.

Wohlers, T., 2013. Additive manufacturing and 3D printing State of the industry, *Wohlers Associates,* Fort Collins, CO.

Wohlers, T., 2018. 3D printing and additive manufacturing state of the industry: *Wohlers Associates,* Fort Collins, CO.

Wu, H. C., and Lin, H. J., 2010. Effects of actuating pressure waveforms on the droplet behavior in a piezoelectric inkjet, *Materials Transactions*, 51, 12, 2269–2276.

Wu, H. C., Lin, H. J., and Hwang, W. S., 2005. A numerical study of the effect of operating parameters on drop formation in a squeeze mode inkjet device, *Modelling and Simulation in Materials Science and Engineering*, 1317–34.

Yadroitsev, I., Shishkovsky, I., Bertrand, A. P., and Smurov, I., 2009. Manufacturing of fine- structured 3D porous filter elements by selective laser melting, *Appl Surf Sci*, 25, 5523–7.

Yamaguchi, K., Sakai, K., Yamanaka, T., and Hirayama, T., 2000. Generation of three-dimensional micro structure using metal jet, *Precision Engineering*, 24, 1, 2–8.

Yang, J. C., Chien, W., King, M., and Grosshandler, W. L., 1997. A simple piezoelectric droplet generator, *Experiments in Fluids*, 23, 5, 445–447.

Yokoyama, Y., Endo, K., Iwasaki, T., and Fukumoto, H., 2009. Variable-size solder droplets by a molten-solder ejection method, *Journal of Microelectromechanical Systems,* 18, 2, 316–321.

Zarzalejo, J. L., Schmaltz, S. K., and Amon, H. C., 1999. Molten droplet solidification and substrate remelting in microcasting Part I: numerical modeling and experimental verification, *Heat. Mass Transf.*, 34, 477–485.

Zhang, D., Qi, L., Luo, J., Yi, H., and Hou, X., 2017. Direct fabrication of unsupported inclined aluminum pillars based on uniform micro droplets deposition, *International Journal of Machine Tools and Manufacture,* 116, 18–24.

Zhang, D., Qi, L., Luo, J., Yi, H., Xiong, W., and Mo, Y., 2019. Parametric mapping of linear deposition morphology in uniform metal droplet deposition technique, *Journal of Materials Processing Technology,* 264, 234–239.

Zhong, S. Y., Qi, L. H., Luo, J., Zuo, H. S., Hou, X. H., and Li, H. J., 2014. Effect of process parameters on copper droplet ejecting by pneumatic drop-on-demand technology, *Journal of Materials Processing Technology*, 214, 12, 3089-3097.

Zhong, S., Qi, L., Tang, Y., and Luo, J., 2014. Development and experimental research of aluminium alloy droplet generator based on mechanical vibration, *In Procedia Engineering*, 81, 1583–1588.

CURRICULUM VITAE

Volkan KORKUT, He received his BSc. from Department of Mechanical Engineering in Ege University in 2013, and MSc. from Department of Mechanical Engineering in Ege University, respectively. He has been working as a Research Assistant in Department of Mechanical Engineering in Adana Alparslan Türkeş Science and Technology University since 2017. His research areas are, additive manufacturing, rapid prototyping, MEMs, direct material deposition, droplet based manufacturing and control techniques.

APPENDIX

A.1. PUBLISHED ARTICLES

Korkut, V., and Yavuz, H., 2022a. In-space additive manufacturing based on metal droplet generation using drop-on-demand technique, *Journal of Materials Engineering and Performance,* In Production (10.1007/s11665-022-06865-7)

Korkut, V., and Yavuz, H., 2022b. Sustainable metal droplet formation via open-source, cost-effective, and modifiable droplet generator, *Proceedings of the Institution of Mechanical Engineers, Part C: Journal of Mechanical Engineering Science*, OnlineFirst Publication: https://doi.org/10.1177/09544062211065347

Korkut, V., and Yavuz, H., 2022c. Examining the influential parameters on reducing both energy and time requirements in open-source 3D printers, *Journal of the Institute of Science and Technology*, 12, 1, 403-411.

Korkut, V., and Yavuz, H., 2020. Enhancing the tensile properties with minimal mass variation by revealing the effects of parameters in fused filament fabrication process, *Journal of the Brazilian Society of Mechanical Sciences and Engineering*, 42, 10.

A.2. CONFERENCE PAPERS

Korkut, V., and Yavuz, H., 2020. An investigation of the energy consumption during a FFF based printing operations. *International Conference on Energy, Environment and Storage of Energy*, November 19-21, Kayseri, Turkey.

Korkut, V., and Yavuz, H., 2019. The importance of pressure supplement in metal jetting mechanism. *6th International Multidisciplinary Studies Congress*, April 26-27, Gaziantep, Turkey.

Korkut, V., and Yavuz, H., 2019. Recent advances over metal part manufacturing using 3d printing technology based on droplet generation method. *6th International Multidisciplinary Studies Congress*, April 26-27, Gaziantep, Turkey.

Korkut, V., and Yavuz, H., 2018. Trending techniques in additive manufacturing with their advantages and disadvantages. *3rd International Energy Engineering Congress.* October 18-19, Gaziantep, Turkey.

Korkut, V., and Yavuz, H., 2018. Available and emerging metal additive manufacturing techniques for direct metal part manufacturing. *3rd International Energy Engineering Congress.* October 18-19, Gaziantep, Turkey.

Korkut, V., and Yavuz, H., 2018. Comparison and evaluation of various material jetting technologies in terms of additive manufacturing. *5th International Conference on Materials Science and Nanotechnology for Next Generation.* October 4-6, Cappadocia, Turkey.